Ablation of Retbindin, the Riboflavin Binding Protein, Exacerbates Retinal Degenerative Phenotypes in Mouse Models of Human Retinal Diseases

by
Ayse Mine Genc

A dissertation submitted to the Biomedical Engineering Department,

of Cullen College of Engineering

in partial fulfillment of the requirements for the degree of

Doctor of Philosophy

in Biomedical Engineering

Chair of Committee: Muna I. Naash

Committee Member: Muayyad R. Al-Ubaidi

Committee Member: Shannon M. Conley

Committee Member: Laura J. Frishman

Committee Member: Jinsook Roh

University of Houston

May 2020

Dedication

I dedicate this dissertation to my dearly husband, Alptekin Genc, who has been supportive and considerate throughout the duration of my graduate school. I am very thankful for having you in my life. I dedicate this work also to my lovely children Yusuf and Yusra. Thank you for understanding of your mom's desire for science and not complaining about mom being busy all the time. I love you to the moon and back. I dedicate this work also to my beloved parents, Faruk Kusbeoglu and Inci Kusbeoglu and to my dearly siblings who have always been constant source of encouragement in my life.

Acknowledgments

I would like to express my heartiest gratitude and sincere to my advisor, Dr. Muna Naash, for allowing me to work in her lab, contribute to the present work, and funding my time as a graduate student. She has been a very supportive and motivating mentor which made my accomplishments possible. I owe so much to her for encouraging me to learn different techniques and challenging me so that I could become a stronger and better scientist and engineer.

I would like to extent my sincere gratitude to Dr. Muayyad Al-Ubaidi, who has actively provided guidance and mentorship through my time working together. I have learnt a lot from his experience, scientific knowledge, intellectuality, and technical guidance. Special thanks to Dr. Shannon Conley for her contribution to my present work. I am inspired from her working ethics, energy, organization and dedication to her work. I appreciate how approachable she is and how clearly explains complex topics and nuances. I would like to thank Dr. Laura Frishman and Dr. Jinsook Roh for their support, insights and service on my dissertation committee. I deeply appreciate them for generously giving their time.

I am grateful to the University of Houston and the Biomedical Engineering Department. I extend my gratitude to our department chair, Dr. Metin Akay, who took students under his wings and supports continuously. I am indebted to my master program advisor, Dr. Richard Gunasekera, who never hesitated to support me and encouraged me to pursue a carrier in research.

I acknowledge Mustafa Makia for helping me with the morphometric analysis and being a helpful lab manager. I would also like to thank Tirthankar Sinha for helping me with the flavin quantification analysis and training me on HPLC. I am thankful to my lab mate and close friend Larissa Ikelle for having stimulating scientific conversations with me and keeping me company through this long walk. Thank you to my other lab mates Mashal Kakakhel, Haarthi Sakthivel, Ryan Crane, Lars Tebbe, Alexander Ferrer, and Xue Zhao for their support and friendship.

\

Abstract

Retbindin (Rtbdn) is a retina-specific, riboflavin binding protein, expressed only by the rod photoreceptor cells. Riboflavin is the precursor of flavin mononucleotide (FMN) and flavin adenine dinucleotide (FAD) which are essential co-factors for enzymes involved in wide-range of metabolic processes. Since flavins are directly linked to the metabolism and metabolic dysregulation is a hallmark of degeneration, we hypothesized that Rtbdn, as a riboflavin binding protein, plays a role in modulating the degenerative process. In support of our hypothesis, we found that Rtbdn is significantly upregulated in the retinas of mouse models of late-onset cone rod dystrophy (*Prph2*^{R172W}), retinitis pigmentosa (*Rho*$^{P23H/+}$) and pattern dystrophy (*Prph2*$^{Y141C/+}$). We investigated the effect of Rtbdn ablation in these retinal degenerative models in order to elucidate the function of this novel protein in retinal health and disease. Although, the ablation of Rtbdn alone (*Rtbdn*$^{-/-}$) had no deleterious effects on retinal function up to postnatal day (P) 120, eliminating Rtbdn in the models led to significant reductions in both scotopic and photopic electroretinographic amplitudes, compared to the single mutants. Histologic assessments revealed severe thinning of diseased retinas upon elimination of Rtbdn. While the outer nuclear layer (ONL) cell counts in wild type (WT) and *Rtbdn*$^{-/-}$ were not significantly different from each other, we observed significant loss of ONL cells in the *Prph2*^{R172W}*/Rtbdn*$^{-/-}$*, Rho*$^{P23H/+}$*/Rtbdn*$^{-/-}$*, and Prph2*$^{Y141C/+}$*/Rtbdn*$^{-/-}$ in comparison to the single mutants. Ultrastructural analyses revealed shorter, malformed and disorganized photoreceptor outer segments, swollen inner segments and dilated Bruch's membrane in the retinas of degenerative models in absence of Rtbdn. In addition, elimination of Rtbdn in the

diseased retina led to vascular pathologies and appearance of neovascular tufts secondary to cell loss. We observed model-dependent alterations in the riboflavin, FAD, and FMN levels. Our data demonstrate the potential protective role of Rtbdn, making it a strong candidate as a therapeutic target in retinal degenerative diseases. Our future work will focus on investigating that potential by studying the effects of overexpression of Rtbdn in slowing the retinal degenerative process in models of human retinal degeneration.

Table of Contents

List of Tables

List of Figures

List of Abbreviations

ATP	adenosine triphosphate
ERG	electroretinography
FAD	flavin adenine dinucleotide
FLAD	FAD synthase
FMN	flavin mononucleotide
FT	flow through
GFAP	glial fibrillary acidic protein
IPM	interphotoreceptor matrix
IS	inner segment of the photoreceptor
mAb	monoclonal antibody
ONL	outer nuclear layer of photorecceptors
OS	outer segment of the photoreceptor
P	postnatal day
P23H	proline to histidine change at codon 23 of rhodopsin gene
pAb	polyclonal antibody
PC	pre-clear
PR	photoreceptor
Prph2	peripherin 2 (aka Rds)
R172W	arginine at position 172 mutated to tryptophan on Prph2 gene
RBP	Riboflavin binding protein of chicken oviduct
RfBP	Riboflavin binding protein
Rho	Rhodopsin
Rd	retinal degeneration
RFVT	riboflavin organic ion transporters RFVT1-3 (*SLC52A1-A3*)
RP	retinitis pigmentosa
RPE	retinal pigment epithelium
Rtbdn	retbindin
WT	wild type
Y141C	Y141C mutation in the Prph2 gene

Chapter 1- Introduction

This chapter introduces the Retbindin (Rtbdn) protein. In order to provide the context of Rtbdn- related research, the first section of introduction covers the visual system, structure of the retina and its photoreceptor cells. The retinal degenerative mouse models used in this dissertation; *Prph2*^{R172W}, *Prph2*$^{Y141C/+}$ and *Rho*$^{P23H/+}$ are also introduced.

1.1 Anatomy of the Eye

1.1.1 The principal components of the eye ball

Vision is the perception of objects in the surrounding environments by means of light that they emit or reflect. The eyes, the organ of the visual system, detect light and convert it into electro-chemical impulses. The eyeball is composed of three principal layers: (1) the outer fibrous layer; (2) the middle vascular layer; and (3) the inner layer that consists of the neural components [1]. The outer fibrous layer is divided into two regions as the sclera and cornea. Sclera is the white outer coat of the eye that is perforated by blood vessels and nerves, protects the delicate structures inside the eye. The cornea is the anterior transparent region of the sclera that transmits and focuses light into the eye. The middle vascular layer of the eyeball consists of three regions; the choroid, ciliary body, and iris. The choroid is a highly vascularized layer that lines back between the sclera and retina and supply the retina with nutrition.

The ciliary body is an extension of the choroid that includes muscles. It supports the iris and lens. The lens that is composed of transparent cells that focuses light rays onto the retina. The iris is the pigmented part of the eye. The iris controls the diameter of pupil, which is the central opening, to regulate the amount of light entering the eye. The space between the iris and the lens is filled with aqueous humor that is secreted by the ciliary body. In addition to all these, the central cavity of the eye behind the lens is filled with transparent jelly substance called vitreous humor. The Fig 1.1 that is taken from https://www.umkelloggeye.org/conditions-treatments/anatomy-eye shows the sagittal section of the human eye. The innermost layer of the eye ball consists of the neural components; the retina and the beginning of the optic nerve. More detailed information about the retina will be provided in the next section.

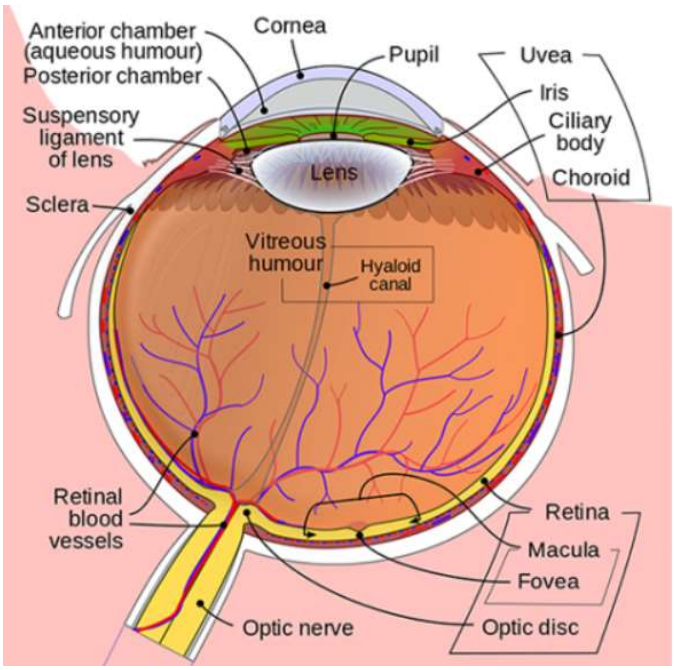

Figure 1.1. Sagittal section of the eye.

1.1.2 Retina

The retina is the innermost layer lining the back of the eyeball. It is the sensory tissue of the eye and considered to be a part of the brain. The light rays enter the eye and focus on the retina by the help of cornea and lens. The light energy is converted into chemical and nervous signals in the retina and transported to the brain via the optic nerve. Finally, these signals are converted into images in the visual centers of the brain [1].

There is a darkly pigmented layer called retinal pigment epithelium (RPE) in the most posterior part of the retina. The most obvious function of the RPE is the absorption of excess light so photoreceptors can give a clearer signal. RPE also nourishes the retina, regenerates the visual pigment and move waste from the retina. The retina consists of three layers of neurons: (1) photoreceptor cells, (2) second order neuron and (3) ganglion cells as it can be seen from the schematic taken from Fu et al. [2] (Fig. 1.2). Photoreceptors are the cells that absorb light and generate signals that can stimulate biological processes. The details about the photoreceptors are discussed later in the next section. Photoreceptors synapse with the dendrites of bipolar cells which are the second order neurons of the visual pathway. Bipolar cells synapse with the ganglion cells which are the largest neurons in the retina. They are the third order neurons of the visual pathway and line up in a single row in mouse retina. Most bipolar cells receive input from multiple photoreceptor cells and the ganglion cells receive input from multiple bipolar cells. Ganglion cell exons form the optic nerve that carry visual signals from retina to the brain. There are also two other types of cells in

the retina; horizontal cells and amacrine cells. They form horizontal connections among photoreceptors and bipolar cells to enhance the perception of contrast and the edges of objects. In addition to all these cell types, there are also astrocytes and other types of glial cells in the retina. Müller cells are the most common type of glial cells in the retina. They are vital for the health of retina such as mediating ion, water and bicarbonate transport, providing trophic and anti-oxidant support to photoreceptor cell, and controlling the composition of extracellular fluid [1]. Minimizing intraretinal light scattering, protecting neuronal cells in case of mechanical trauma, modulating the neural activity, and differentiation to neural progenitor cells are recently discovered new functions of Müller cells [3].

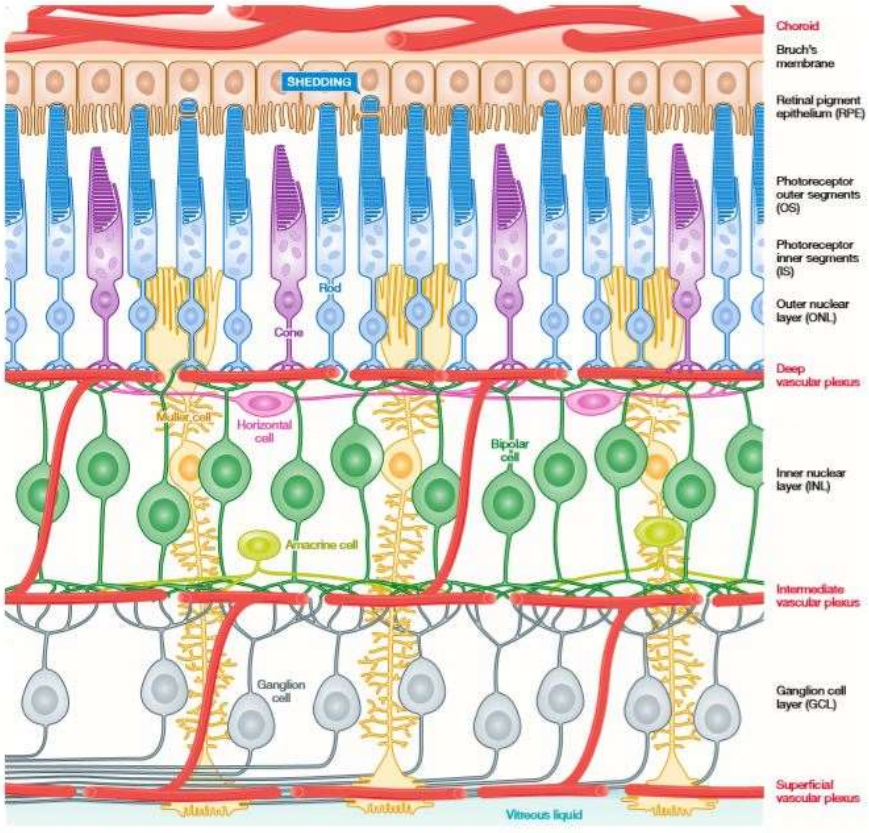

Figure 1.2. Cellular layout of the retina.

1.1.3 Photoreceptor cells

Photoreceptors are the cells in the retina that convert light energy to chemical or electrical signal. There are two types of photoreceptor cells in the human eye: rods and cones. They are derived from the same stem cells that produce ependymal cells of the brain. Rods are responsible for dim light/night (scotopic vision) that produce images only in shades of gray. While cones function in brighter light so, they are responsible for day (photopic) vision. Both rods and cones have outer segment (OS) and inner segment (IS) regions as can be seen from the schematic taken from Fu et al. [2] (Fig. 1.3). These segments are separated from each other by connecting cilium in the middle. The OSs are modified cilium that specialized in light absorption while ISs are where the mitochondria and other organelles are. The base of the photoreceptors contains the nucleus and the processes to synapse with neurons in the next layer. The OS of the rods are in cylindrical shape. Each rod OS composed of nearly 1000 neatly aligned stacks of discs which are enclosed by a plasma membrane [1]. Each disc is densely packed with a protein called rhodopsin (Rho). Rho is the visual pigment of the rods. The cone OSs taper to a point that is why they are called cones. Although the discs of rod OSs are completely detached from the plasma membrane, cone OSs contain open discs that are infoldings of the plasma membrane in addition to the closed ones. The visual pigment in the cones are called photopsin. Both Rho and photopsin consist of two moieties: a protein (opsin) and a vitamin a derivative (retinal). The retinal moieties are the same for rods and cones. However, the opsin moiety of the cone has a different amino acid sequence which determines the

absorption maximum wavelength of the light. There are three types of cones in humans: for short wavelengths; S (blue) cones, medium wavelength; M (green) cones, and long wavelength; L (red) cones. While mice lack L cones, so, they cannot see the red light. Our perception of different colors is based on mixture of the signals received from different types of cones [4].

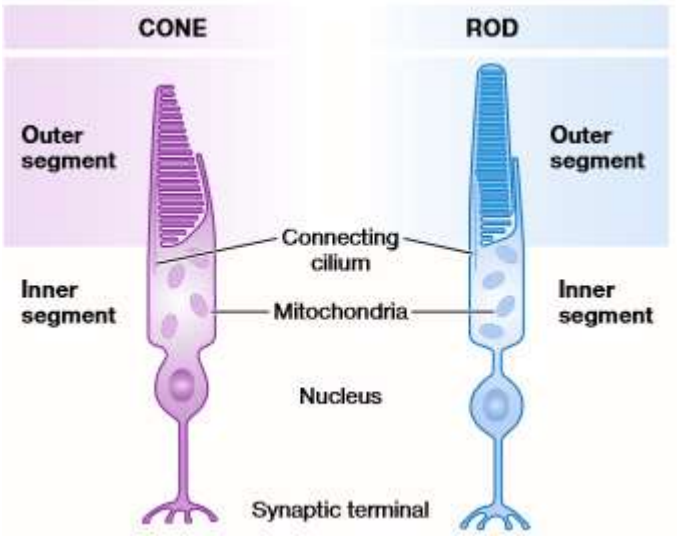

Figure 1.3. Structure of rod and cone photoreceptor cells.

The macula is a pigmented area near the center of the retina of the primate eyes. A tiny pit area called fovea in the macula provides the clearest vision of all. Although the number and ratio of rod and cones varies among species, the number of rods far exceeds the number of cones. The human retina contains about 91 million rods and 4.5 million cones [5]. Although the cones are present at a low density throughout the retina, their number increases ~200 fold in the center of the fovea. Conversely, rod density presents a sharp decline in the fovea. Mouse models have

greatly assisted our research on retinal diseases. Although the mouse retina does not contain macula, the rod to cone ratio is similar between mouse and human [6].

The photoreceptor nuclei layer is called outer nuclear layer (ONL) and the area where nuclei of bipolar cells and other second order neurons reside is called inner nuclear layer (INL). The third single raw of nuclear layer is called the ganglion cell layer (GCL). The light comes from the direction of the vitreous humor and passes through the entire retina before it reaches the photoreceptors in the outer layer (actually the innermost layer from the vitreous side). The extra light that passes through the retina is absorbed by the RPE. The neural signals pass in the reverse direction through photoreceptors, bipolar cells and finally reach the ganglion cells that carry the image away from the retina through the optic nerve [1].

The way how light is converted into electrical signal by the rods and cones are similar. Yet, cones are significantly less sensitive than rods and their photo-responses are much faster. Also, they recover their sensitivity several times faster than rods and adapt wide over a range of background lights [7, 8]. Here, the photo-transduction cascade in the rods is explained. In the dark, positively charged sodium (Na^+) ions flow to the rod cells through ion channels at the plasma membrane that are activated by their ligand, cyclic guanosine monophosphate (cGMP). The influx of positively charged ions causes the cells to remain in a depolarized state, meaning the continuous release of the neurotransmitters (glutamate) from the photoreceptors. In dark, the retinal in the Rho molecule is in the cis-retinal conformation. When it absorbs light, its conformation changes to the trans-retinal. Trans-retinal breaks away from opsin and

activates transducin, a G-protein. Then, transducin activates the enzyme phosphodiesterase which breaks down the cGMP. As cGMP levels fall the ion channels, that are open by cGMP, begin to close. Thus, less Na+ enters the cell and cell becomes hyperpolarized due to the potassium (K) ions that regularly leave the cell. Consequently, glutamate release from the base of the cell decreases. The bipolar cells are sensitive to these on/off pulses of glutamate secretion. Since some bipolar cells are inhibited by glutamate, they are excited when glutamate levels are reduced by rising light intensities. Finally, they stimulate ganglion cells to produce action potentials. These changes provide visual signals to the brain via the optic nerve [1, 8].

1.2 Diseases of the Retina

Vision is dependent on the precise structure of the retina so, any defect of this exquisite tissue is critical. There is a wide range of retinal disease conditions.

1.2.1 Pathogenesis of retinal diseases

The underlying reason of the retinal pathogenesis can be categorized as following:

Genetic: Inherited retinal diseases are caused by one of more than 250 different genes [9] (http://www.sph.uth.tmc.edu/RetNet/). There are several types of inherited retinal diseases but the following is a small list: retinitis pigmentosa (most common one), Best's disease, pattern dystrophy, Stargardt's disease, rod-cone dystrophy, cone-rod dystrophy, central areolar choroidal dystrophy. Depending on the disease, some people experience gradual loss of vision, while others experience vision

loss in early childhood. Unfortunately, there is no cure for the hereditary forms of retinal diseases. Therapeutic options are focused on slowing down the disease progression and they are currently limited. In addition to pharmacotherapy, gene therapy, stem cell therapy, optogenetics, and retinal prostheses are other potential treatment techniques and studies have already shown promising results [10].

Metabolic: Ocular manifestations occur in various metabolic disorders. The mechanism by which metabolic disease contributes to ophthalmologic problems is not well understood. Toxic byproducts of the altered metabolism, deficient energy production or the accumulation of metabolites due to errors of synthetic pathways are suggested as possible mechanisms [11, 12]. Diabetes, hyperlipidemia, thyroid eye disease, pituitary adenoma are some of the conditions that present with retinal manifestations. Although many of the retinal diseases have not been considered to be metabolic in nature, metabolic dysregulation has been shown to contribute to retinal pathologies. The occurrence of retinitis pigmentosa in metabolic disorders is an example of this situation.

Vascular: Retinal vascular disorders refer to eye diseases that affect the blood vessels that generally involve a blockage of blood flow, neovascularization and leakage or rupture of a retinal vessel. These conditions may be linked to existing vascular diseases, such as high blood pressure, high cholesterol, diabetes, central retinal vein occlusion, branch retinal vein occlusion, hypertension retinopathy, central retinal artery occlusion, branch retinal artery occlusion, retinopathy of prematurity.

Also, some of the ocular diseases are associated with pathological retinal neovascularization and edema such as wet age-related macular degeneration, proliferative diabetic retinopathy and diabetic macular edema. Anti-Vascular endothelial growth factor agents have been developed for the treatment of these diseases [13].

Inflammation: Ocular inflammation and its related complications are critical and can lead to severe vision loss. The term uveitis describes a group of inflammatory diseases that cause swelling and damage to the eye. Anterior Uveitis, Posterior Uveitis, VKH/Panuveitis, bacterial infections such as TB, Lyme disease, syphilis, and parasitic infections such as toxoplasmosis and giant cell arteritis are conditions affecting the retina due to inflammation, although the eye has been considered as an immune privileged tissue. Moreover, recent studies demonstrated the effect of inflammation on the pathogenesis of multiple diseases including AMD [14], retinitis pigmentosa [15], diabetic retinopathy[16], and retinal vein occlusion [17]. Altered retinal homeostasis due to genetic conditions, metabolic or vascular abnormalities, and aging may initiate inflammatory cascades. Secondary to these conditions, dysregulated immune response itself may be detrimental and contributes to the pathogenesis of the retinal disease.

Tumors/Cancer: Retinoblastoma is a cancer of the retina that is the most common intraocular cancer type in children. It occurs when nerve cells develop genetic mutations. Mutations in RB1 gene initiates the tumor growth [18, 19].

Choroidal nevus, choroidal melanoma, metastatic disease, intraocular lymphoma are the other tumor based pathologies affecting the retina. Most cancers affecting the retina usually occur in the choroid. Since the retina depends on the choroid in terms of nutrition and oxygen supply, cancer in the choroid likely to affect the retina and so vision.

Nutritional: There is plenty of evidence showing relationship between nutrition and retinal health. Low combined levels of vitamin C&E, zeaxanthin, and zinc were associated in with wet AMD [20]. Another study showed that increased intake of lutein and zeaxanthin could improve early functional abnormalities of the central retina [21]. The effects of Omega-3 fatty acids in the prevention of advanced AMD [22, 23] and protection of cellular function in diabetic retinopathy [24] are also shown. Theoretically, antioxidants supplementation should be beneficial in terms of limiting the effects of oxidative damage. Phototoxicity, plaquenil toxicity, phenothiazine toxicity, tobacco/alcohol amblyopia, and vitamin A deficiency are the other factors affecting the health of the retina. Evidence has also linked riboflavin (vitamin B) to the protection of retinal cells from death by oxidative stress and apoptosis [25]. The impact of riboflavin in retinal health is discussed in detail in a separate section in this chapter.

The retinal diseases can also be presented according to their anatomical location: macula and peripheral retina. Age related macular degeneration (AMD), Diabetic macular edema, myopic macular degeneration, macular pucker or macular

pole, macular edema due to CRVO, BRVO, BRAO, post-cataract surgery cystoid macular edema, central serous chorioretinopathy are the conditions affecting the macula. While, posterior vitreous detachment, retinal tear, retinal detachment form tear, retinal detachment from exudative process, lattice degeneration/axial myopia are the conditions affecting the peripheral retina.

1.2.2 Selected mouse models of inherited retinal diseases

This section introduces the late onset cone-rod dystrophy (*Prph2*^{R172W}), retinitis pigmentosa (*Rho*$^{P23H/+}$), and pattern dystrophy (*Prph2*$^{Y141C/+}$) mouse models which were employed for the studies presented in this dissertation. These are clinically relevant models which mimic disease phenotypes and progression in patients. The other reason why these models have been chosen is that both rhodopsin (Rho) and Peripherin-2 (Prph2, aka RDS/ retinal degeneration slow) are frequently mutated in patients. Over 40 pathogenic mutations in the Rho gene and more than 80 pathogenic mutations in Prph2 gene [26] have been identified. Both Rho and Prph2 are essential proteins for photoreceptor morphogenesis.

Prph2^{R172W} *(Cone-rod dystrophy mouse model)*

Prph2, a membrane protein, is a photoreceptor specific protein that is essential for the formation of both rod and cone OSs [27-29] and localizes to the rim region of photoreceptor discs. The C-terminus of Prph2 plays an important role in OS targeting and membrane fusion [30]. Retinas of Prhp2 knock out (*Prph2*$^{-/-}$) mice lack OSs [31]and mutations in Prph2 cause diverse pathologic conditions including central

areolar choroidal dystrophy, autosomal dominant retinitis pigmentosa, various form of macular degeneration, and pattern dystrophy simulating Stargardt / fundus flavimaculatus [26]. Prph2 is a tetraspanin protein with 4 transmembrane domains and it interacts with its homologue Rom1 [32, 33]. Prph2 and Rom1 have a large extracellular D2 loop that is essential for their oligomerization into tetramers [34]. Prph2 form homo- and hetero-tetramers with itself and Rom1 in the IS and traffic to the OS [35]. The tetramers further assemble into covalently linked complexes which is required for proper OS formation and growth.

R172W transgenic mice carry mutation in codon 172 of the *Prph2* gene. This point mutation results in the substitution of arginine to tryptophan at that position. R172W is the first Prph2 mutation that associated with cone-rod dystrophy [36]. Although, a marked clinical phenotype variation has been observed among the R172W affected individuals [37], they often display reduced central vision usually starting at the 2nd or 3rd decade of life. Some patients complain of night blindness as well. The affected individuals have abnormal electroretinography (ERG) measurements and speckled fundus appearance [38]. Although the majority of the patients have the disease limited to macula, several of the others show marked cone-rod dystrophy phenotype. In addition, non-penetrance has been observed and different levels of gene expression thought to be associated with this [36, 37]. Since pathogenesis of this Prph2 mutation in patients is still unresolved, it is an interesting target for investigation of disease progression and exploring possible therapeutic targets. For further investigation of the pathogenicity, R172W transgenic mouse line was

generated previously [36]. Consistent with the observations in human, the R172W mice were reported to develop cone loss followed by secondary rod loss [36].

$Rho^{P23H/+}$ (Retinitis Pigmentosa mouse model)

Retinitis pigmentosa, an inherited retinal dystrophy, occurs in 1 out of 4000 people worldwide [39], and effects 100,000 individuals in the United States alone [40]. Retinitis pigmentosa is characterized by a progressive photoreceptor loss with no effective clinical treatment is currently available. Thus, identifying elements that promote photoreceptor survival in retinitis pigmentosa is crucial for the management of this disease.

In the majority of retinitis pigmentosa cases, rod photoreceptors of the peripheral retina begin to degenerate and patients become night blind gradually. This may be accompanied by vascular alterations, pale optic disc and precipitation of bone spicules [41]. Rod loss is followed by gradual cone photoreceptor death. As peripheral vision worsens, patients are reduced to tunnel vision. This situation may end up with total blindness. The disease phenotype is heterogeneous; there is a wide spectrum of disease severity with different features. This makes it more challenging to discover treatment strategy. Although the disease mechanism of retinitis pigmentosa is still unclear, recent studies has associated retinitis pigmentosa with oxidative stress during rod and cone photoreceptor degeneration [42, 43].

To date, ~30% of the retinitis pigmentosa cases have been linked to mutations in the Rho gene. A proline to histidine change at codon 23 (P23H) in Rho is the most common (~15%) and is the cause of Rho-related retinitis pigmentosa in the US [44-

46] and it was the first retinitis pigmentosa mutation identified in human patients. Various transgenic animal models have been utilized for the investigation of the P23H mutation. Among such models, the heterozygous P23H knock-in ($Rho^{P23H/+}$) mouse best mimics the patients phenotype and disease progression [47].

Photoreceptor degeneration in the $Rho^{P23H/+}$ retina starts just after the eye opening. At early ages, the $Rho^{P23H/+}$ mouse model exhibits greater functional deficits in rods, while there is less cone dysfunction. Later, around P60, cone defects become apparent [47]. Histological analysis of $Rho^{P23H/+}$ revealed shorter rod OSs but most survived for several months. No abnormal aggregates were detected in their ISs. Lack of chromophore in the $Rho^{P23H/+}$ retina resulted in accelerated cell death suggesting an interaction between healthy opsin and P23H opsin which cause malformation of rod OSs. The retinal toxicity of P23H protein enhances with the absence of 11-cis retinal [47]. Opposing the P23H transgenic models, in the $Rho^{P23H/+}$ knock in model, mutated protein didn't found to be accumulated in the endoplasmic reticulum. Instead, it goes to OSs and disrupts the discs. Most of the P23H protein degrades, only a small fraction of P23H protein (1-10%), which are not properly glycosylated, traffic to the OSs. It remains elusive that how such small amount of mutation protein can be this much toxic to the OSs. Ultrastructural analysis of $Rho^{P23H/+}$ eye sections revealed perpendicularly aligned discs [47]. In the $Rho^{P23H/+}$ mouse model, P23H opsin found to be causing abnormally fast photo-responses. There are sagittally oriented primordial discs in the young rods of $Rho^{P23H/+}$ retina, in addition to transversely oriented ones [48]. At normal circumstances (healthy retina), the primordial discs shift to a

transverse orientation as retina develops. However, in $Rho^{P23H/+}$ retina, sagittally oriented discs keep their sagittal orientation and enlarge. While the transverse orientation in the $Rho^{P23H/P23H}$ is completely absent [48]. Altogether, suggesting that P23H opsin disturbs the process of disc reorientation.

$Prph2^{Y141C/+}$ (Pattern Dystrophy mouse model)

Pattern dystrophy is the group of retinal dystrophies with characteristic pigment changes. The gene linked to the mutations causing pattern dystrophy is Prph2. When Prph2 protein is mutated, the integrity of photoreceptor disc membrane is disrupted that leads to degeneration of the photoreceptor cells and ultimately resulted in accumulation of lipofuscin in the RPE that characterize the pattern dystrophy [49]. In this study, we elected to work with $Prph2^{Y141C/+}$ knock-in pattern dystrophy mouse model. The Y141C associated retinal disease is dominantly inherited. Heterozygous mice represent the patients' genetic cases. This $Prph2^{Y141C/+}$ mouse model exhibits decreased rod and cone function, retinal degeneration and wide spread yellow flecks in the fundus images [50].

The patients carrying Y141C mutation display inter- and intra-familial phenotypic variability [49, 51]. Although patients are mostly diagnosed with pattern dystrophy, some of them display retinitis pigmentosa symptoms [52]. Y141C patients often exhibit macular changes, RPE pigmentation, durusen like deposits and chorioretinal atrophy [26]. They can develop choroidal neovascularization at later stages [53]. Unfortunately, there is no current strategy to prevent progression of atrophy, which results in poor vision.

Y141C-Prph2 form abnormal high molecular weight Prph2/Rom1 complexes [50]. Surprisingly, these large protein complexes escape the endoplasmic reticulum (ER) and traffic to the OS. Y141C-Prph2 is able to initiate OS formation, however, the mutant protein accumulates in abnormal vesicular structures and cannot support the proper disc growth. The altered Y141C-Prph2 complexes in the OS is toxic to the surrounding tissues; the secondary effect on the RPE and the late onset fundus abnormalities have been associated with the toxic effect of the Y141C-Prph2. The phagosomes packed with abnormal Prph2 complexes have been proposed as an extra stress factor to the RPE. Although the oligomerization of Prph2 with Rom1 is a prerequisite for OS formation, absence of Rom-1 shifts the pattern dystrophy phenotype to retinitis pigmentosa [54].

We utilized these three well characterized mouse models (*Prph2*^{R172W}, *Prph2*^{R172W}, and *Rho*$^{P23H/+}$) to explore the role of Retbindin protein in the development and progression of retinal degeneration.

1.3 Retbindin: A novel retina specific protein

Retbindin (Rtbdn) is a novel protein that was identified during expressed sequence tag analysis of human retinal RNA [55]. Organ northern blot analysis showed a band for Rtbdn only in the retina [55]. Our lab confirmed the retina specific-expression of Rtbdn [56].

Rtbdn gene is only present in mammals [56] that is located on chromosome 19p13 in human and 8C3 in mouse [57]. The gene has 6 exons, the first of which is

noncoding. The Rtbdn sequence contains an open reading frame of 229 amino acids in human and translated into a 247 amino acid protein in mouse. We detect a ~30 kDa protein on our immunoblots of mouse retina lysates using polyclonal anti-rtbdn antibody. Adding reducing agent does not change Rtbdn' s size on the SDS-PAGE gel which suggests that it does not form intermolecular disulfide linkages between the cysteines. The amino acid sequence of the protein can be viewed from NCBI website using the following ID: Accession NP_659178.1. Although Rtbdn sequence contains conserved glycosylation sites [55], the protein is not sensitive to PNGAse treatment [56].

According to GenBank database, Rtbdn shares a significant homology with the riboflavin binding protein of chicken (RBP) (27% identity over 135 residues) and distant similarities with some folate receptors. Considering this, Rtbdn is believed to belong to a superfamily involved in binding cyclic or polyunsaturated molecules. RBP is responsible for the riboflavin storage in the egg that is required for the development of embryo [58, 59]. The tertiary structures of Rtbdn and RBP show noticeable similarities [56]. RBP contains 12 cysteines that are conserved in Rtbdn.

To study the localization of Rtbdn, retinal sections were co-labeled with Rtbdn and Rho, wheat germ agglutin (WGA), peanut agglutin (PNA), S-opsin, and ezrin. No co-localization was observed between Rtbdn and Rho, suggesting that Rtbdn is not a disc component. Rtbdn was not observed at close proximity to neither PNA nor S-opsin. In contrast, co-localization of Rtbdn and WGA was observed, which suggests that Rtbdn could be part of the extracellular matrix, the IPM, surrounding rods.

Moreover, co-localization of Rtbdn with ezrin at the RPE microvilli was observed. The IPM is a highly organized structure surrounding the photoreceptors and extends throughout the subretinal space. Immunochemical analysis of Rtbdn shows predominant localization at the tips of the rod OSs directly adjacent to the RPE microvilli in the IPM that is a dynamic interface where oxygen, nutrients and metabolites exchange. The second pool of Rtbdn is around the ISs and in the perinuclear area in the ONL (Fig. 1.4). In order to investigate the subcellular localization of Rtbdn in the IS pool, retinal sections of dark adapted mice eyes were double labeled with Rtbdn and arrestin and no co-localization was observed. This was again suggestive of an extracellular localization of Rtbdn. Altogether, suggest that Rtbdn exclusively expressed by rod photoreceptor cells and secreted into the IPM [56].

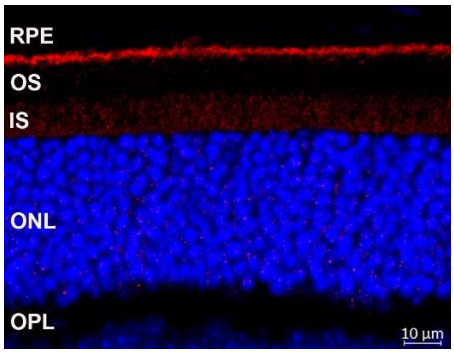

Figure 1.4. Expression pattern of Rtbdn. Shown is a representative confocal image of retinal cross-section taken from adult healthy mouse labeled for Rtbdn (red) with nuclei stained with DAPI (blue).

Biochemical analyses revealed that Rtbdn is associated with the membranous fractions. Peripheral membrane proteins were stripped using a buffer containing Na_2CO_3 and Rtbdn was found exclusively in the Na_2CO_3 soluble fraction, while Prph2

remained in the Na_2CO_3 insoluble fraction as a transmembrane protein. This data shows that Rtbdn is a peripheral membrane protein. Next, retinal insoluble IPM preparations were treated NaCl to detach electrostatistically linked peripheral membrane proteins and Rtbdn was found to be in the NaCl soluble fraction while Prph2 remained in the NaCl insoluble fraction, suggesting that Rtbdn is localized extracellularly. Altogether shows that Rtbdn is secreted into the IPM and anchors itself to the plasma membrane via electrostatic forces [56].

The similarities between Rtbdn and RBP guided the prediction that Rtbdn binds to riboflavin. This binding was confirmed by *in vitro* [56] and *ex vivo* [60] analyses. Moreover, the protective effect of Rtbdn on immortalized photoreceptor cells against riboflavin mediated light damage was also demonstrated *in vitro* [56]. Finally, flavins quantification in the retina and RPE from Rtbdn knock out ($Rtbdn^{-/-}$) mice showed significant reduction in levels [60]. These data indicated that Rtbdn is a key player in flavin homeostasis in the retina. Since Rtbdn does not contain any transmembrane domains or membrane anchoring moieties, it is not likely for it to be a transporter. Instead, it may be participating in the shuttling of riboflavin to specialized transporters.

Elimination of Rtbdn leads to age and dose-dependent retinal photoreceptor degeneration of both rods and cones. The significant functional and structural manifestations of Rtbdn absence was observed starting at post-natal day (P) 120 and P240, respectively [60]. Metabolome analysis of $Rtbdn^{-/-}$ retina suggest the

misregulation of the citric acid cycle and subsequent ATP production as the reason behind photoreceptor cell death [61].

1.4 Flavins and their importance for the health of the retina

Riboflavin [7,8-dimethyl-1O(l'-D-ribityl) isoalloxazine], also known as Vitamin B2, is a water soluble vitamin that is essential for cell maintenance and growth. It is the precursor of flavin adenine dinucleotide (FAD) and flavin mononucleotide (FMN) coenyzmes. These structural variants are formed by the modification of riboflavin (Fig. 1.5). Flavoproteins that contain a flavin group, catalyze oxidation/ reduction steps in almost every metabolic pathway using FAD and FMN [62, 63]. The available data regarding the flavin levels in tissues supports the notion that apo-flavoenzymes are responsible for binding and retention of riboflavin in the body.

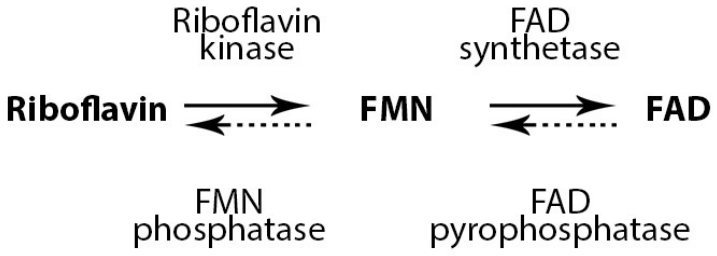

Figure 1.5. Formation and degradation of flavin coenzymes.

Riboflavin plays an important role in a broad spectrum of biological activities including, DNA repair, energy metabolism, amino acid synthesis [64], protein folding

[65] and, normal immune function [66]. Riboflavin also acts as an antioxidant and its deficiency cause oxidative damage and cell stress response [67]. Growth retardation, hair loss, anemia, nerve deficits, hearing loss and vision abnormalities are some of the problems observed in humans deficient in riboflavin [68]. Lesions of the cornea, cataract formation, degeneration of retinal ganglion cells have been reported as ocular changes in human receiving insufficient riboflavin [69].

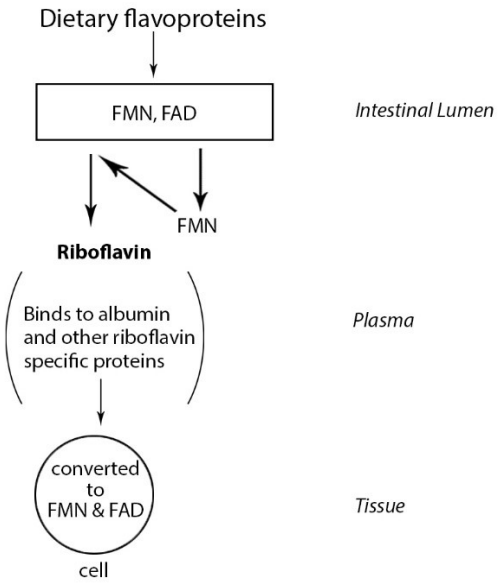

Figure 1.6. Conversion of dietary flavoproteins to riboflavin and its release to the systemic circulation.

Riboflavin is primarily found in its co-enzymatic forms in the biological fluids and tissues. The utilization of riboflavin in the tissues starts with the conversion of riboflavin to FMN by riboflavinkinase (RFK) enzyme and further adenylation of FMN to FAD by Flavin synthetase (FLAD1) (Fig. 1.5). FMN and FAD are widely distributed in tissues and mostly present in the cytosol [70].

Mammals cannot produce riboflavin by biosynthesis so, and it needs to be acquired from diet [71]. In addition to the free riboflavin, FAD, FMN and flavoproteins are also obtained from diet. The riboflavin derivatives and flavoproteins are hydrolyzed to riboflavin in small intestine and delivered to various tissues in circulating blood for absorption [72] (Fig. 1.6 [71]). Riboflavin mainly binds to albumin, B-globulin, a-globulin, I-globulin and fibrinogen in human plasma. It is mostly bound to albumin; the immunoglobulins and other plasma proteins function when there is not enough albumin. Excess riboflavin is excreted in urine.

Although the exact mechanism of riboflavin absorption is not well defined yet, results from various studies suggests the involvement of carrier mediated components and presence of active riboflavin uptake mechanism. The retina acquires riboflavin through the choroidal and retinal blood supplies. Various riboflavin transporters were identified in different tissues in the human body however, little is known about the mechanism behind the riboflavin transport from circulating blood to retina and its absorption in the retina. Kubo and colleagues suggest the involvement of RFVT2 and RFVT3 riboflavin transporter at the outer and inner blood retinal barriers [73, 74]. However, no retinal riboflavin transporter has been identified in the retina yet.

The retina has one of the highest oxidative metabolism rates per tissue weight in the body due to light exposure and phototransduction. Glutathione is a typical scavenger of free radicals [75]. Retinal ganglion cells highly express glutathione reductase which is involved in the enzymatic conversion of glutathione. Furthermore, glutathione reductase requires FAD as coenzyme to function. Riboflavin has ability to

reduce the level of pro-inflammatory mediators as well. This information suggests that riboflavin is important to protect retina from oxidative stress [76]. The flavin levels were found to be highly concentrated in the retina compared to other tissues [77-79]. In particular, it was almost 20 fold higher compared to the levels in the blood, which means that the retina accumulates riboflavin against a concentration gradient, which suggests a special flavin concentrating mechanism. Ca^{++}-calmodulin modulated uptake of riboflavin in the RPE and retinoblastoma cells were showed by *in vitro* analyses [80-82], which suggests an interconnected flavin acquisition mechanism between RPE and retina. However, no flavin concentration mechanism or flavin binding protein in the retina was proposed before. Though flavins are essential for various biological activities, unbound flavins has been reported to have adverse effects. Their exposure to light results in production of reactive oxygen species and subsequent lipid peroxidation [79, 83]. Giving the importance of flavins and their susceptibility to light suggest that they should be tightly regulated in the retina.

Chapter 2- Elimination of a retinal riboflavin binding protein exacerbates degeneration in a model of cone-rod dystrophy

Ayse M. Genc, Mustafa S. Makia, Tirthankar Sinha, Shannon M. Conley[#], Muayyad R. Al-Ubaidi[*] and Muna I. Naash[*]

Department of Biomedical Engineering, University of Houston, Houston, Texas, 77204, United States of America.

[#]Department of Cell Biology, University of Oklahoma Health Sciences Center, Oklahoma City, OK, 73104, United States of America

This study is accepted for publication in IOVS in April, 2020. Formatting changes and minor adjustment has been made from the submitted version to conform the overall dissertation.

2.1 Introduction

Retbindin (Rtbdn) is a novel retina-specific protein located in the interphotoreceptor matrix (IPM) at the tips of photoreceptor outer segments (OS) [55, 56]. In the IPM metabolites and nutrients are exchanged between photoreceptors and the retinal pigment epithelium (RPE) [84]. Rtbdn is secreted into the IPM and peripherally anchored to the plasma membrane via electrostatic forces, and we showed that mice lacking Rtbdn (*Rtbdn*$^{-/-}$) exhibit retinal degeneration as well as defects in rod and cone function [56, 60]. Our previous studies using both degenerative models that lack rods but retain some cones and models in which GFP is knocked into cells that express Rtbdn, have shown that Rtbdn expression is limited to rods [56, 60]. Rtbdn

shares significant homology with the riboflavin binding domain of chicken oviduct riboflavin binding protein (RBP) [55, 56]. Subsequently, we determined that Rtbdn binds riboflavin *in vitro*[56] and that flavin levels were reduced in *Rtbdn*$^{-/-}$ mice [60].

Riboflavin is not synthesized by the body, and is the precursor of flavin mononucleotide (FMN) and flavin adenine dinucleotide (FAD), essential enzymatic cofactors [85-87]. FMN and FAD are involved in many processes, including antioxidant systems (where they are cofactors for glutathione reductase) and energy generation. Cellular energy production involves the utilization of FAD/FMN in the electron transport chain [88] and during beta-oxidation of fatty acids [89]. Retinal flavin levels are several-fold higher than blood levels [79], reflecting the extraordinarily high demand for energy in photoreceptors and retinal susceptibility to oxidative stress. Combined these observations have led us to hypothesize that Rtbdn may play a role in the ability of the retina to concentrate flavins.

Flavin levels are decreased in models of rapid retinal degeneration such as the *rd1* and *rd10* [90]. However, it is not clear what role Rtbdn or flavin metabolism may play during retinal degeneration. To begin evaluating this, here we examine the role of Rtbdn in a model of cone-rod dystrophy, the R172W peripherin-2 transgenic mouse model (*Prph2*^{R172W}) [36]. Peripherin-2 is essential for the formation of rod and cone OSs [31, 91]. The R172W mouse model has been well characterized, and mimics many of the cone-rod dystrophy phenotypes seen in patients carrying the R172W mutation [36, 37, 92, 93], including functional defects in cones and late onset retinal degeneration.

Here, we report that Rtbdn levels are significantly upregulated in *Prph2*^{R172W} retinas before and during degeneration. Furthermore, eliminating Rtbdn in the R172W model (*Prph2*^{R172W}*/ Rtbdn*$^{-/-}$) exacerbated structural and functional degeneration associated with the R172W mutation. Interestingly, retinal flavin levels were elevated in the *Prph2*^{R172W}*/Rtbdn*$^{-/-}$ retinas. Our results clearly demonstrate that Rtbdn has a role during degeneration and suggest that the contribution of retinal flavins during degeneration is complicated.

2.2 Materials and Methods

Animals

Rtbdn knockout (*Rtbdn*$^{-/-}$) and R172W-Prph2 transgenic mice were generated and characterized as reported previously [56, 60, 94]. The *Prph2*^{R172W} mice on wild-type (WT) peripherin 2 background were cross-bred into the *Rtbdn*$^{-/-}$ background to generate the *Prph2*^{R172W}*/Rtbdn*$^{-/-}$ mice. WT, *Rtbdn*$^{-/-}$ and *Prph2*^{R172W} mice were included for comparisons. Animals are backcrossed onto our in-house WT line, a strain that was created by breeding FVB mice to C57BL/6, eliminating the rd1 and rd8 mutations and then inbreeding for over 10 generations. PCR genotyping confirmed that none of the mice used in this study carry the rd8 mutation. Animals were housed under 30-50 lux cyclic light 12 h light: 12 h dark. Both genders were equally included into the analyses. All procedures were approved by University of Houston Institutional Animal Care and Use Committee (IACUC). For sample collection, animals were euthanized using CO_2 asphyxiation and retinas were collected as

described before [95] and immediately frozen in liquid nitrogen and stored at -80°C until used.

Protein Chemistry

Immunoblot analyses were performed as detailed previously [56]. N=5-6 independent retinal extracts per age/genotype. Rtbdn levels were measured densitometrically using Bio-Rad Image lab v4.1 software and normalized to actin. Soluble IPM, cytoplasmic and membrane fractions were prepared by placing intact freshly extracted post-natal day (P)30 retinas in 1X PBS (pH 7.2) containing 1X protease inhibitors on ice for 15 min without agitation. The supernatant (soluble IPM fraction) was collected after centrifugation at 113 x g for 5 min using Eppendorf centrifuge 5427R. The pellets were incubated in hypotonic buffer (0.1X PBS, pH 7.2 containing 1X protease inhibitors) on ice for 15 min then extracted with a hand held motor and pestle tip homogenizer and centrifuged at 50,000 x g for 30 min. The supernatant (cytoplasmic fraction) was removed and the pellet (membrane fraction) was re-suspended/solubilized in 1X PBS (pH 7.2) containing 1% Triton X-100 and 1X protease inhibitors then homogenized with sonication. After 1 h incubation at 4°C, samples were centrifuged at 16,128 x g for 5 min. The supernatant was considered to contain the membrane bound proteins. Antibodies used are described in Table 1.

Immunofluorescence

Whole eyes were harvested and fixed in the Davidson's fixative (32% ethanol, 11% acetic acid, 2% formaldehyde) overnight as indicated before [56], washed in 1×

PBS, and then soaked sequentially in 70%, 80%, 90%, and 100% ethanol for 30 min each and transferred to xylene for clearing. After incubating in 2x xylene for 30 min each, samples were embedded in paraffin. Eyes were sectioned at 10 µm thickness using a microtome (Thermo Fisher Scientific, #62248, Waltham, MA). After rehydration and antigen retrieval (20 min boiling in 10 mM citrate buffer, pH 6.0), sections were blocked and probed for Rtbdn as previously described [56]. Primary antibody incubation for Rtbdn labeling was 30 min at room temperature [56], and for GFAP labeling was overnight at 4°C (antibody details are described in Table 1). After washing, slides were incubated with secondary antibodies (see Table 1) for 2 hours at room temperature. DAPI (Thermo Fisher Scientific, #62248, Waltham, MA) was used at a concentration of 0.1µg/mL for 15 min at room temperature. Slides were mounted with Prolong Gold antifade mountant (#P36934, Thermo Fisher Scientific) and images were captured using Zeiss 800 LSM confocal system with an Airyscan detector and processed in Zen 2 lite software (Thornwood, NY). Images in figure 2.1B (upper panel) and figure 2.5 were collected under epifluorescent conditions at 40x. Images in figure 2.1B (lower panel) were captured at 63x and shown are airyscan processed collapsed planes from a confocal stack. Images in figure 2.3B were collected at 20x and are collapsed views of confocal images with 6 planes (1 µm each). For cone counts, sections were labeled with peanut agglutinin (PNA) and imaged 200 µm inferior and superior to the optic nerve. For each animal, the number of cones in the superior and inferior images was averaged to obtain a single value for that animal. N=3 animals/genotype and age.

Electroretinography

Full-field ERG was performed at P30, P60 and P90 under scotopic and photopic conditions as described previously [54, 96] using UTAS system (LKC, Gauthersburg, MD, USA). N=10-19 animals for each genotype/age. + indicates comparisons between WT and *Prph2*^{R172W}/*Rtbdn*$^{-/-}$ as well as between *Rtbdn*$^{-/-}$ and *Rtbdn*$^{-/-}$/*Prph2R*^{172W}. & indicates comparisons between WT and *Rtbdn*$^{-/-}$, * indicates comparisons between WT and *Prph2*^{R172W}, and ¥ indicates comparison between *Prph2R*^{172W} and *Prph2*^{R172W}/*Rtbdn*$^{-/-}$.

Light histology and morphometry

Eyes were collected, fixed, embedded and sectioned as described above. Slides with the sections along the optic nerve were chosen and rehydrated, soaked in the Hematoxylin (MHS16, Sigma, Burlington, MA) for 4 min and rinsed under tap water for 1 min. After 3-4 dips in 0.3% acid alcohol, sections were rinsed under running tap water for another min and soaked in Eosin (HT110116, Sigma) for 2 min. Slides were rinsed with tap water once again, exposed to a dehydration and clearing process, and then mounted using Permount mounting medium (SP15100, Fisher Scientific). Images were captured every 200 μm through the superior and inferior sides of the sections starting from the optic nerve using Zeiss Axioskop 50. Outer nuclear layer cells were counted within the areas enclosing 100 μm length every 200 μm intervals. N=3 independent retinal sections for each genotype/age.

Light and transmission electron microscopy

Following euthanasia, the superior hemisphere of the eyes were marked then harvested, punctured at the ora serrata and fixed in mixed aldehyde fixative (2% paraformaldehyde, 2% glutaraldehyde, 100 mM cacodylate, 0.025% $CaCl_2$ (pH 7.4)) for 2 h. Cornea and lens were removed and eye cups were returned back to the fixative and incubated at 4ºC overnight. The globes were embedded in plastic resin, sectioned and stained with Osmium tetroxide as explained elsewhere [54, 97]. Ultrastructural imaging was performed as previously described [54].

Fundus and fluorescein angiography

Fundus and fluorescein angiogram imaging was performed as described previously [98] using Phoenix Micron IV system (Phoenix Research Laboratories, Pleasanton, CA). After capturing bright field images, mice were intraperitoneally injected with clinical grade (Akorn Ak-fluor 10%) fluorescein at a dose of 0.01ml per 10 gm weight of the animal. Almost 30 seconds past injection, they were examined for fluorescein angiogram using the 451.5 – 486.5 nm excitation and 488 nm emission GFP filter. All of the animals were exposed to the same amount of light at same voltage and gain. Images were obtained using Discover-1.2 software.

Flavin quantification by HPLC

Animals were fasted for 6 h prior of euthanasia to prevent any feeding variability among animals. Retinas were collected and snap frozen in liquid nitrogen

and kept at -80 ºC until used. Micro-extraction and quantification of flavins (riboflavin, FAD, and FMN) was carried out as previously described [90] using Waters HPLC system (Waters, Milford, MA, USA).

Quantification of cellular ATP levels

The total levels of cellular ATP in freshly collected retinal samples were measured using Abcam (ab113849) luminescent ATP detection Assay kit as previously described [60]. In brief, retinas were placed in 110 µl 1X PBS (pH 7.4) and 1% PIN and homogenized using sonication and centrifuged at 16,128 x g for 5 min. 100 µl of the supernatant for each sample was transferred to a single well of 96 well plate and then 50 µl of detergent in the kit was added to each well and incubated at room temperature for 10 min on an orbital shaker at 450 rpm to lyse the cells and activate ATPases. Then, 50 µl of substrate solution was added to each well and incubated for 15 min at room temperature on the same orbital shaker. All of these procedures were performed under dim red light. The plate was immediately placed in the microplate reader (Spectramax M5, Molecular devices, Sunnyvale, CA). The ATP levels of each sample in random luminescence units was converted to micro molar using standard curve.

Statistical Analysis

Statistical analyses, were done using one- or two-way ANOVA with Tukey's post-hoc comparison. One symbol $P<0.05$, two symbols $P<0.01$, three symbols

P<0.001 and four symbols P<0.0001. Data for all experiments were expressed as ± SEM. Graphpad Prism v.8 was used for all analysis.

2.3 Results

2.3.1 Rtbdn levels are upregulated in Prph2^{R172W} retinas

To begin evaluating whether Rtbdn is important during photoreceptor degeneration, we assessed its levels in retinal extracts harvested from the *Prph2*^{R172W} mice. This mouse line carries endogenous wild-type Prph2 and a R172W mutant Prph2 allele, resulting in expression of R172W protein at levels equivalent to ~40% of endogenous Prph2 levels [36]. Previously we showed that overexpression of WT Prph2 is not toxic to the retina, but R172W animals exhibit gradual structural and functional retinal degeneration [36, 92]. Immunoblot analysis showed that Rtbdn levels were 2.5 fold higher in *Prph2*^{R172W} than non-transgenic wild-type (WT) at P30 (Fig 2.1A), and critically that levels continued to rise in *Prph2*^{R172W} from P30 to P90, 3.7 fold higher than WT at P90.

Our previous biochemical studies showed that Rtbdn is an extracellular protein, which co-localizes with the IPM marker wheat germ agglutinin (but not the disc component rhodopsin) [56]. Rtbdn is normally found in two areas; the IPM between the apical edge of the OSs and the RPE, and surrounding the inner segments [56]. Immunofluorescence labeling at P30 demonstrated that *Prph2*^{R172W} retinas

exhibit labeling in these areas, but rather than a layer of labeling restricted to the apical OS/RPE junction, *Prph2*^{R172W} retinas exhibit Rtbdn (red) labeling throughout the OS layer (Fig. 2.1B).

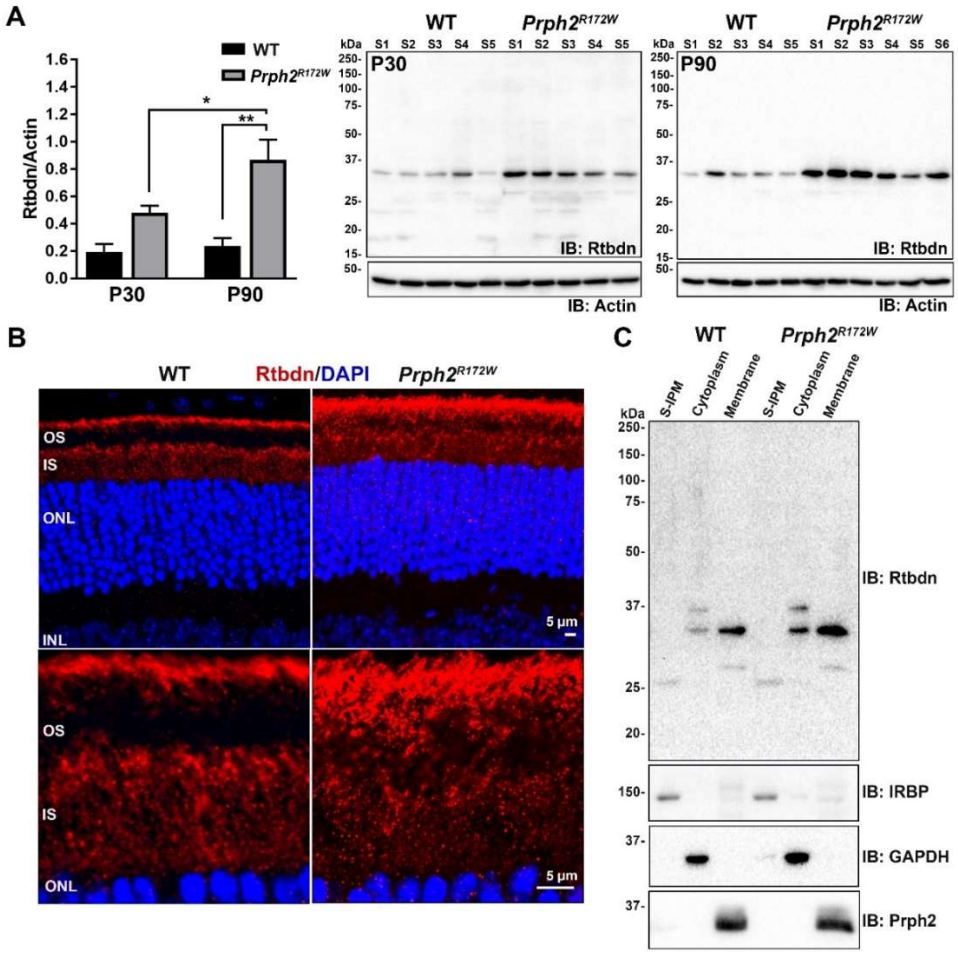

Figure 2.1. Rtbdn is upregulated in the *Prph2*^{R172W} retinas. A. Immunoblot analysis of Rtbdn. **B.** Confocal images of P30 retinal cross-sections. **C.** Western blot analysis of retinal extracts separated into subcellular fractions.

We previously found that Rtbdn is an extracellular membrane associated component of the insoluble IPM. To determine whether this subcellular localization is preserved in the *Prph2*^{R172W}, we fractionated retinas into the soluble IPM, retinal

membranes, and retinal cytoplasm. The majority of Rtbdn in both the WT and *Prph2*^{R172W} is found in the membrane fraction (Prph2 shown as a positive control), with no significant Rtbdn in the soluble IPM (IRBP as a positive control) (Fig. 2.1C). A small portion of total Rtbdn is found in the cytoplasmic fraction and interestingly, two Rtbdn bands are detected. These likely reflect newly synthesized immature (upper band) and mature Rtbdn (lower band), and suggests that Rtbdn undergoes post-translational modification/processing.

2.3.2 Rtbdn ablation exerts negative functional and structural effects on Prph2^{R172W} retina

The observed upregulation of Rtbdn in *Prph2*^{R172W} retinas supported the idea that Rtbdn plays a role during retinal degeneration. To help understand whether this upregulation was a protective response (i.e., to help protect the retina in the face of a degenerative insult) or a contributor to degeneration, we backcrossed the *Prph2*^{R172W} mice onto the *Rtbdn*$^{-/-}$ background. We conducted full-field scotopic and photopic electroretinography (ERG) to measure rod and cone function, respectively (Fig. 2.2A). Consistent with previous findings, elimination of Rtbdn (*Rtbdn*$^{-/-}$) had no deleterious effects on retinal function up to P90 [60]. In contrast, eliminating Rtbdn in the *Prph2*^{R172W} retina led to statistically significant reductions in both cone and rod responses at all three ages in comparison to WT and single mutants (Fig. 2.2B). Eliminating Rtbdn in *Prph2*^{R172W} mutants had a larger effect on rod function than cone function; for example, at P30, rod function (scotopic a-wave) in the *Prph2*^{R172W}/ *Rtbdn*$^{-/-}$ was reduced 52% compared to the *Prph2*^{R172W}, while cone function (photopic

b-wave) was reduced by 21%. However, this difference may be due to the fact that the R172W mutation affects cones more than rods, and when compared to WT, the *Prph2*^{R172W}*/Rtbdn*$^{-/-}$ had similar reductions in both rod and cone function (to 38% and 40% of WT, respectively at P90). Scotopic b- wave is a measure of second-order neuron signaling, and here we find that scotopic a- and b- waves were reduced fairly proportionally.

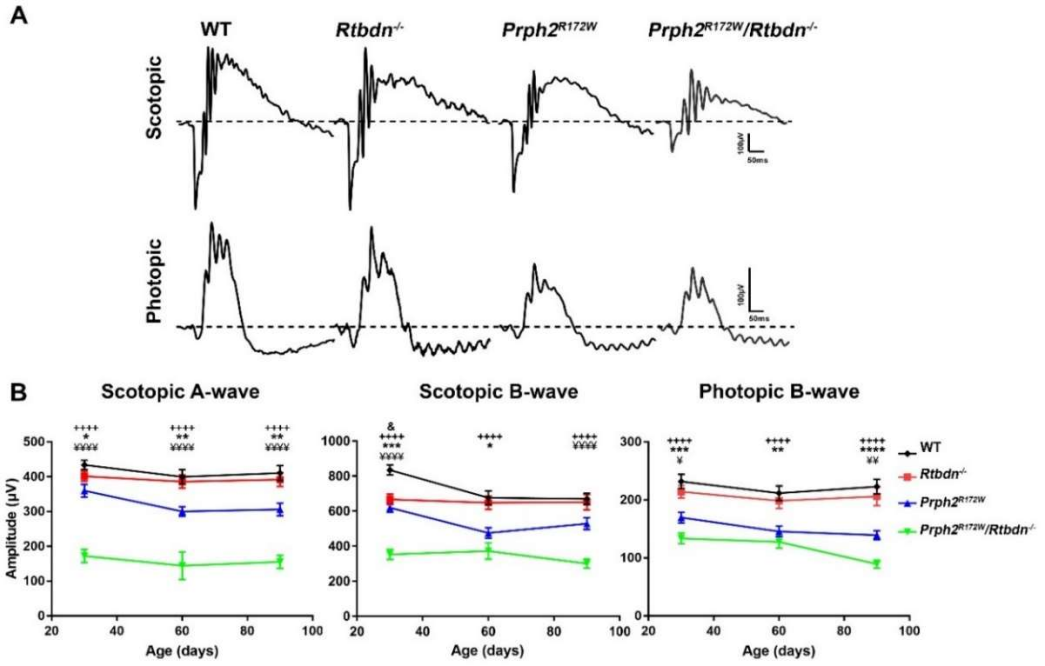

Figure 2.2. Lack of Rtbdn in the *Prph2*^{R172W} mutant causes defect in rod and cone functions. A. Representative waveforms of ERG responses of P30 mice. **B.** Average amplitudes of maximum scotopic a-b- waves and photopic b-waves.

Histologic analyses showed no obvious signs of retinal degeneration at P30 in the *Prph2*^{R172W} or the *Rtbdn*$^{-/-}$, however there is evident thinning of the outer nuclear layer (ONL) as well as the OS and inner segment (IS) layers in the *Prph2*^{R172W}*/Rtbdn*$^{-/-}$ retina (Fig. 2.3A). To quantify this degeneration, we counted ONL nuclei (95-97%

rods) across the retina (Fig. 2.3C). ONL counts in WT, *Rtbdn*$^{-/-}$, and *Prph2*^{R172W} were not significantly different from each other at P30, but there was a ~25% reduction in ONL nuclei in the *Prph2*^{R172W}/ *Rtbdn*$^{-/-}$ central retina compared to WT (Fig. 2.3C, left). At P90, this was even more pronounced, with ~65% reduction in ONL cells in the *Prph2*^{R172W}/*Rtbdn*$^{-/-}$ central retina compared to WT. In striking contrast the *Rtbdn*$^{-/-}$ still shows no degeneration at P90 and the *Prph2*^{R172W} only shows a very small reduction in the ONL at P90 (Fig. 2.3C, right

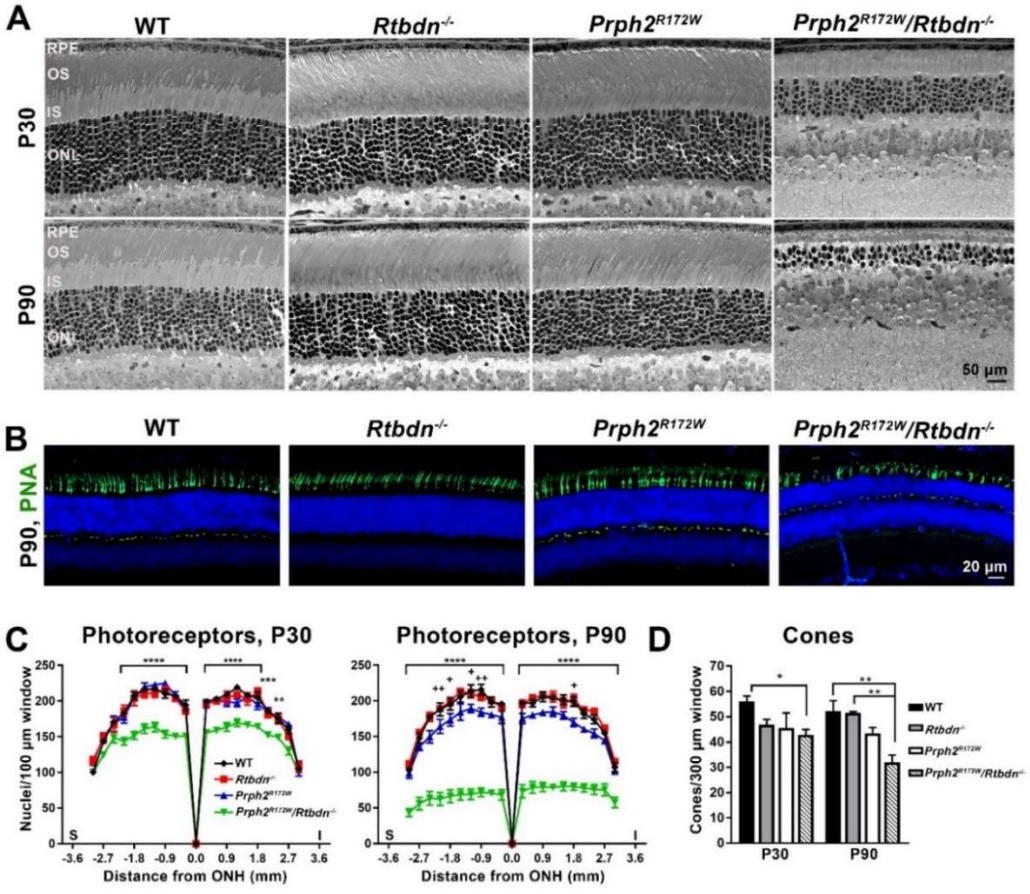

Figure 2.3. Photoreceptor degeneration is accelerated in the *Prph2*^{R172W}/*Rtbdn*$^{-/-}$.
A. Light micrographs of retinal sections. **B.** Cones were labeled using PNA. **C.** Photoreceptor nuclie counts. **D.** Cone counts from PNA labeled sections.

Although Rtbdn is expressed only in rods, long-term Rtbdn deficiency led to rod and cone defects [56]. Here we saw exacerbated cone functional deficits in the *Prph2*^{R172W}*/Rtbdn*$^{-/-}$ retina so, we counted cone photoreceptors in the central retina labeled with peanut agglutinin (Fig. 2.3B, D). Similar to rods, we observed significant loss of cone cells in the *Prph2*^{R172W}*/Rtbdn*$^{-/-}$ retinas at both P30 and P90 (Fig. 2.3D).

Ultrastructural examination showed that, unlike the WT and the single mutants that exhibited nicely aligned stacks of discs, most OSs in the *Prph2*^{R172W}*/Rtbdn*$^{-/-}$ were highly disorganized (asterisks, Fig. 2.4A) and ISs were swollen (white arrowheads, Fig. 2.4A) at P30 and P90. This disorganization is clearer at higher magnification (Fig. 2.4B); some OS discs in the *Prph2*^{R172W}*/ Rtbdn*$^{-/-}$ retina are misaligned (blacked asterisks, Fig. 2.4B), shorter (black arrow heads, Fig. 2.4B) or totally disrupted (black arrows, Fig. 2.4B). OS disorganization is exacerbated at P90 where swirls are present in *Prph2*^{R172W}*/ Rtbdn*$^{-/-}$ retinas (white arrowheads, Fig. 2.4B) next to fairly organized OSs (white arrows, Fig. 2.4B). In addition, RPE cells showed marked vacuolization in the *Prph2*^{R172W}*/ Rtbdn*$^{-/-}$ (black arrows, Fig. 2.4B). These vacuoles often contain membranous debris (Fig. 2.4A, inset), possibly undigested OS. However, in contrast to photoreceptor defects which are much more severe in the *Prph2*^{R172W}*/Rtbdn*$^{-/-}$ than in WT or single mutants, RPE defects are seen in both double mutants and *Prph2*^{R172W}, suggesting RPE changes may be primarily due to the R172W mutation.

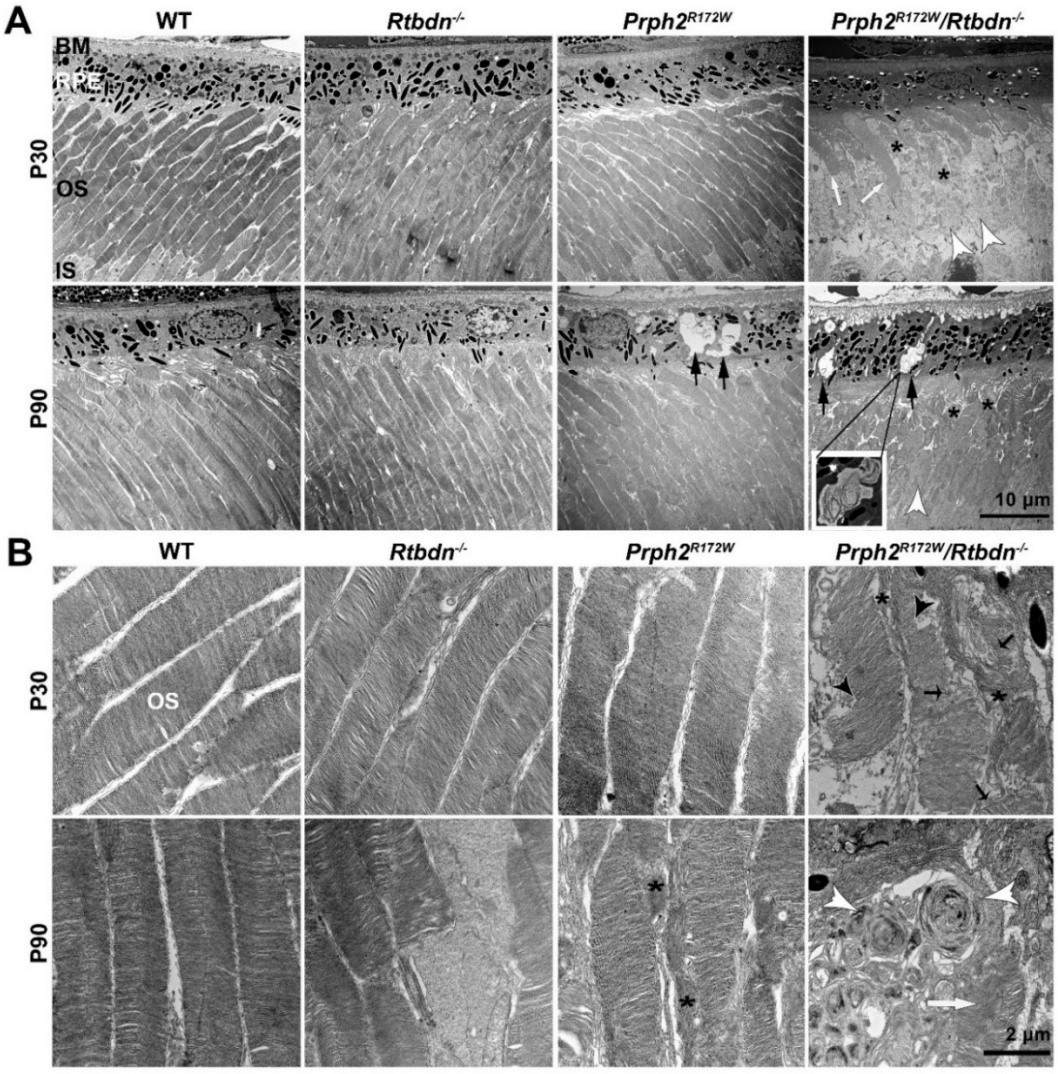

Figure 2.4. Rtbdn ablation in the *Prph2^{R172W}* retina causes ultrastructural changes. A. Representative EM images of OS and RPE for the indicated genotypes. **B.** Representative EM images of OSs.

2.3.3 Ablation of Rtbdn in the Prph2^{R172W} retina leads to retinal gliosis

One sign of retinal stress and gliosis [99-101] is upregulation of glial fibrillary acidic protein (GFAP) in Müller cells. Reactive gliosis can be neuroprotective, but chronic gliosis can contribute to vascular and other retinal pathologies [102]. At P30,

GFAP was restricted to the nerve fiber layer as expected. However, by P90 GFAP labeling was increased in the *Prph2*^{R172W}*/Rtbdn*$^{-/-}$ retina, with Müller cell labeling extending into the inner plexiform and inner nuclear layer, consistent with gliosis (Fig. 2.5, arrows).

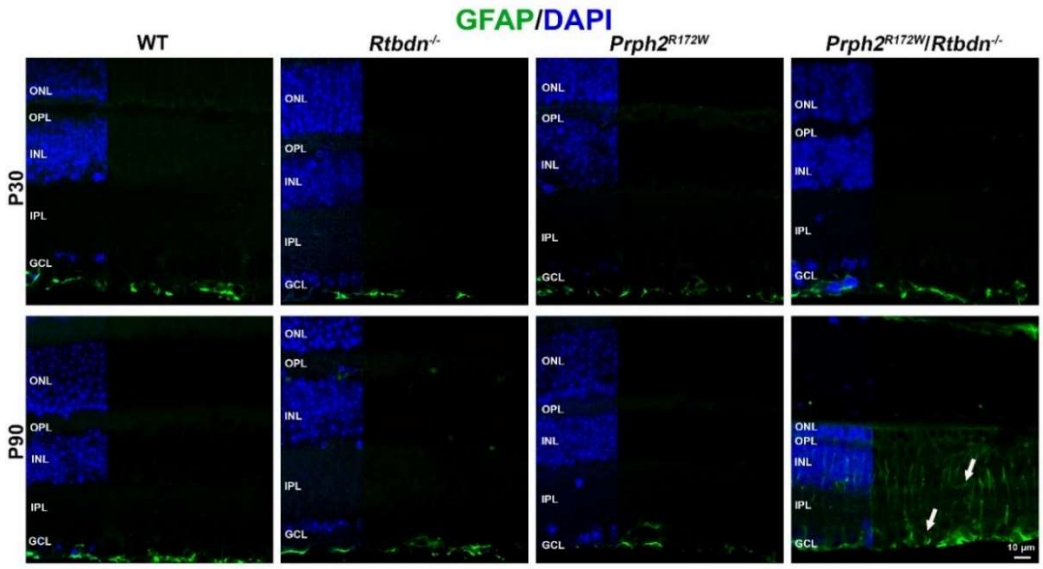

Figure 2.5. *Prph2*^{R172W}*/ Rtbdn*$^{-/-}$ retina shows altered pattern of GFAP labeling. Representative images of retinal sections probed for GFAP (green) and DAPI (blue). Arrows highlight increased gliosis at P90.

2.3.4 Prph2^{R172W}*/Rtbdn*$^{-/-}$ *mice exhibit fundus and retinal vascular abnormalities*

Humans and mice carrying the R172W mutation exhibit alterations in retinal vasculature with varying degrees of penetrance [37, 92]. To assess whether eliminating Rtbdn had any effect on retinal vasculature we performed fundus imaging and fluorescein angiography at multiple time points.

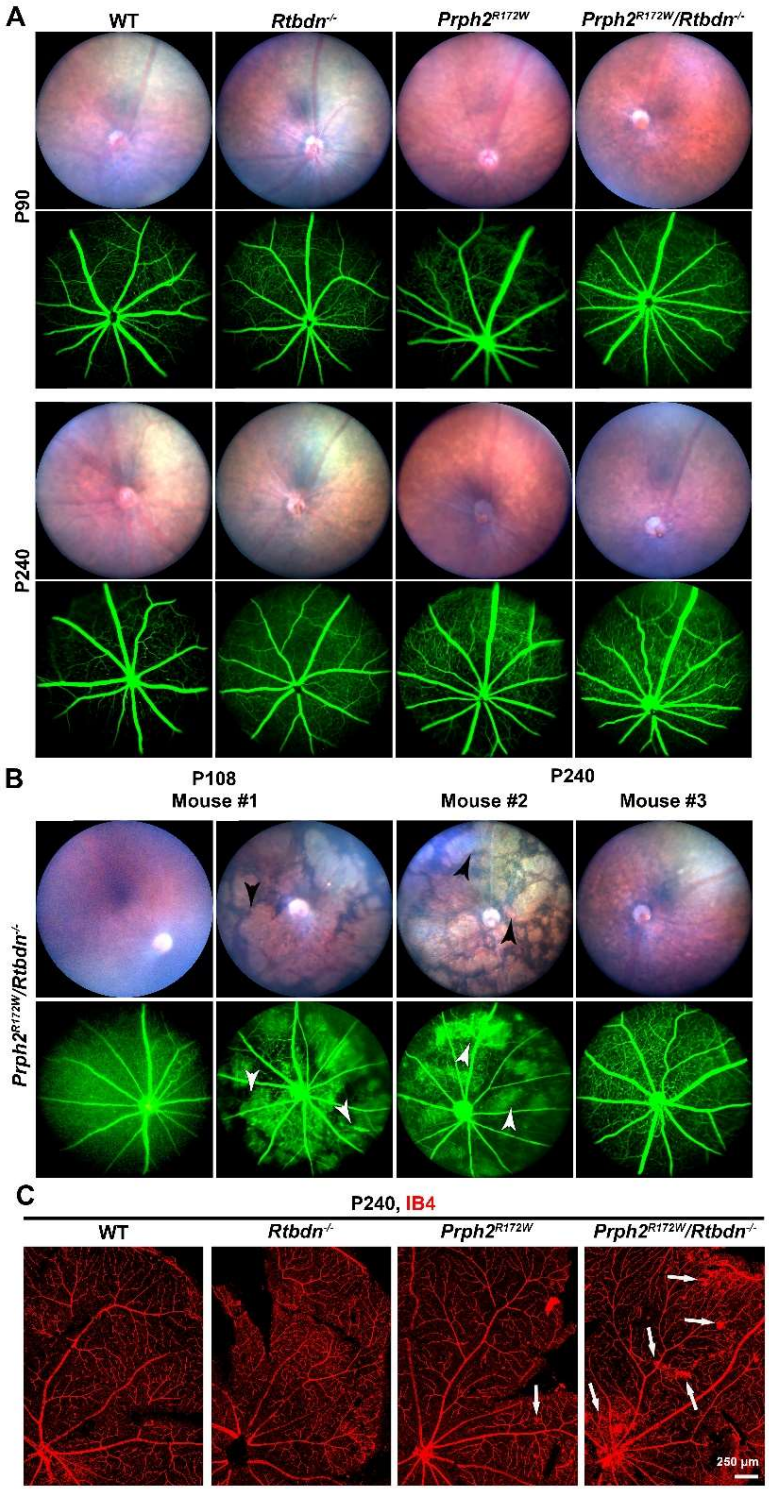

Figure 2.6. *Prph2*^{R172W}*/Rtbdn*$^{-/-}$ mice exhibit fundus and vascular abnormalities. **A.** Fundus images and fluorescein angiograms. **B.** Fundus and fluorescein angiograms from three additional mice. **C.** Isolectin-B4 stained retinas.

There were no overt changes in fundus appearance of fluorescein angiogram at P90 (Fig. 2.6A), but by P240, *Prph2*^{R172W}/*Rtbdn*$^{-/-}$ eyes start to exhibit changes (Fig 2.6A-B). On fundus images, large degenerative patches become evident (black arrowheads Fig. 2.6B), and correlate with areas where diffuse GFP signal from the choroid can be seen (white arrowheads, Fig. 2.6B). This phenotype is variable among age-matched mice (Fig. 2.6B). In P240 *Prph2*^{R172W}/*Rtbdn*$^{-/-}$ animals, 12/13 animals showed neovascular tufts, and 3/13 exhibited splotchy degenerated areas (on fundus images). These phenotypes also occurred in the *Prph2*^{R172W}, 5/9 animals exhibited neovascular tufts and 5/9splotchy degenerative areas. In contrast, none (out of 7) *Rtbdn*$^{-/-}$ mice exhibited these phenotypes at P240 and only 1/7 wild-type mice had a very small number of neovascular tufts. To help better visualize these neovascular tufts, we labeled blood vessels on retinal flat mounts using isolectin B4 (red, Fig. 2.6C). Capillary tufts (white arrows) were observed in the central and peripheral areas of *Prph2*^{R172W} retinas, a phenotype that was worsened in *Prph2*^{R172W}/*Rtbdn*$^{-/-}$ retinas.

2.3.5 Changes in flavin processing in the Prph2^{R172W}*/Rtbdn*$^{-/-}$

Riboflavin and its cofactors FMN and FAD are essential for retinal health [103-105], and flavin levels are significantly reduced in the *Rtbdn*$^{-/-}$ retina [60]. We observe that at P30, riboflavin, FAD, and FMN levels are decreased in the *Rtbdn*$^{-/-}$ and *Prph2*^{R172W} (compared to WT, Fig. 2.7A-C, left). P30 FMN levels are also reduced in the *Prph2*^{R172W}/*Rtbdn*$^{-/-}$, however, riboflavin levels are elevated at P30 (compared to the *Rtbdn*$^{-/-}$). This finding is more pronounced at P90 where both FMN and riboflavin

levels are increased in the *Prph2*^{R172W}*/Rtbdn*$^{-/-}$ compared to *Rtbdn*$^{-/-}$ (Fig. 2.7A-B). Interestingly, while riboflavin and FMN levels are elevated in the *Prph2*^{R172W}*/Rtbdn*$^{-/-}$, FAD levels in the *Prph2*^{R172W}*/Rtbdn*$^{-/-}$ retina remain reduced over time, similar to the *Rtbdn*$^{-/-}$ (Fig. 2.7C).

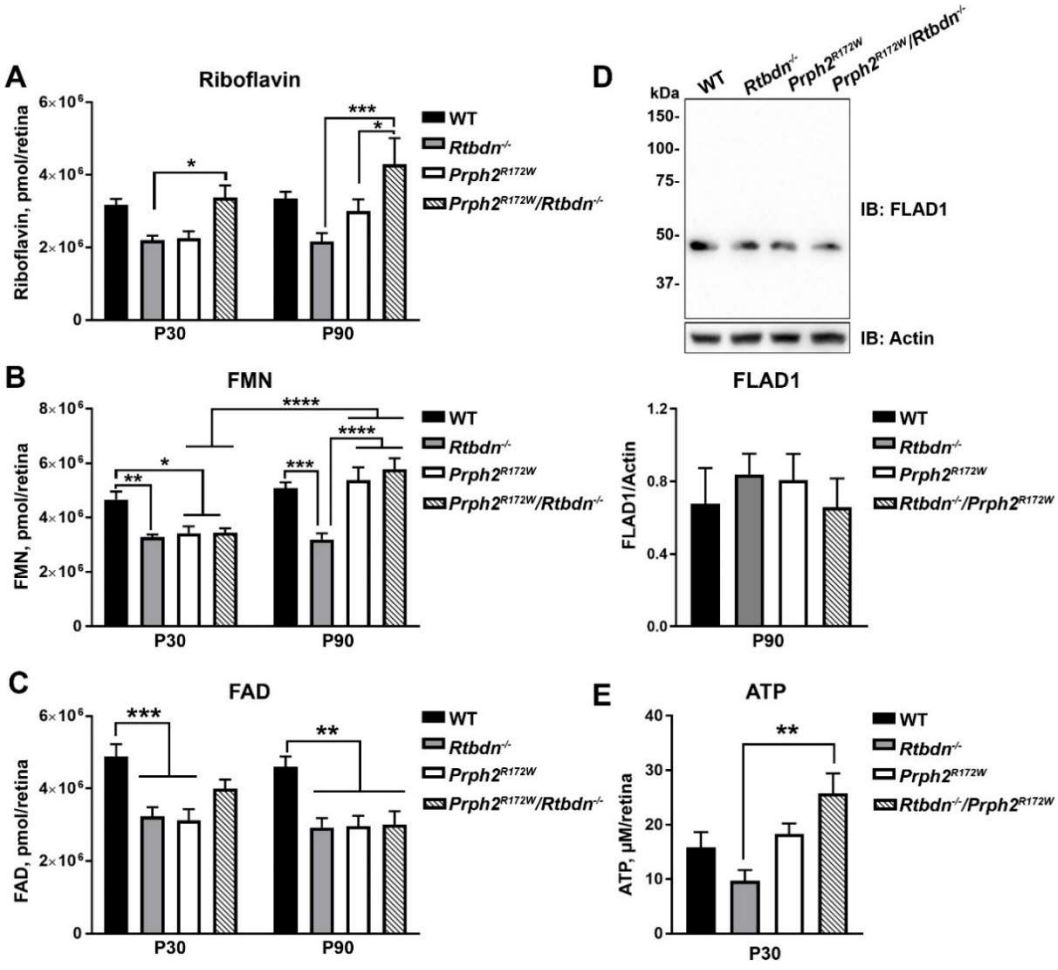

Figure 2.7. Retinal flavins are altered in the *Prph2*^{R172W}*/Rtbdn*$^{-/-}$ retina. Flavin quantification (riboflavin-**A**, FMN-**B**, FAD-**C**) of retinal samples. **D.** Immunoblot analysis for FLAD1. **E.** ATP analysis of retinal samples.

Within cells, FAD synthase (FLAD1) catalyzes the adenylation of FMN to form FAD. The increased levels of riboflavin and FMN (Fig. 2.7A-B) without concomitant increases in FAD (Fig. 2.7C) prompted us to ask whether FLAD1 protein levels were changed in the *Prph2*^{R172W}*/Rtbdn*$^{-/-}$ retina. However, retinal FLAD1 levels were not significantly different in any group (Fig. 2.7D).

2.3.6 Prph2^{R172W}*/Rtbdn*$^{-/-}$ *retina harbors increased ATP levels*

Apoptosis and energy metabolism are tightly coupled processes and it is well known that deficiencies in energy metabolism can lead to visual dysfunction and neuronal degeneration [106]. We previously found that elimination of Rtbdn led to reduced ATP levels in the retina [60]. Therefore, ATP levels were measured in *Prph2*^{R172W}*/Rtbdn*$^{-/-}$ retinas. ATP levels were reduced in the *Rtbdn*$^{-/-}$ as expected but were significantly elevated in the *Prph2*^{R172W}*/Rtbdn*$^{-/-}$ (Fig. 2.7E).

2.4 Discussion

Eliminating Rtbdn in a model of inherited cone-rod dystrophy (R172W) caused exacerbation in degenerative phenotypes such as rod and cone functions, rod and cone cell loss, and retinal gliosis. These phenotypes were much more severe in the *Prph2*^{R172W}*/Rtbdn*$^{-/-}$ than either the *Rtbdn*$^{-/-}$ or *Prph2*^{R172W} alone. Retbindin levels are significantly increased in the R172W model at P30, and these two factors combined suggest that Rtbdn plays a protective role for both rods and cones (though it is only expressed in rods [56]) during photoreceptor degeneration. Our results also

suggest that Rtbdn is essential for retinal homeostasis. We hypothesized that one important function of Rtbdn is to facilitate enrichment of retinal flavins. In the *Rtbdn*$^{-/-}$, riboflavin, FAD, and FMN levels are all reduced, consistent with this idea. This idea is also largely supported by data from the *Prph2*^{R172W} line. Young *Prph2*^{R172W} retinas have reduced flavin levels, possibly due to increased energy demands either to promote apoptosis or cell survival in a retina facing degenerative insults. However, in this model, Rtbdn levels are elevated, and by P90, riboflavin and FMN levels are back to WT levels.

Our current data also suggest an additional role for Rtbdn. Flavins are delivered to the retina via inner retinal blood vessels and the RPE [73, 74], and potentially taken into retinal cells through riboflavin organic ion transporters RFVT1-3 (*SLC52A1-A3*) [107, 108]. In the blood, flavins bind to albumin and immunoglobulins, and inside cells they bind as cofactors to the enzymes of the riboflavin proteome. This protein binding is essential; unbound flavins that are exposed to light (such as in the retina) undergo photoreduction and are converted to reactive species that can initiate lipid peroxidation and cellular toxicity [109-111]. Thus it is logical to hypothesize that an additional function of Rtbdn is to bind flavins in the IPM to prevent this photoreduction-associated toxicity. Support for this hypothesis comes from our previous *in vitro* experiments showing that Rtbdn was capable of preventing light-induced riboflavin-associated cell death [112]. This function may also explain why degeneration in the *Prph2*^{R172W} was so exacerbated by removal of Rtbdn; indeed, elevated flavin levels coupled with a lack of flavin binding

proteins (i.e., Rtbdn) may translate to increased lipid peroxidation and oxidative stress-induced cellular toxicity.

However, analysis of flavin levels in the *Prph2*^{R172W}*/Rtbdn*$^{-/-}$ adds a layer of complication. In spite of the absence of Rtbdn, both riboflavin and FMN are up at P90 in the *Prph2*^{R172W}*/Rtbdn*$^{-/-}$ compared to the *Rtbdn*$^{-/-}$. Why should introducing the Prph2 R172W mutation "rescue" the *Rtbdn*$^{-/-}$ phenotype of reduced flavin levels? One hypothesis is that the exacerbated retinal degeneration in the *Prph2*^{R172W}*/Rtbdn*$^{-/-}$ might lead to increased flavin levels compared to the *Rtbdn*$^{-/-}$. Energy is required during apoptotic cell death [113] which is occurring in Prph2-associated retinal degeneration, and flavins play a role in cellular energy generation [114]. Yet this hypothesis is inconsistent with our previous findings. At P30, the *rd1* and r*d10* models both show decreases in flavin levels [90], and the amount degeneration we see at P90 in the *Prph2*^{R172W}*/Rtbdn*$^{-/-}$ (at which point flavin levels are increased) is in between that seen at P30 in the *rd1* and r*d10*.

Another interesting finding is that although FMN and riboflavin levels are elevated in the *Prph2*^{R172W}*/Rtbdn*$^{-/-}$ and *Prph2*^{R172W} compared to *Rtbdn*$^{-/-}$, FAD levels remain reduced. This raises the question of whether FMN, specifically, is in high demand during the photoreceptor degeneration seen in the *Prph2*^{R172W}. The majority of the enzymes that use flavins utilize FAD rather than FMN (84% vs. 16% [108, 115]). However, FMN-dependent enzymes are involved in a wide variety of cellular processes including energy generation in the electron transport chain; synthesis of methionine, coenzyme A, and tRNAs; and pyrimidine breakdown, among other

functions. Further investigation will be needed to understand whether increased FMN levels during retinal degeneration are tied to increased demand for FMN as a cellular cofactor.

Support for the idea that there is increased demand for flavins as cofactors in energy generation in this degenerative model comes from our observation that there are elevated levels of total ATP in *Prph2*^{R172W}*/Rtbdn*$^{-/-}$ retinas. Apoptosis is a highly regulated process which requires ATP at many different steps, and there are mixed findings regarding levels of ATP in tissues undergoing apoptosis [116-118]. However, it has been shown that apoptotic signals can lead to necrotic cell death if there is insufficient ATP [119-121]. Thus the increased ATP levels in the *Rtbdn*$^{-/-}$ */Prph2*^{R172W} retinas may reflect a mechanism to protect surrounding tissues [122], i.e., by ensuring that apoptosis can be completed rather than defaulting to necrosis. Future studies may more precisely evaluate cell death mechanisms ongoing in these models.

One interesting observation is that the absence of Rtbdn in the *Prph2*^{R172W} retina resulted in vascular pathologies such as the appearance of neovascular tufts. However, we didn't observe vascular pathology at early ages, at time points when retinal function and photoreceptor structure were already significantly affected. This suggests the vascular pathology is a secondary effect to retinal degeneration in the *Prph2*^{R172W}*/Rtbdn*$^{-/-}$ retina. Early photoreceptor dysfunction in rats is predictive of ensuing neurovascularization [123], and other studies demonstrated that photoreceptor energy demand controls the vascular supply and drive vessel growth [124-126]. Given the role of flavin-binding enzymes in cellular metabolism and the potential role of

Rtbdn in flavin processing in the retina, it is logical to hypothesize that retinal metabolism is altered in *Rtbdn*$^{-/-}$ retinas during degeneration, thus accelerating associated vascular pathologies.

It has become increasingly apparent that metabolism and cellular bioenergetics are essential to cellular homeostasis and that aberrations in these processes play a major role in a widening circle of pathologies. As a result, understanding the mechanisms by which retinal nutrient balance is generated and maintained is absolutely essential. Our findings here support the importance of a clearer understanding of the mechanisms underlying retinal homeostasis: by removing Rtbdn and altering flavins in the retina, degeneration is accelerated in a model of inherited retinal disease. This study indicates that Rtbdn is essential for retinal health and suggests it may play a protective role during retinal degeneration. Our findings also raise a large number of questions about the role of flavins in retinal homeostasis and disease, about the role of Rtbdn as a flavin binding protein in the retina, and about potential other roles for Rtbdn. They also highlight unique tissue-specific biology. While flavins are essential cofactors in all cells, the unique, light-rich tissue microenvironment of the retina coupled with the high metabolic rate create a tissue with unique demands for flavin and flavin binding proteins. The study of Rtbdn is quite new, and there is much we still do not know about its function in the retina. This study advances our understanding of the role of Rtbdn in models of retinal pathology, and we look forward to future mechanistic studies help further our understanding of its function. Our ultimate goal is to identify therapeutic targets related to Rtbdn that will

help promote cellular homeostasis in a variety of disease states. With the current availability of tools for precisely measuring mitochondrial energetics and assessing metabolome profiles, coupled with these unique animal models, we have an unparalleled opportunity to explore retinal homeostasis at the most fundamental cellular level.

Chapter 3- Retbindin ablation accelerates the disease progression in P23H knock-in mouse model of Retinitis Pigmentosa

This study will be submitted at a later date

3.1 Introduction

Retbindin (Rtbdn) is a novel retina-specific protein that is exclusively expressed by retinal rod photoreceptor cells [56]. Post expression, Rtbdn is secreted into the inter photoreceptor matrix (IPM) and anchors itself to the plasma membrane via electrostatic forces. Immunohistochemical analysis of Rtbdn shows predominant localization at the tip of the rod outer segments (OS), adjacent to retinal pigment epithelium (RPE) microvilli [56]. The similarities between Rtbdn and riboflavin binding protein (RBP) of chicken [55] guided the prediction that Rtbdn binds to riboflavin, which was later confirmed *in vitro* [56] and *ex vivo* [60]. Subsequent investigation revealed significantly reduced levels of riboflavin and its derivatives in the retinas of Rtbdn knockout (*Rtbdn*$^{-/-}$) mice [60]. Furthermore, *Rtbdn*$^{-/-}$ mice exhibited a decline in rod and cone functions at P120 concomitant with a reduction in photoreceptor numbers at P240.

Riboflavin (Vitamin B2) is a water soluble vitamin that is essential for cell growth and function [127]. Intracellularly, it is primarily found in its redox active co-enzymatic forms, flavin adenine dinucleotide (FAD) and flavin mononucleotide (FMN). Flavins are associated with various proteins and play vital roles in a variety of processes including the citric acid cycle, β-oxidation, amino acid synthesis, protein folding, DNA repair, and normal immune function [128]. The retina and specifically

the photoreceptors are metabolically active [129], hence it is not surprising that retinal flavin levels are almost 20 fold higher compared to blood [78, 79]. This suggests that the retina has a unique, flavin acquisition and concentration mechanism and that proper flavin regulation is necessary to maintain photoreceptor metabolic state over time.

Due to its homology to RBP, its localization at the dynamic interface where metabolites and nutrients are exchanged [56], its riboflavin binding capability [56, 60] and reduced flavin levels in the knockout retinas [60], Rtbdn has been tied to the regulation of retinal flavin. Since metabolic dysregulation is a hallmark of photoreceptor cell death [130] and flavins are directly linked to metabolism [128], we investigated Rtbdn role in the degenerative retina of a retinitis pigmentosa model.

Retinitis pigmentosa (RP), an inherited retinal dystrophy, occurs in 1 out of 4000 people worldwide [39]. RP is characterized by a progressive photoreceptor loss with no effective clinical treatment is currently available. Thus, identifying elements that promote photoreceptor survival in RP is crucial for the management of this disease. A proline to histidine change at codon 23 (P23H) of the rhodopsin (Rho) gene is the most common (~15%) cause of Rho-related RP in US [44-46]. The P23H knock-in ($Rho^{P23H/+}$) mouse, which expresses wild type (WT) and P23H Rho, is the model of choice to determine the role of Rtbdn in the progression of the degenerative process.

In this study, we show that levels of Rtbdn are significantly upregulated in the $Rho^{P23H/+}$ retina compared to age matched WT control. This rise likely reflects

increased metabolic activity and energy demand by the degenerating retina either as a protective mechanism or to execute the energy dependent cell death. To investigate which of these possibilities is more likely, we studied the effect of Rtbdn ablation on the *Rho*$^{P23H/+}$ retina. Herein, we report that Rtbdn absence in the *Rho*$^{P23H/+}$ mice exacerbated the degenerative phenotype. In addition to functional decline and increased cell loss, lack of Rtbdn in the *Rho*$^{P23H/+}$ retina resulted in fundus abnormalities and neovascularization. This study demonstrates that Rtbdn plays a protective role during the degenerative process hence making Rtbdn a potential therapeutic target for inherited retinal degenerations.

3.2 Materials and Methods

Animals

Rtbdn knockout (*Rtbdn*$^{-/-}$) and *Rho*$^{P23H/+}$ knock-in mice were generated and characterized as reported previously [48, 60]. *Rho*$^{P23H/P23H}$ (homozygous) (B6.129S6(Cg)-*Rho*$^{tm1.1Kpal}$/J, stock number: 017628, Jackson Laboratory) mice were bred onto the *Rtbdn*$^{-/-}$ background to generate *Rho*$^{P23H+/-}$*/Rtbdn*$^{-/-}$mice. WT, *Rtbdn*$^{-/-}$ and *Rho*$^{P23H/+}$ mice were also included in the present study as controls. All *Rho*$^{P23H/+}$ mice analyzed for this study were heterozygous for the knock-in gene and carried one endogenous copy of wild Rho gene. All of the animals were in the C57BL/6-129SV background and they were free of rd8 and rd1 mutations. Mice were raised under 12 hour (h) dim light (30-50 lux) and 12 h dark conditions. Males and females were equally included into the analyses. All animal procedures and experiments were

approved by University of Houston institutional Animal Care and Use Committee (IACUC). For the sample collection, animals were euthanized using CO_2 asphyxiation. Retina samples for western blot and HPLC analyses were collected by winkling method [95] and immediately frozen in liquid nitrogen and stored at -80°C until used.

Immunoblotting

Immunoblot analyses using Rtbdn antibody were performed as described previously [56]. N= 7 independent retinal extracts for each genotye/age. Sub-cellular fractionation of the retina samples was performed as following: Intact P30 fresh retinas were incubated in 1X PBS (pH 7.2) containing 1% PIN, on ice for 15 min. Supernatant was collected and saved as soluble IPM fraction. The pellets were exposed to a hypotonic environment by incubating them in 0.1X PBS containing 1% PIN on ice for 15 min to bust the cells open. Then, they were extracted with the hand held motor and pestle tip homogenizer and centrifuged at 50,000g for 30 min. The supernatant was considered as cytosolic components of the cells. The pellets were re-suspended in 1X PBS (pH 7.2) containing 1% Triton X-100 and 1% PIN then homogenized with sonication. After 1 h incubation period at 4°C, samples were centrifuged at 16,128 g for 5 min. The supernatant was considered to contain the membrane bound proteins. Finally, the fractions were analyzed via immunoblotting using the Rtbdn antibody. Prph2 (RDS-2B7) mouse monoclonal antibody was used as membrane marker (1:1000), which was produced by Precision Antibodies and characterized earlier [131]. Anti-IRBP rabbit polyclonal was used as soluble IPM

marker, in the dilution of 1:1000 [132]. GAPDH mouse monoclonal antibody was from abcam (ab8245) and used as cytosolic marker. The blots were imaged using Bio-Rad ChemiDoc™ MP imaging system and quantified densitometrically, using Bio-rad Image Lab v4.1 software.

Immunofluorescence

Whole eyes were harvested from the euthanized mice and fixed in Davidson's fixative (32% ethanol, 11% acetic acid, 2% formaldehyde) overnight. They were soaked sequentially in 70%, 80%, 90%, and 100% absolute ethanol for 30 min each and transferred to xylene for clearing (1 hour) and embedded in paraffin. 10 μm sections were obtained using microtome. Immunolabeling with Rtbdn was performed as described previously [56]. The following antibodies/reagents were used: Anti-Rtbdn (in house, 1:500), anti-rhodopsin (1D4) (in house, 1:1000), PNA (1:500), wDAPI (Thermo Fisher Scientific, 62248, 0.1μg/mL). Slides were washed and mounted with Prolong Gold antifade mountant (P36934, Thermo Fisher Scientific) and images were captured using Zeiss 800 LSM confocal system and processed in Zen 2 lite software. Experiments were repeated 3 times using 3 independent retinal sections.

Electroretinography recordings

Full field ERG was performed at P15, P30, P60 and P90 as described previously [133] using UTAS system (LKC, GAuthersburg, MD, USA). The scotopic measurements were recorded against a response to the 157.7 cds/m^2 single flash. After

5 min light (intensity 29.03 cd/$m^{2)}$ adaptation, animals were exposed to 25 flashes at 79 cd s/m^2 intensity. Results obtained from the right and left eyes were averaged and plotted in GraphPad Prism 7 software. N=10-19 animals for each genotype/age.

Light Histology and Quantitative morphometry

Paraffin sections along the optic nerve were chosen and rehydrated, soaked in the Hematoxylin (MHS16, Sigma, Burlington, MA, USA) for 4 min and rinsed with water. After 4 quick dips in to the 0.3% acid alcohol, sections were rinsed with water and soaked in to the Eosin (HT110116, Sigma, USA) for 2 min. The slides were rinsed again with water to remove the excess stain, and mounted using permount mounting medium (SP15100, Fisher Scientific), after the dehydration and clearing steps. Light microscopic images were captured from the inferior side, 500 μm away from the optic nerve using Zeiss Axioskop 50. Outer nuclear cells pertaining to the length of 100 μm at intervals of 200 μm were counted across the retina.

Cone counting in whole mounted retinas

Whole eyes were harvested from mice and fixed in 4% PFA overnight. Lens and cornea were removed and retinas isolated from the eye cups and four incisures were cut to flatten the retinas. The retinas were washed with 1XPBS and blocked with 0.5% Triton X-100 and 5% bovine serum albumin in 1XPBS (pH 7.4) at room temperature for 2 hours. The retinas were then incubated in PNA (1:500), which diluted in blocking solution, overnight at 4 °C. Retinas were washed extensively and mounted flat (photoreceptor side up) using permount mounting medium (SP15100,

Fisher Scientific). Whole mounted PNA labeled retinas were imaged with Zeiss 800 LSM confocal system using 40x objective. Captured images, enclosing 135 × 135 μm^2 area, were from 350 μm away from the optic nerve for each quadrant. The cone count number of four quadrants were averaged to give a value for each sample.

Transmission electron microscopy

Mice at P30 were euthanized, and their whole eyes were harvested after marking the superior hemisphere. A puncture was made on the ora serrata and placed in EM grade fixative (2% paraformaldehyde, 2% glutaraldehyde, 100mM Cacodylate, 0.025% $CaCl_2$ (pH 7.4 final mixture)) for 2 h. The whole eyes were cut at the ora serrata to remove the Cornea and lens. Then, eye cups were returned back to the fixative and kept in it overnight at 4 °C. The enucleated eyes were embedded in plastic resin and sectioned as explained elsewhere [131]. The plastic sections were in 600-800 Å thickness, stained with 2% (v/v) uranyl acetate and Reynold's lead citrate and imaged with JEOL 100CX microscope.

Fundus and Fluorescein Angiogram Imaging

Fundus and fluorescein angiogram imaging was performed using Phoenix micron IV system (Phoenix Research Laboratories, Pleasanton, CA). Animals were anesthetized by intramuscular injection of 85 mg/kg ketamine and 14 mg/kg xylazine and their eyes were dilated with 1% cylopentalate to prepare them for imaging. Bright field fundus images were captured and then, mice were intraperitoneally injected with clinical grade (Akorn Ak-fluor 10%) fluorescein at a dose of 0.001ml/gm. Almost 30

seconds past fluorescent injection, mice were subjected to the fluorescent angiogram imaging using the 451.5 – 486.5 nm excitation and 488 nm emission GFP filter. Images were obtained from all of the animals under the same light, voltage and gain conditions.

Flavin quantification by HPLC

Micro-extraction and quantification of flavins in the retina samples using the Waters HPLC system (Waters, Milford, MA, USA) was performed as previously described [90]. Extraction of the samples were performed under red dim light to minimize the photo degradation of flavins. Flavin amounts were measured by calculating the area under the curve (AUC) using the Breeze 2 software (Waters, Milford, MA, USA). The AUC raw data was converted to pmol per retina for final analysis.

Quantification of ATP levels in retina

The cellular ATP levels were measured using abcam (ab113849) Luminescent ATP Detection Assay Kit following the supplier's protocol. Briefly, retinas were collected and immediately placed in to 1X PBS (pH 7.4) containing 1% PIN and homogenized using sonication. They centrifuged at 16,128g for 5 min and supernatant was transferred to a single well of 96 well plate. In order to lyse the cells, 50 µl of detergent in the kit was added to each well and incubated at room temperature for 10 min on a shaker. Then, 50 µl of substrate solution was added, incubated for another 15 min at room temperature and the plate was placed in the microplate reader

(Spectramax M5, Molecular devices, Sunnyvale, CA) to measure total cellular ATP levels. This experiment was performed under dim red light.

Statistical Analysis

Statistical analyses were performed using one or two way ANOVA with Tukey's post-hoc comparison. One symbol $P<0.05$, two symbols $P<0.01$, three symbols $P<0.001$ and four symbols $P<0.0001$. Data for all experiments were expressed as ± SEM. Graphpad Prism 7 was used for the quantitative analysis.

3.3 Results

3.3.1 Rtbdn is upregulated in the $Rho^{P23H/+}$ retina

To evaluate whether Rtbdn is modulated in the $Rho^{P23H+/-}$ retina, levels of Rtbdn were determined. As shown in Figure 3.1 (solid blue bar) levels of Rtbdn were found to be upregulated by >1.8 folds in the postnatal day (P) 15 and 30 $Rho^{P23H/+}$ retinas compared to age matched WT controls (solid black bar). At P90, Rtbdn levels in $Rho^{P23H/+}$ retinas were about similar to that of WT (Fig. 3.1A).

Due to the degenerative status of the retinas in $Rho^{P23H/+}$ mice, we reassessed the levels of Rtbdn overexpression in that model taking in account the number of remaining rod photoreceptors. As shown in Figure 3.1A (open bars), when the levels of Rtbdn are normalized to the number of remaining rods, it seems that those rods were still overproducing Rtbdn.

The subcellular localization of a protein provides information regarding the physiological context for its function, and any abnormal localization may contribute to pathogenesis of the disease [134]. In order to address whether the increased amount of Rtbdn continues to be, as in the WT [56], extracellular, cellular fractionation was performed on $Rho^{P23H/+}$ retinas. As shown in Figure 1B, despite the increased levels, Rtbdn was still localized to membrane fraction in the $Rho^{P23H/+}$, as has been described before in the healthy retina [56]. The Rtbdn band observed in the cytoplasmic fraction is likely the newly synthesized Rtbdn.

We have previously shown that Rtbdn is extracellularly localized and restricted to two areas, at the tip of the OSs and around the inner segment (IS)s [56, 60]. To determine whether the distribution of upregulated Rtbdn in the $Rho^{P23H/+}$ retina is altered, we performed immunohistochemical localization on P30 WT and $Rho^{P23H/+}$- retinal sections (Fig. 3.1C). As shown before in the WT retina, Rtbdn was observed in a band at the RPE/OS junction while another pool was localized around the ISs. Surprisingly, we observed that the band of Rtbdn that is normally observed at the junction of RPE/OS was diffused in the $Rho^{P23H+/-}$ retina (Fig. 3.1C) and the signal was concentrated in patchy structures around the OSs and displayed reduced presence at the IS area. (Fig. 3.1C). To evaluate whether these structure are aberrant rod OSs or cone OSs, we performed co-immunostaining with Rtbdn and Rho or peanut agglutinin (PNA), which is known to label cone sheaths [135-137]. The patchy Rtbdn immunostaining localized to neither rod OSs nor to cones (Fig. 3.1C).

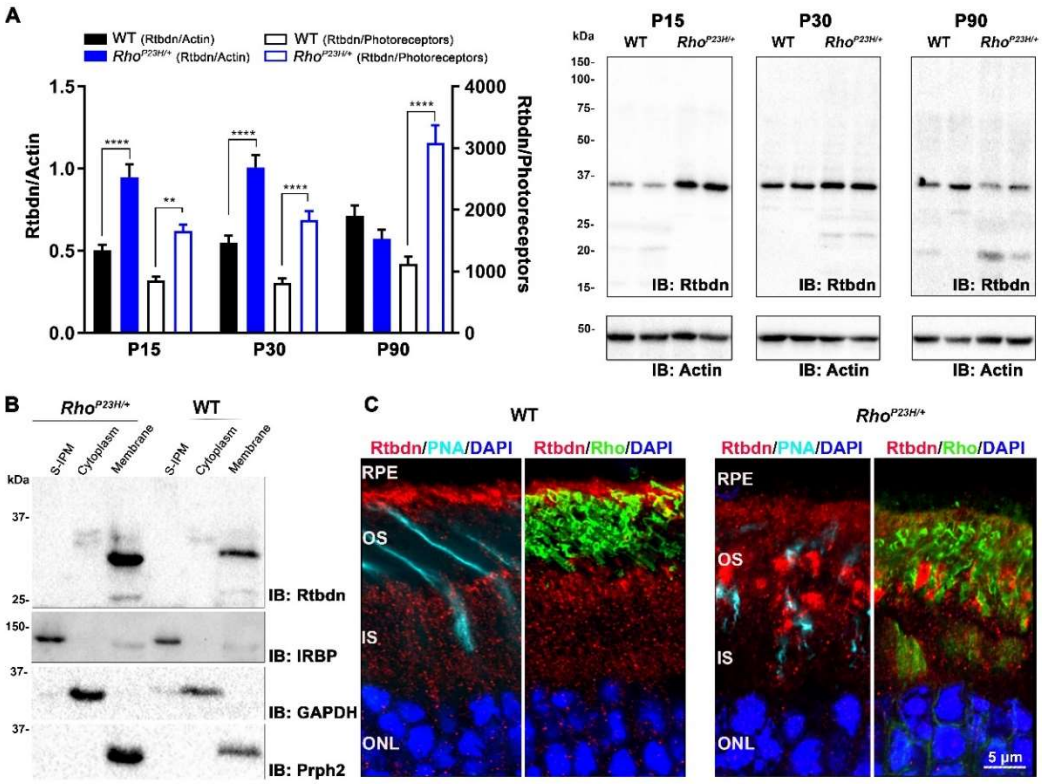

Figure 3.1. Rtbdn upregulation and its cellular localization in *Rho*$^{P23H/+}$ retina. **A.** Immunoblot analysis of Rtbdn. **B.** Western blot analysis of retinal extracts separated into subcellular fractions **C.** Confocal images of P30 retinal sections.

3.3.2 The pattern of Rtbdn labeling is altered in the compromised retinal homeostasis

Redistribution of proteins can be a mechanism to *adapt* or respond to *changing* environments [138-140]. Data in Figure 3.1 showed that as the levels of Rtbdn increased in *Rho*$^{P23H/+}$ retina, its association with the membrane was retained. However, the cellular distribution was altered whereby Rtbdn (red) was not limited to the RPE/OS junction and around the IS. Instead, Rtbdn was observed diffused at the RPE/OS junction, patchy localization at the OS and reduced presence at the IS (Fig. 3.1C). To gain insight into the pattern of Rtbdn immunostaining at different stages of

degeneration, we examined immunostaining characteristic of the *Rho*$^{P23H/+}$ retina at different ages (Fig. 3.2). Retinal sections from P15 (early developmental age, initial stage of degeneration), P30 (adolescent, mid-stages of degeneration), and P90 (adulthood, advanced stage of degeneration) *Rho*$^{P23H/+}$ and age-matched WT control retinas were double-stained with antibodies against Rtbdn (red) and Rho (green). Confocal microscopic analyses showed that in WT retinas, Rho is localized to the OS, except at P15 where it is also present at base of ISs (white arrowhead, Fig. 3.2, P15). However, in *Rho*$^{P23H/+}$ retinas, Rho is observed at the IS and ONL layers, in addition to its main localization in OS. The corresponding spatial distribution of Rho fluorescence in the selected areas from the confocal images, represented by a 2.5-D view, revealed that most of the Rho is localized to OS in P30 *Rho*$^{P23H/+}$ retina (Fig. 3.2, P30) and almost all of Rho is localized to OS in the P90 *Rho*$^{P23H/+}$ retina (Fig. 3.2, P90).

The developmental pattern of expression of the majority of Rtbdn in the WT retina is limited to the apical portion of IS with diffused expression in rest of IS and OS (Fig. 3.2, P15). As the retina matures, Rtbdn is confined mostly to the apical side of the OS and diffused expression around the IS (Fig. 3.2, P30 & 90). However, in the P15 *Rho*$^{P23H/+}$ retina Rtbdn is mostly present in patches (white arrow) in OS with diffused presence in IS (Fig. 3.2, P15). As the *Rho*$^{P23H/+}$ retina matures, the pattern remains with clear presence in the ONL (Fig. 3.2, P30). Finally, with the progression of the degenerative process, Rtbdn is mostly present in the OS patches (Fig. 3.2, P90).

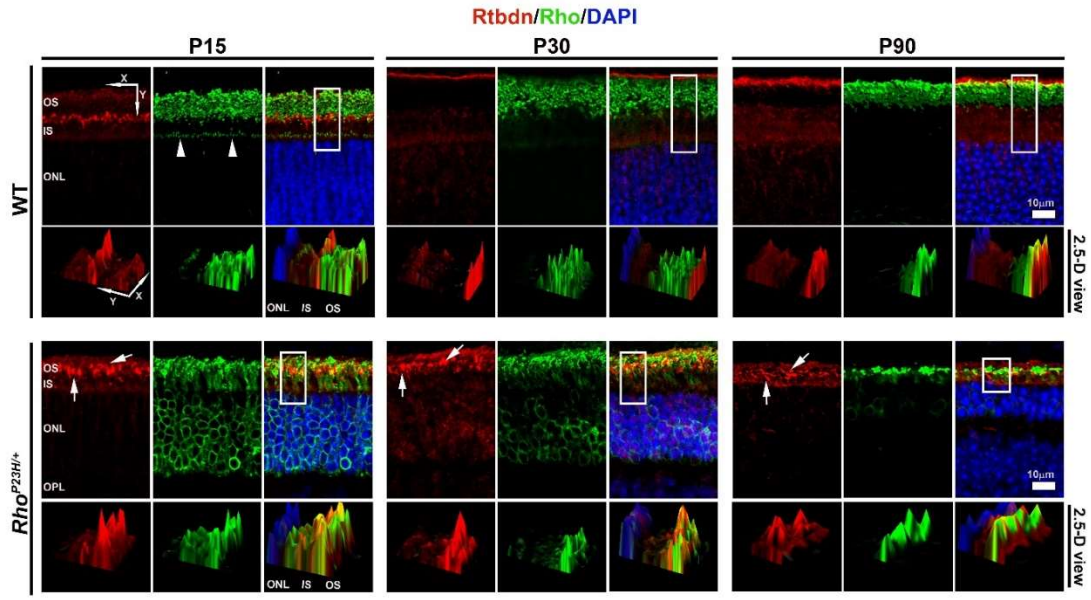

Figure 3.2. Rtbdn immunostaining during postnatal development and in adults. Representative single-plane confocal images of retinal cross-sections. The 2.5-D reconstruction of the area enclosed within the white rectangles are shown.

3.3.3 Elimination of Rtbdn leads to functional decline in the Rho$^{P23H/+}$ retina

Upregulation of Rtbdn in the *Rho*$^{P23H/+}$ retina suggests that it influences, positively or negatively, the progression of the degenerative disease. To investigate this, we crossbred *Rho*$^{P23H/+}$ mice into the background of *Rtbdn*$^{-/-}$. We first investigated retinal functionality in absence of Rtbdn by conducting full-field developmental electroretinography (ERG) on the *Rho*$^{P23H/+}$/*Rtbdn*$^{-/-}$ mice and compared results to those for *Rho*$^{P23H/+}$, *Rtbdn*$^{-/-}$ and WT controls. Consistent with our previous studies, *Rtbdn*$^{-/-}$ exhibited normal ERG responses until P120 [60]. While Rtbdn ablation showed no effect on retinal function at P15, elimination of Rtbdn in the *Rho*$^{P23H/+}$ retina at P30 caused significant reduction in both scotopic a- and photopic b-waves amplitudes (Fig. 3.3).

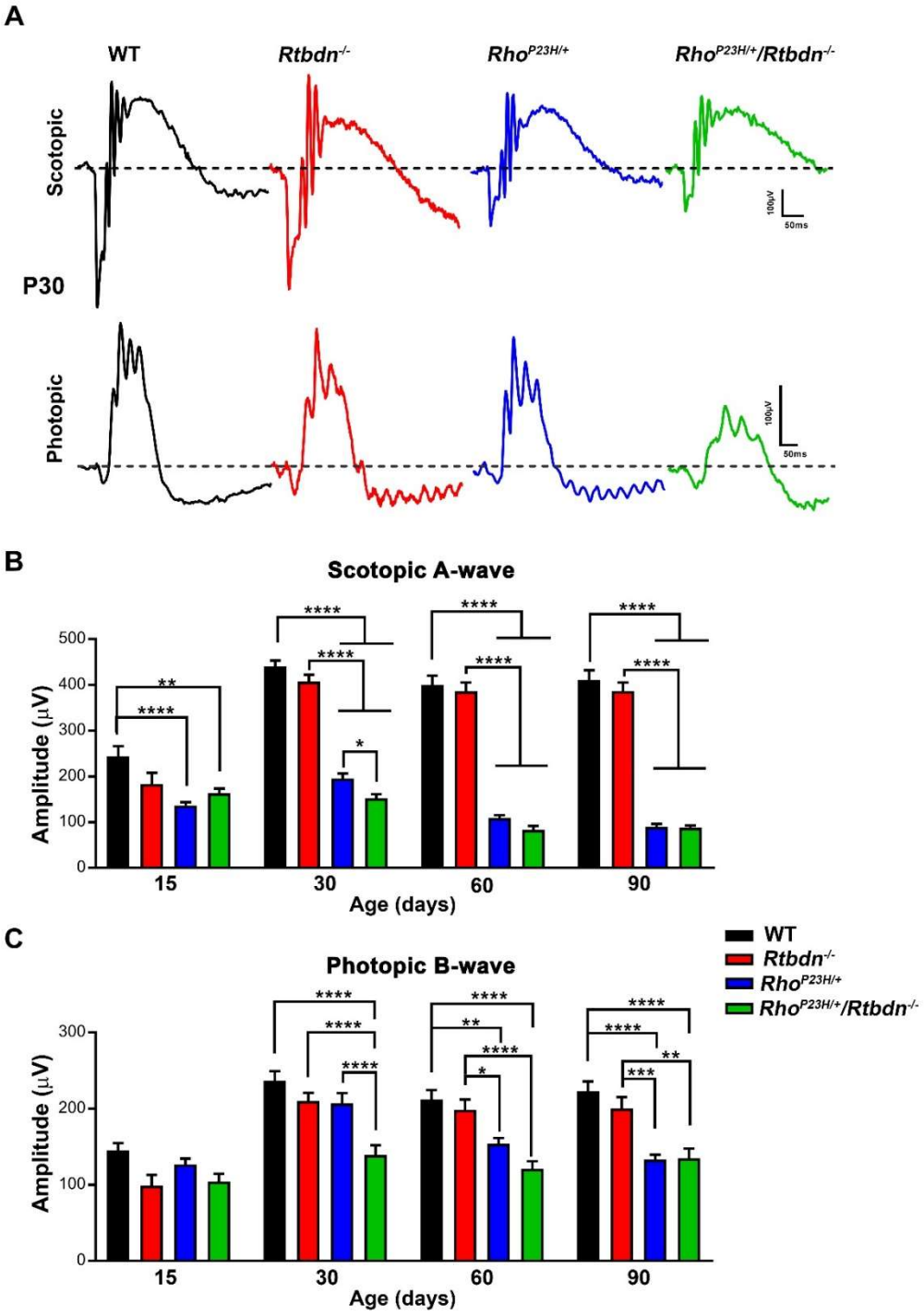

Figure 3.3. Functional consequences of Rtbdn elimination in the *Rho*$^{P23H/+}$ retina. **A.** Representative waveforms of scotopic-A and photopic-B ERG responses **B, C.** The average amplitudes of maximum scotopic-A and photopic-B waves.

At P30, the *Rho*$^{P23H/+}$/*Rtbdn*$^{-/-}$ mice showed reduced rod photoreceptor function by ~22% (Fig. 3.3B) and cone photoreceptor functional reduction of ~33% when compared to the *Rho*$^{P23H/+}$ (Fig. 3.3C). It is interesting to observe this significant decline in cone function of the *Rho*$^{P23H/+}$/*Rtbdn*$^{-/-}$ mice, although cone function was not affected neither in the *Rho*$^{P23H/+}$ nor the *Rtbdn*$^{-/-}$ ones. However, *Rtbdn*$^{-/-}$ mice showed reduced photopic function at P120 [60] despite the fact that cones do not express Rtbdn [56]. The decline in retinal function disappears as the animals age, likely due to the advanced degeneration (Fig. 3.3B&C).

3.3.4 Ablation of Rtbdn in the Rho$^{P23H/+}$ retina exacerbates rod photoreceptor degeneration and triggers early cone photoreceptor loss

Light microscopic (Fig. 3.4A) and morphometric (Fig. 3.4B) analyses were performed to determine if structural abnormalities are responsible for the functional decline in the *Rho*$^{P23H/+}$/*Rtbdn*$^{-/-}$ mice in comparison to *Rho*$^{P23H/+}$ or *Rtbdn*$^{-/-}$. There is a significant OS, IS, and outer nuclear layer (ONL) thinning in the *Rho*$^{P23H/+}$/*Rtbdn*$^{-/-}$ retinal sections compared to the controls at P15 and P30 (Fig. 3.4A). Our ONL cell count data reveals that Rtbdn absence in the *Rho*$^{P23H/+}$ background causes ~21% (superior), ~18.2% (inferior) reduction at P15 and ~19.4% (superior), ~16.3% (inferior) reduction at P30 compared with *Rho*$^{P23H/+}$. The difference between the *Rho*$^{P23H/+}$/*Rtbdn*$^{-/-}$ retinas and the *Rho*$^{P23H/+}$ controls, disappears at P90, consistent with the functional analysis at this age (Fig. 3.4B) and likely due to the advanced degeneration.

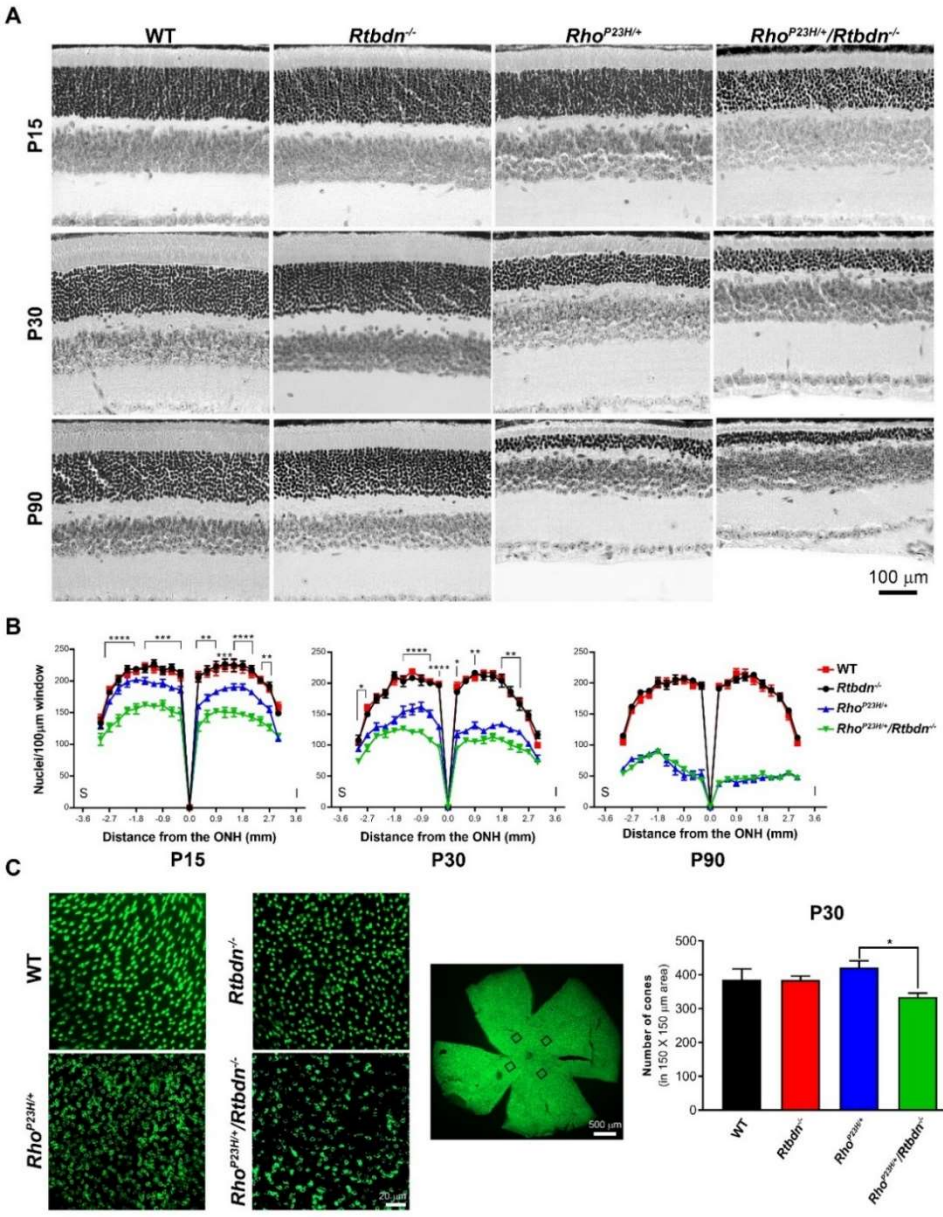

Figure 3.4. Morphometric analysis and cone counts of *Rho$^{P23H/+}$/Rtbdn$^{-/-}$* retina.
A. Light microscopic images of H&E stained retinal sections **B.** Photoreceptor nuclei count **C.** Cone photoreceptors of the P30 whole mounted retinal sections

To determine whether any structural changes are also responsible for the decline in the function of the cones, the number of cone photoreceptors in the central retina was counted on whole retinal mounts. A significant cone cell loss (~21%) in

the *Rho*$^{P23H/+}$/*Rtbdn*$^{-/-}$ retinas compared to the *Rho*$^{P23H/+}$ones was observed (Fig. 3.4C). This result emphasizes the role of Rtbdn in the viability of cones or cone pathways, although Rtbdn is exclusively expressed by the rods [56].

3.3.5 Elimination of Rtbdn leads to ultrastructural abnormalities in the Rho$^{P23H/+}$ *retina*

Rtbdn$^{-/-}$ retinas were characterized by minor ultrastructural changes that could not account for the functional decline [60]. Expression of the P23H mutation in Rho led to shorter and disorganized OSs with perpendicularly aligned discs [47, 48]. Our light microscopic examination showed that the degeneration in *Rho*$^{P23H/+}$ *retinas* is exacerbated by the elimination of Rtbdn (Fig. 3.4A). To determine whether deleterious ultrastructural changes had occurred after the elimination of Rtbdn, we examined ultrathin sections from P30 *Rho*$^{P23H/+}$/*Rtbdn*$^{-/-}$ retina and the age matched control retinas with transmission electron microscopy (TEM) (Fig. 3.5). Although less of them are present overall, *Rho*$^{P23H/+}$ retina exhibited shorter and miss-oriented OSs (Fig. 3.5, white arrowheads). While the ultrastructure of *Rtbdn*$^{-/-}$ retina resembles that seen in WT retinas in which OSs are composed of well aligned stacks of discs, elimination of Rtbdn in the *Rho*$^{P23H/+}$ retina led to total reduction in number of photoreceptors with much shorter and disorganized OSs (Fig. 5 white arrows). There are sagittally oriented and transversely oriented discs (Fig. 3.5, black arrowheads) in the P23H mutant retinas. However, unlike *Rho*$^{P23H/+}$ retina, *Rho*$^{P23H/+}$/*Rtbdn*$^{-/-}$ OSs were severely malformed (asterisk and black arrows, Fig. 3.5). The presence of unflatten discs were also very common in those retinas (Fig. 3.5, black arrows). We

also observed thicker Bruch's membrane in the *Rho*$^{P23H/+}$/*Rtbdn*$^{-/-}$ compared to the *Rho*$^{P23H/+}$ (BM, Fig. 3.5). No significant RPE phenotype difference was observed between the *Rho*$^{P23H/+}$ and *Rho*$^{P23H/+}$*Rtbdn*$^{-/-}$ sections.

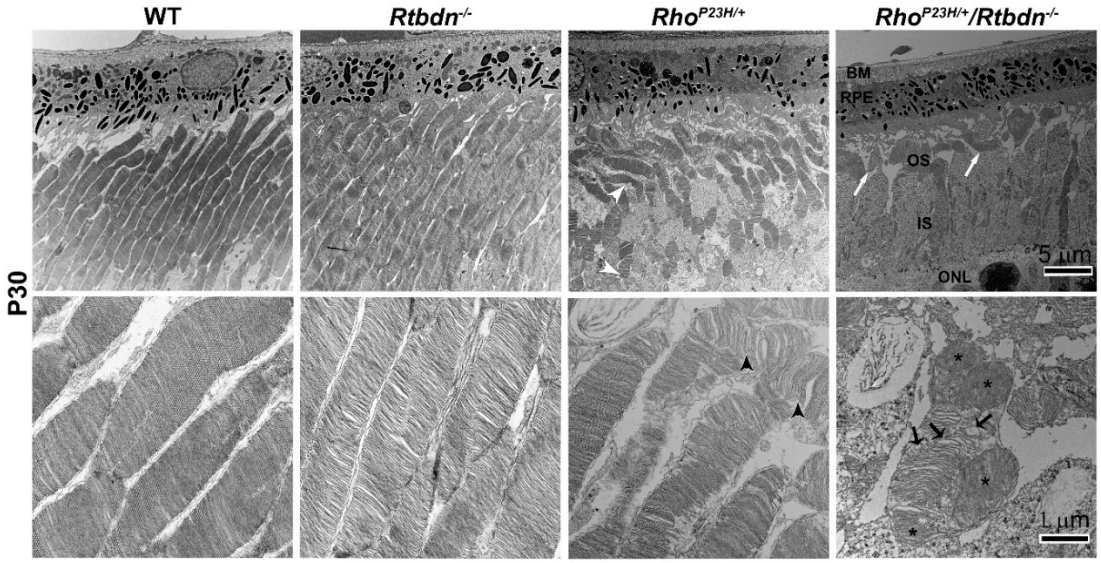

Figure 3.5. Ultrastructural effect of Rtbdn ablation in the *Rho*$^{P23H/+}$ retina.
A. Representative EM images of outer retina/RPE (upper panel) and the OS (lower panel) of the photoreceptor cells in the indicated genotypes at P30.

3.3.6 Ablation of Rtbdn in the Rho$^{P23H/+}$ *retina leads to retinal vascular changes*

To determine whether lacking Rtbdn in the *Rho*$^{P23H/+}$ retina leads to other abnormalities in addition to the functional and histological manifestations, we performed fundus imaging and fluorescein angiography (Fig. 3.6). At P90, *Rtbdn*$^{-/-}$ mice exhibited normal fundus appearance similar to WT. Fundus images of *Rho*$^{P23H/+}$/*Rtbdn*$^{-/-}$ mice showed minor changes (Fig. 3.6A, black arrows) when compared to *Rho*$^{P23H/+}$. While blood vessels were attenuated in the *Rho*$^{P23H/+}$ retina, (Fig. 3.6A) fluorescein angiography of *Rho*$^{P23H/+}$/*Rtbdn*$^{-/-}$ retinas revealed denser capillary bed and presence of neovascular tufts (Fig. 3.6A, white arrows)

Liu et al. showed that retinal capillary degeneration in *Rho*$^{P23H/P23H}$ mutants is appreciable while photoreceptors are still present, however, it slows after photoreceptor degeneration (Fig. 3.6B; [141]). Aging the *Rho*$^{P23H/+}$/*Rtbdn*$^{-/-}$ animals to P240, an advanced stage of the disease, worsened the attenuation of retinal vessels, black patches appeared and vessels became leaky (Fig. 3.6B). However, these features were also present, to a lesser extent, in the *Rho*$^{P23H/+}$ (Fig. 3.6B). The data here suggests that lack of Rtbdn makes the degenerative retina more prone to develop extra vasculature, likely to compensate for the extra need for nutrients and/or oxygen.

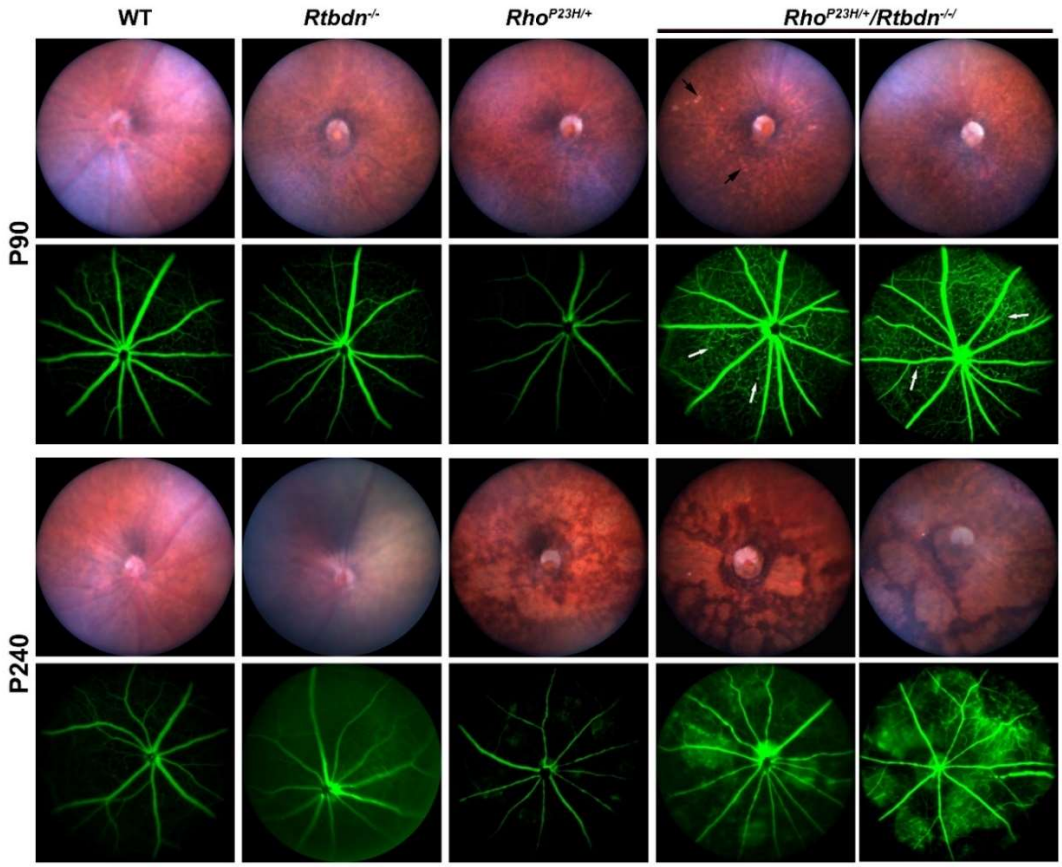

Figure 3.6. Fundus abnormalities and subretinal neovascularization in the *Rho*$^{P23H/+}$/*Rtbdn*$^{-/-}$ mice. A. Bright field fundus and fluorescein angiograms. Two different *Rho*$^{P23H/+}$/*Rtbdn*$^{-/-}$ mice were displayed for each age.

3.3.7 Lack of Rtbdn in the Rho$^{P23H/+}$/Rtbdn$^{-/-}$ resulted in reduced FMN levels

Since Rtbdn binds riboflavin [56] and it is upregulated in the degenerative retina (Fig. 1), levels of riboflavin and its derivatives were measured in WT, *Rtbdn* $^{-/-}$, *Rho*$^{P23H/+}$ and *Rho*$^{P23H/+}$/*Rtbdn*$^{-/-}$ retinas. At P15, there were no significant differences between the different genotypes (Fig. 3.7A-C). At P30, the analysis revealed reduced levels of riboflavin, FMN and FAD in the *Rtbdn*$^{-/-}$ retinas, compared to the WT controls, confirming our previous findings [60]. Despite the fact that the levels of Rtbdn are elevated in the degenerating retina of *Rho*$^{P23H/+}$ mice (Fig. 3.1), levels of riboflavin were reduced (Fig. 3.7A). Surprisingly, levels of FMN, although reduced compared to WT, were higher than expected from the drastic reduction in riboflavin levels. Elimination of Rtbdn in *Rho*$^{P23H/+}$ retina, led to levels of riboflavin and FAD reflective of those in *Rtbdn*$^{-/-}$ retinas (Fig. 3.7A&C), but to reduced levels of FMN (Fig. 3.7B).

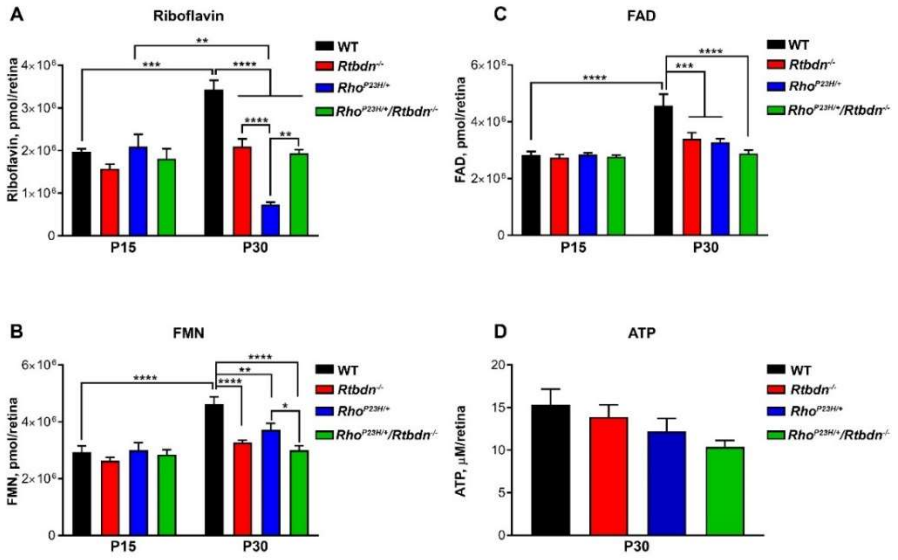

Figure 3.7. Steady state levels of flavins (Riboflavin, FAD, FMN) and ATP in retina of adult WT, *Rtbdn*$^{-/-}$, *Rho*$^{P23H/+}$ and *Rho*$^{P23H/+}$/*Rtbdn*$^{-/-}$ mice.

Since disturbances in flavin homeostasis are expected to lead to implications for energy production [68] and several retinal disorders are associated with compromised energy metabolism, we measured ATP levels (Fig. 3.7D). A statistically insignificant trend was observed toward a decrease in steady state ATP levels following the pattern: WT> *Rtbdn*$^{-/-}$ > *Rho*$^{P23H/+}$ > *Rho*$^{P23H/+}$/ *Rtbdn*$^{-/-}$.

3.4 Discussion

This study focused on determining the role of Rtbdn, the retina specific riboflavin binding protein, in retinal degenerative disorders. We showed that levels of Rtbdn are significantly increased prior and during the degenerative process in the *Rho*$^{P23H/+}$ model of retinitis pigmentosa. To understand its role in the degenerative process caused by the P23H mutation, we eliminated Rtbdn by crossing *Rho*$^{P23H/+}$ mice onto *Rtbdn*$^{-/-}$ mice. Although there was no obvious phenotype in the *Rtbdn*$^{-/-}$ retinas until P120, ablation of Rtbdn in the *Rho*$^{P23H/+}$ mice accelerated the onset of the retinal degeneration and increased its severity.

Disturbance of metabolic homeostasis is a contributing factor for the degenerative process [142-144]. Since Rtbdn binds riboflavin and flavins play critical roles in various metabolic processes, upregulation of Rtbdn during cell death likely reflects the stress response of the degenerating cells which require more energy either for cell death or survival. In order to investigate its impact on the degenerative process, we ablated Rtbdn in the *Rho*$^{P23H/+}$ mice. Characterization of mice that express the mutant rhodopsin in absence of Rtbdn showed rapid functional decline

associated with structural changes and the appearance of neovascular tufts and denser capillary bed. Surprisingly, the elimination of Rtbdn led to cone functional decline and degeneration that is not observed in the P23H mutant mice in presence of Rtbdn.

In the $Rho^{P23H/+}$ model, surviving photoreceptors operate in a toxic environment. Most of the P23H protein degrades, only a small fraction (1-10%), which is not properly glycosylated, traffic to the OSs, and disrupt the discs [47]. Accelerated photoreceptor cell death of $Rho^{P23H/+}/Rtbdn^{-/-}$ mice suggest that Rtbdn ablation either increases the cytotoxic effect of P23H opsin or exacerbates the photoreceptor degeneration due to the elimination of a protective factor (i.e., Rtbdn). Unbound flavins that expose to light can generate toxic by-products and activated oxygen species [109-111]. Thus, it is logical to hypothesize that absence of Rtbdn as a flavin binding protein may lead to photo-oxidative stress in the retina.

We did not observe changes in levels of flavins at P15 even when Rtbdn was eliminated. This may reflect the fact that the retina is still in the developmental stages and due to low levels of all flavins, compared to adult, the minor differences may not be apparent. Those differences became clear as the retina matured. At P30, the reduced flavin levels in the $Rho^{P23H/+}$ retinas compared to WT, agrees with our previous data whereby reduced flavin levels in the rd1 and rd10 mouse models [90] were observed. Reduction of the flavin levels in the $Rho^{P23H/+}$ retina despite the upregulation of Rtbdn might be either due to excessive flavin consumption or the reduction in the alive photoreceptor cell number.

We observed slightly reduced FAD (albeit insignificant) and significantly reduced FMN levels in the $Rho^{P23H/+}/Rtbdn^{-/-}$ retinas compared to $Rho^{P23H/+}$ as expected due to the elimination of Rtbdn. However, riboflavin levels in the $Rho^{P23H/+}/Rtbdn^{-/-}$ retinas were 2.5 fold higher. This might be due to the increased riboflavin flux as a result of retinal neovascularization and leakage we observed in the $Rho^{P23H/+}/Rtbdn^{-/-}$ mice. There is no strong evidence to claim about how elimination of Rtbdn in the $Rho^{P23H/+}$ retina triggers neovascularization, however, previous studies suggested disordered energy metabolism as the reason of aberrant neovascularization of the retina [145]. Structure and permeability of ocular blood vessels has been associated with the metabolic demand of retinal neurons and alterations are affecting the photoreceptor and the postreceptoral function [146]. The main source of nutrients for the metabolic activity of photoreceptors comes from choroidal circulation while inner retina is mainly nourished from retinal vasculature. Reduced nutrient and oxygen availability give rise to misguided neovascularization in retinal pathologies [147]. Considering the Rtbdn's potential function in the enrichment of retinal flavins and the essential role of flavins in cellular metabolism, it is plausible to suggest that absence of Rtbdn in the diseased photoreceptors likely drives neovascularization of the retina to accommodate to the altered metabolic conditions. Moreover, retinal degeneration is severe in the P30 $Rho^{P23H/+}/Rtbdn^{-/-}$ retina; means there is no much cells left to be able to use FMN and FAD. Thus, flavins might accumulate in the form of riboflavin.

In conclusion, elimination of Rtbdn in the $Rho^{P23H/+}$ retina exacerbates the photoreceptor degeneration. The presence of increased Rtbdn immunostaining and its

redistribution in the *Rho*$^{P23H/+}$ retina suggests that Rtbdn upregulation is an adaptive mechanism to protect photoreceptors from insult. This study indicates that Rtbdn is essential for retinal homeostasis and advances our understanding of the role of Rtbdn in model of RP. The outcome of this study should help to define the metabolic changes occurring during the degenerative process and to identify new therapeutic targets. Although these results so far support the notion that Rtbdn has the capability of ameliorating disease progression, we should also determine whether excess amount of Rtbdn is actually part of a protective mechanism. Thus, metabolomic analysis should also be done for the *Rho*$^{P23H/+}$ and *Rho*$^{P23H/+}$*/Rtbdn*$^{-/-}$ retinas to identify the pathways affected by Rtbdn absence and upregulation. The ultimate goal of this study is to identify therapeutic targets related to Rtbdn and consider Rtbdn as a target for gene therapy.

Chapter 4- Retbindin upregulates in pattern dystrophy model and its absence accelerates the disease progression

This study will be submitted to a later date.

4.1 Introduction

Retbindin (Rtbdn) is a retina specific, riboflavin binding protein, expressed only by rod photoreceptor cells [56, 60]. Riboflavin (aka Vitamin B2) is the precursor of flavin monoculeotide (FMN) and flavin adenine dinucleotide (FAD), which are redox active cofactors required for the functionality of various flavoproteins [148] that are involved in several reactions in metabolism [149]. Riboflavin is acquired from diet and its utilization in the tissues starts with the conversion to FMN and further adenylation to FAD.

Retina is metabolically very active, thus flavin concentration is ~20 fold higher in it compared to blood [79]. Recent studies demonstrated the carrier mediated transport of riboflavin across the outer [73] and inner [74] blood retinal barriers. However, the uptake, transport, concentration and control mechanism of flavins in the retina remains elusive. Our *in-vivo* and *ex-vivo* analyses showed Rtbdn binding to riboflavin [56, 60]. We also demonstrated significantly reduced flavin levels in the Rtbdn knock out ($Rtbdn^{-/-}$) retinas [60], which indicates that Rtbdn plays a role in retinal flavin homeostasis. There is a wealth of literature suggesting that metabolic aberrations may underlay or at least contribute to the degeneration [142, 143]. Since flavins are involved in enzymatic reactions in metabolism, we hypothesized that

Rtbdn, as a flavin binding protein, plays a role in modulating the degenerative process in the retina.

In support of our hypothesis, we found that the levels of Rtbdn increase during retinal degeneration in different mouse models of inherited retinal diseases. The upregulation of Rtbdn during degenerative process could be due to its protective response or as a result of increased energy demand of the dying photoreceptor cells. In this study, we explore the role of Rtbdn in development and progression of pattern dystrophy. For this purpose, we utilized the Y141C knock in mutation in the Peripherin-2 (Prph2) gene. The heterozygous mice (*Prph2*$^{Y141C/+}$) that carry 1 allele of healthy Prph2 and 1 allele of Y141C-Prph2, represent genetic case in patients. Individuals, carrying Y141C mutation, display inter- and intra-familial phenotypic variability [49, 51]. Y141C patients often exhibit macular changes, RPE pigmentation, durusen like deposits and chorioretinal atrophy [26]. They can develop choroidal neovascularization at later stages [53]. Unfortunately, there is no current strategy to prevent progression of atrophy, which results in poor vision. Y141C-Prph2 form abnormal high molecular weight Prph2/Rom1 complexes [50]. Surprisingly, these large protein complexes escape the ER and traffic to the photoreceptor outer segments (OS). Y141C-Prph2 is able to initiate the OS formation, however, it accumulates in abnormal vesicular structures and cannot support the proper disc growth. Moreover, the altered Y141C-Prph2 complexes in the OS is toxic to the surrounding tissues.

In this study, we observed significant upregulation of Rtbdn in the *Prph2*$^{Y141C/+}$ retinas. Although, loss of Rtbdn in wild type (WT) background had no gross effect in photoreceptor function till the advanced ages, its absence in the *Prph2*$^{Y141C/+}$ mice accelerated the disease progression. *Prph2*$^{Y141C/+}$*/Rtbdn*$^{-/-}$ mice exhibited significantly reduced rod and cone functions, as well as increased photoreceptor cell loss, compared to the *Prph2*$^{Y141C/+}$ control mice. Our flavin quantification analysis revealed Rtbdn dependent changes, supporting its possible function in retinal flavin enrichment. Lack of Rtbdn in the *Prph2*$^{Y141C/+}$*/Rtbdn*$^{-/-}$ mice resulted in the signs of retinal neovascularization. We also showed the presence of auto fluorescent granules, presumably lipid particles, in the Bruch's membrane (BM) of the Rtbdn lacking mice. Our ultrastructural examination suggests that Rtbdn deficiency facilitates the formation of sub- BM and RPE materials and hence may contribute to the exacerbated pathogenesis of pattern dystrophy in the *Prph2*$^{Y141C/+}$*/Rtbdn*$^{-/-}$ mice.

4.2 Materials and Methods

Mice

Rtbdn knockout (*Rtbdn*$^{-/-}$*)* and *Prph2*$^{Y141C/+}$ knock-in mice were previously characterized [50, 60]}. *Rtbdn*$^{-/-}$*/Prph2*$^{Y141C/+}$ mice were generated by crossing *Prph2*$^{Y141C+/+}$ mice to *Rtbdn*$^{-/-}$ mice. For controls, age-matched WT, *Rtbdn*$^{-/-}$ and *Prph2*$^{Y141C/+}$ mice were used. All of the animals were on the C57/BL6 background and they were free of rd8 and rd1 mutations. Mice were housed on a 12 hour (h) light (30-50 lux)/12 h dark cycle. All animal procedures and experimental protocols were

approved by Institutional Animal Care and Use Committee (IACUC) of University of Houston. Mice of both sexes were used and they were euthanized using CO_2 asphyxiation at the indicated time points for tissue collection. Retina samples were collected by winkling method [95]and immediately frozen in liquid nitrogen or transferred to the extraction buffer depending on the experimental procedure. Frozen retina samples were stored at -80°C until used.

Subcellular fractionation of the retina

Fresh retinas, collected by winkling method, immediately placed in 1X PBS (pH 7.2) containing 1% PIN and incubated on ice for 15 min. For IPM fraction, supernatant was collected and saved. The pellets were re-suspended in 0.1X PBS containing 1% PIN and incubated on ice for 15 min. Samples were agitated with the hand held motor and pestle tip homogenizer and centrifuged at 50,000g for 30 min. The supernatant (cytosolic fraction) was saved and the pellets were re-suspended in 1X PBS (pH 7.2) containing 1% Triton X-100 and 1% PIN and homogenized with sonication. They were incubated at 4°C for 1 hour and later centrifuged at 16,128 g for 5 min. The supernatant was used for membrane fraction. The subcellular fractions were analyzed via immunoblotting using anti-Rtbdn (1:500; in-house). The blot was dried and re-blotted using the following antibodies, which serve as control for each fraction: anti-Prph2 (membrane marker) (1:1000; [131]), anti-IRBP (soluble IPM marker) (1:1000; [132]) and anti-GAPDH (cytosolic marker) (1:1000; Abcam, Cambridge, MA)

Immunoblot analyses

The detailed protocol for immunoblot analyses using Rtbdn antibody were performed as previously published [56]. Briefly, frozen retinas were placed in 1XPBS (pH 7.2) containing 1% Triton X-100, 1% protease inhibitor cocktail (PIN) and sonicated. After 1 hour incubation at 4C, they were spun at 16,128 g for 5 min and prepared for loading on the gel using Laemmli buffer containing SDS and 5% betamercaptaethanol. Samples were separated by SDS-PAGE, and proteins were transferred to a PVDF membrane. The membrane was blocked with 5% milk and incubated with Rtbdn antibody (1:500; in-house) [56] for 30 min at room temperature. The same blot was dried and reblotted with anti-beta-Actin-HRP (1:50000; A3854 Sigma-Aldrich, St.Louis, MO) for normalization. Blots were imaged using ChemiDoc™ MP imaging system (Bio-rad) and quantification was performed densitometrically, using Bio-rad Image Lab v4.1 software.

Immunohistochemistry

Whole eyes were harvested and immersion fixed in Davidson's fixative (32% ethanol, 11% acetic acid, 2% formaldehyde) overnight. They were dehydrated by submerging in 70%, 80%, 90%, and 100% absolute ethanol for 30 min each and transferred to xylene for clearing for 1 hour and finally embedded in paraffin. 10 μm paraffin sections, obtained using microtome, were subjected to immunolabeling using anti-Rtbdn and anti-Prph2 following procedures described previously [56]. Briefly, slides were re-hydrated, boiled in citrate buffer (pH 6.0 containing 5% Tween) for 20 min for antigen retrieval, and blocked with 2% donkey serum, 1% fish gelatin, 1%

triton, and 1XPBS (pH7.2). Primary antibodies were used as described above. Anti-Prph2 applied overnight, while Rtbdn applied for 30 min at room temperature sequentially. Secondary antibodies were Alexa 647 (rabbit) and Alexa 555 (mouse) (Life technologies, Grand Island, NY, USA).

DAPI (Thermo Fisher Scientific, 62248) was applied after the secondary incubation for 15 min at a concentration of 0.1µg/mL. Slides were washed and mounted and imaged using Zeiss 800 LSM confocal airycan system and processed in Zen 2 lite software.

Electroretinography

Full field ERG was performed as described previously [133] using the UTAS system (LKC, GAuthersburg, MD, USA). In brief, mice were dark adapted overnight and anesthetized with an intramuscular injection of ketamine (85 mg/kg) and xylazine (14 mg/kg). 1% cylopentolate hydrochloride ophthalmic solution by SANDOZ was used to dilate the pupils. Small amount of 2.5% hypromellose ophthalmic demulcent solution by AKORN was applied on each cornea and platinum electrodes were positioned on them. A set of platinum electrodes were inserted into the tail (ground) and forehead (as reference). The rod function (scotopic) was recorded in response to a 157.7 cds/m^2 single flash. Mice were light adapted at 29.03 cd/m^2 intensity for 5 min, and cone function (photopic) was measured by averaging responses to 25 flashes at 79 cd s/m^2 intensity. Scotopic and photopic measurements obtained from right and left eyes were averaged and counted as a single sample.

Light and transmission electron microscopy examination

Mice were euthanized by CO_2 asphyxiation, and their eyes were harvested, and placed in EM grade fixative (2% paraformaldehyde, 2% glutaraldehyde, 100mM Cacodylate, 0.025% $CaCl_2$ (pH 7.4 final mixture)). After 2 hours, the eyes were enucleated and returned back to the fixative and kept at 4°C overnight. The plastic embedding and sectioning were performed as described previously [97]. For light microscopy, 10 μm sections were stained with toluidine blue and images were captured at 40x using Zeiss Axioskop 50. Images were collected from the superior hemisphere, 500 μm distance away from the optic nerve head. For electron microscopy, 600-800 Å thick sections were stained with 2% (v/v) uranyl acetate and Reynold's lead citrate and imaged using JEOL 100CX microscope at 5,000x and 25,000x.

Quantitative morphometry

Paraffin sections that were cut along the optic nerve were chosen. After rehydration steps, they were soaked in Hematoxylin (MHS16, Sigma, Burlington, MA, USA) for 4 min, washed thoroughly and dipped in to the 0.3% acid alcohol for 4 times. The slides were rinsed with water and soaked in to the Eosin (HT110116, Sigma, USA) for 2 min. They were washed again, dehydrated, cleared, and mounted using permount mounting medium (SP15100, Fisher Scientific). To count nuclei, the ONL of entire retina was imaged at 20x objective and the length of 100 μm marked at intervals of 200 μm. The number of nuclei at the corresponding locations were counted manually using image J software.

Cone count

Paraffin sections were obtained and dehydrated as described above. The slides were boiled in EDTA buffer for 20 minutes for antigen retrieval and blocked with 0.5 % Triton X-100, 5% bovine serum albumin and 2% donkey serum in 1XPBS (pH 7.4). Peanut agglutinin (PNA) was applied at 1:500 dilution and kept at 4°C overnight. The sections were mounted and z-stack images were captured 300 μm inferior and superior to the optic nerve. The cone photoreceptors were counted on the collapsed z-stack images. The numbers counted from superior and inferior sides were averaged to obtain a single value for that mouse.

Fundus and Fluorescein Angiography

Mice were anesthetized with ketamine/xylazine and their pupils were dilated. Bright field funduscopic images were captured using Phoenix micron IV system (Phoenix Research Laboratories, Pleasanton, CA), and then mice were intraperitoneally injected with fluorescein (0.001ml/gm; Akorn Ak-fluor 10%). Angiographic images were captured after 30 seconds of fluorescein injection using the same system at a uniform light, voltage and gain conditions for all animals.

HPLC analysis of Flavins

Extraction and quantification of flavins in retinal samples were performed as previously published [90]. Mice were fasted for 6 h prior sample collection to prevent flavin intake variability among each other's. In summary, frozen retinas from them were homogenized in 1XPBS and centrifuged at 10,000g for 10 min at 4 ºC. The

supernatant was collected and 10% TCA was added to it to precipitate proteins. Samples were later filtered through 0.45μm filter and transferred to Waters HPLC system (Waters, Milford, MA, USA) for analysis. Riboflavin, FMN and FAD amounts were analyzed by measuring the area under curve (AUC) for each corresponding peak that appeared at the identified retention time. The AUC raw data was converted to pmol using the standard curve for each component.

Quantification of ATP levels in retina

Retinal ATP levels were quantified using abcam (ab113849) Luminescent ATP Detection Assay Kit following supplier's protocol. In brief, fresh retinas were placed in 1xPBS containing 1% PIN and homogenized using sonication. Samples were centrifuged at 16,128g for 5 min and supernatant was transferred to a single well of 96 well plate. The detergent in the kit was added to each well and incubated at room temperature for 10 min on a shaker. Finally, the substrate solution in the kit was added and incubated for another 15 min at room temperature. The plate was placed in the microplate reader (Spectramax M5, Molecular devices, Sunnyvale, CA) to measure the ATP levels for each sample. This experiment was performed under dim red light.

Statistical Analysis

Statistical significance was determined by one- or two-way ANOVA with Tukey's post-hoc comparison. All values are given as means ± SEM. Graphpad Prism 7 was used for the quantitative analysis.

4.3. Results

4.3.1 Rtbdn upregulation in the Prph2$^{Y141C/+}$ retina

To investigate Rtbdn in pathological condition, we first examined its expression profile in the diseased retina. The *Prph2*$^{Y141C/+}$ retinas that were collected at the age of post-natal day (P) 30 had ~2.35 fold greater Rtbdn expression than the age matched WT retinas ($P<0.0001$) (Fig. 4.1A). At P90, Rtbdn levels of the *Prph2*$^{Y141C/+}$ retinas were comparable to the control group, if normalized to actin. The age-dependent decline of Rtbdn levels in *Prph2*$^{Y141C/+}$ retinas was potentially due to loss of photoreceptor cells. Thus, we normalized the Rtbdn levels with photoreceptor nuclei counted across the retina for each genotype/age. In this case, we observed ~2.34 fold and ~2.13 fold greater Rtbdn levels in the *Prph2*$^{Y141C/+}$ retinas at P30 and P90 respectively ($P<0.0001$).

We examined Rtbdn expression in both healthy and *Prph2*$^{Y14C/+}$ retinas using immunohistochemistry as well and observed stronger Rtbdn immunoreactivity in *Prph2*$^{Y141C/+}$ retinas compared to WT controls (Fig. 4.1B). Rtbdn was detected at the tip of the photoreceptor OSs and around the IS area in WT adult mice, confirming the published data [56, 60]. However, presence of the Y141C mutation altered the distribution of Rtbdn. Instead of concentrating at the tips, the wide spread immunoreactivity in the OS may be attributed to the diffusion of Rtbdn due to perturbed photoreceptors or redistribution of the protein to display its function at the entire span of the photoreceptor layer. Upregulation and altered distribution of Rtbdn suggest a role to Rtbdn in degeneration.

Rtbdn is a membrane bound protein in normal conditions [56]. Here, we addressed the subcellular localization of Rtbdn in diseased retinas and revealed that it remains to be membrane bound during degenerative process (Fig. 4.1C). Both WT and *Prph2*$^{Y141C/+}$ retinas had the majority of Rtbdn expression in the membrane fraction with much lower level in the cytoplasmic portion (likely newly synthesized protein), and non-detectable levels in soluble fraction.

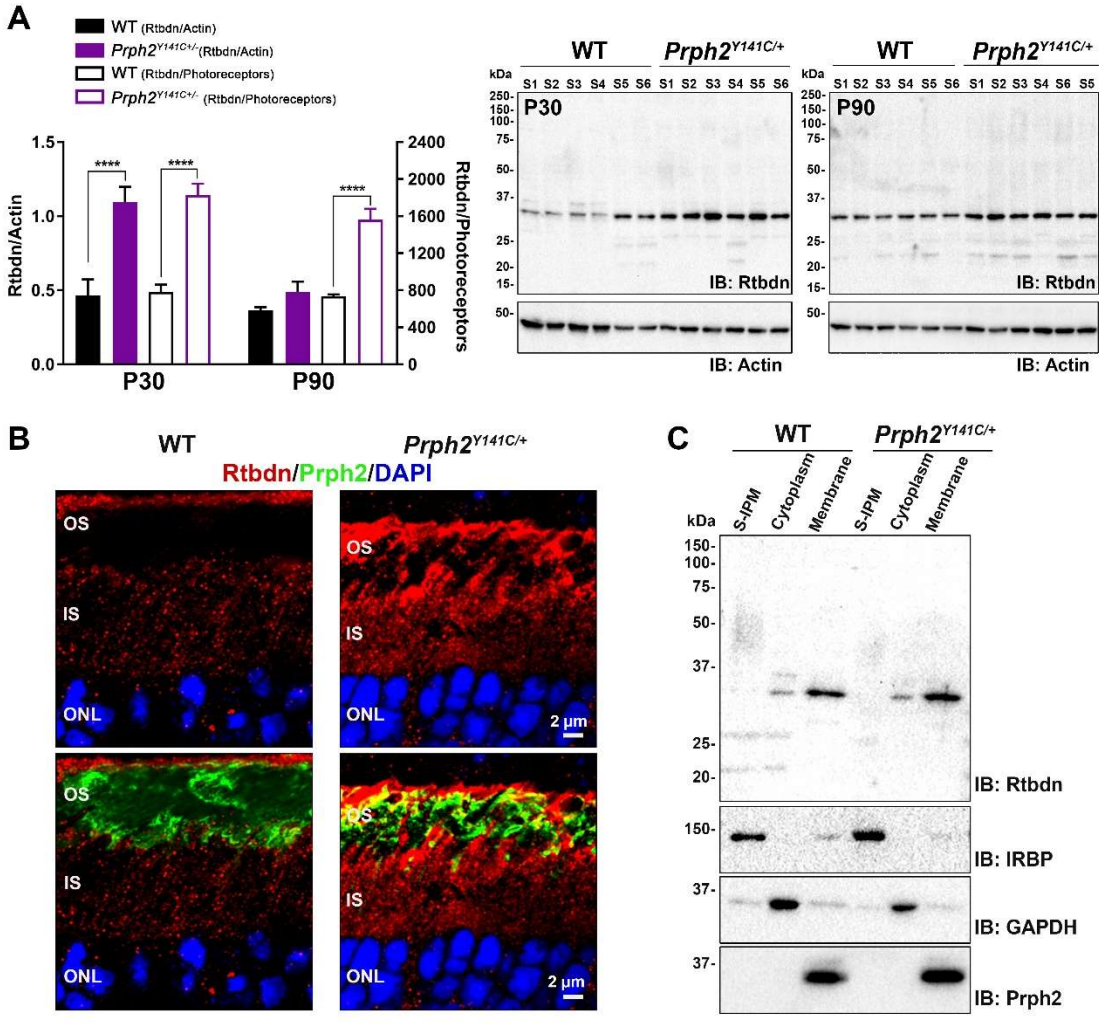

Figure 4.1. Rtbdn upregulation and its cellular localization in *Prph2*$^{Y141C/+}$ retina. **A.** Immunoblots of Rtbdn. **B.** Immunohistochemical analysis of Rtbdn. **C.** Western blot analysis of retinal extracts separated into subcellular fractions.

4.3.2 Elimination of Rtbdn leads to functional decline in the Prph2$^{Y141C/+}$ retina

Upregulation and altered distribution of Rtbdn in the *Prph2*$^{Y141C/+}$ retina prompted us to analyze the genomic deletion of Rtbdn in the *Prph2*$^{Y141C/+}$ mice. To investigate the role of Rtbdn in degenerative process, we crossed Y141C mice with the *Rtbdn*$^{-/-}$ ones. We previously showed that both scotopic and photopic ERG responses of the *Rtbdn*$^{-/-}$ mice were not different than the WT ERG responses till P120 [60]. To determine whether Rtbdn elimination has any functional impact on the diseased retina, we performed ERGs on the *Prph2*$^{Y141C/+}$*/Rtbdn*$^{-/-}$ mice and age matched WT, *Rtbdn*$^{-/-}$ and, *Prph2*$^{Y141C/+}$ controls. Conforming the previous study [60], scotopic- a and photopic b-wave amplitudes of *Rtbdn*$^{-/-}$ mice resembled the WT ERGs (Fig 4.2). However, elimination of Rtbdn accelerated functional decline in the *Prph2*$^{Y141C/+}$; both scotopic a- and photopic b- amplitudes of *Prph2*$^{Y141C/+}$*/Rtbdn*$^{-/-}$ mice were significantly below the *Prph2*$^{Y141C/+}$ amplitudes at P30 and remained lower than *Prph2*$^{Y141C/+}$ for all ages examined (n=9-14) (Fig. 4.3). At P30, compared to *Prph2*$^{Y141C/+}$, the reduction (~34%) in photopic b- wave amplitude of *Prph2*$^{Y141C/+}$*/Rtbdn*$^{-/-}$ mice was proportionally larger than the reduction in scotopic-a wave (~25%). There was no significant changes in the scotopic b- values between *Prph2*$^{Y141C/+}$ and *Prph2*$^{Y141C/+}$*/Rtbdn*$^{-/-}$ at any ages examined (data not shown). Both *Prhp*$^{Y141C/+}$ and *Prph2*$^{Y141C/+}$*/Rtbdn*$^{-/-}$ amplitudes showed minor progressive decline over time. The age dependent reduction in scotopic a- responses from *Prph2*$^{Y141C/+}$*/Rtbdn*$^{-/-}$ mice paralleled that of *Prph2*$^{Y141C/+}$ and lost significant decline over time for photopic b-

amplitudes, suggesting that the functional deficits due to Rtbdn absence initially arose during retinal development.

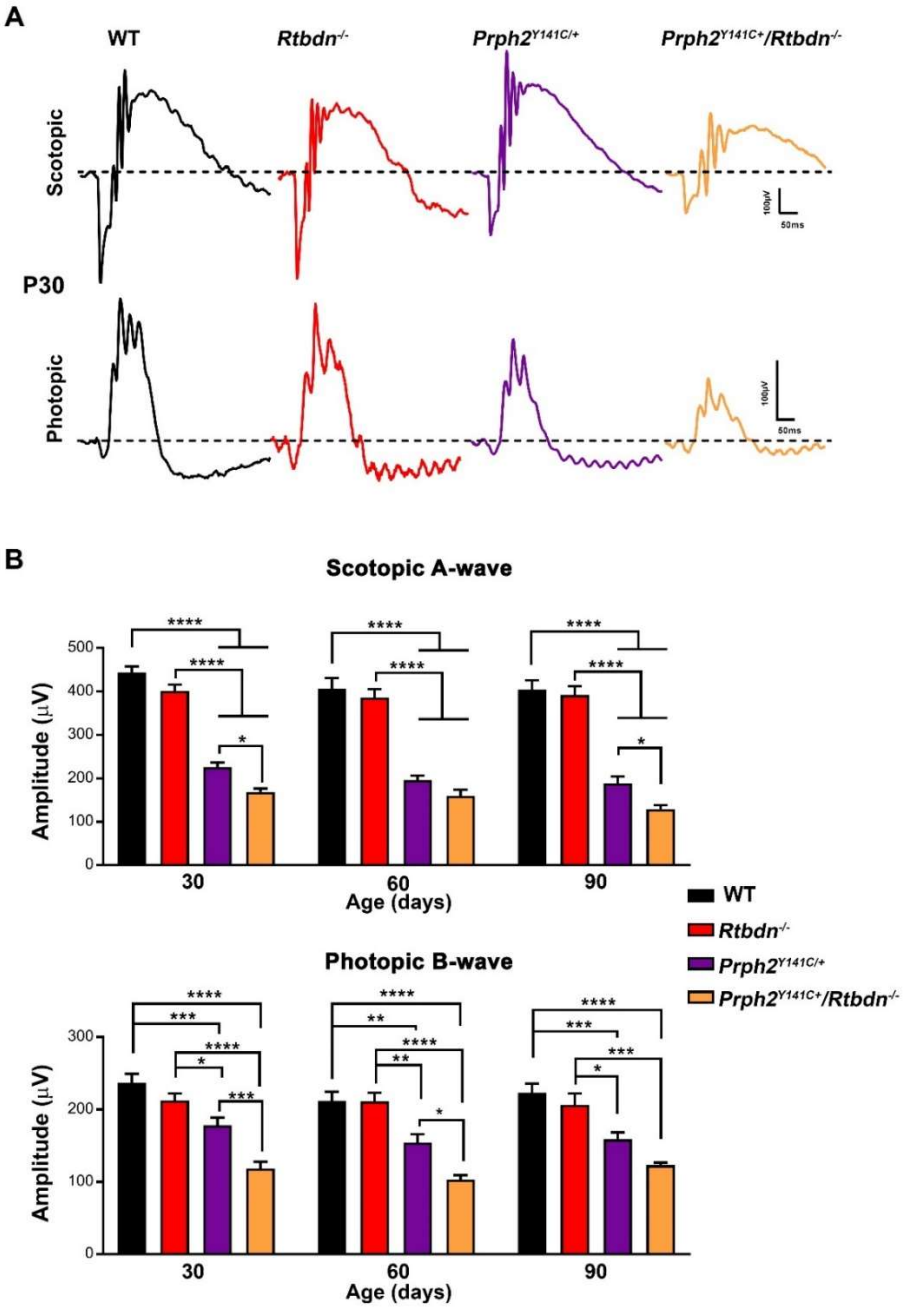

Figure 4.2. Lacking Rtbdn in the *Prph*$^{Y141C/+}$ mice reduce the retinal function. **A.** Representative waveforms of full field ERG responses under scotopic and photopic conditions. **B.** Scotopic a- wave and photopic b- wave amplitudes.

4.3.3 Ablation of Rtbdn in Prph2$^{Y141C/+}$ retina exacerbates the thinning of OSs and photoreceptor loss

The reduced ERG responses of *Prph2$^{Y141C/+}$/Rtbdn$^{-/-}$* mice potentially could arise from degeneration of photoreceptors. Alternatively, this might result from functional changes unrelated to cell loss. To determine the reason of exacerbated functional decline in the *Prph2$^{Y141C/+}$/Rtbdn$^{-/-}$* (Fig. 4.2), we examined the structure of the retinas at light microscopic level (n=4). Histologic assessments of *Rtbdn$^{-/-}$* retinas revealed no degenerative changes neither at P30 nor P90 (Fig. 4.3A). At P30, the outer nuclear layer (ONL) thickness of *Prph2$^{Y141C/+}$* and *Prph2$^{Y141C/+}$/Rtbdn$^{-/-}$* were not significantly different than the WT and *Rtbdn$^{-/-}$* controls. However, *Prph2$^{Y141C/+}$* retinas displayed shorter OSs that was much more severe in the *Prph2$^{Y141C/+}$/Rtbdn$^{-/-}$* ones. By P90, the *Prph2$^{Y141C/+}$* ONL was thinner compared to WT but significantly thicker than the *Prph2$^{Y141C/+}$/Rtbdn$^{-/-}$* ONL. To quantify photoreceptor degeneration, we counted ONL nuclei along the superior and inferior plane. ONL counts in WT and *Rtbdn$^{-/-}$* were not different from each other at neither ages (Fig. 4.3C). At P30, there was a slight reduction in *Prph2$^{Y141C/+}$/Rtbdn$^{-/-}$* retinas compared to *Prph2$^{Y141C/+}$* but the differences was not significant. At P90, ONL counts were significantly reduced in most parts of the *Prph2$^{Y141C/+}$/Rtbdn$^{-/-}$* retina (~19%), compared to *Prph2$^{Y141C/+}$*.

To determine whether photopic b- response reduction, we observed at P30, arise from cone loss, we counted the cone photoreceptors identified by PNA labeling in vertical sections (Fig. 4.3B&D). Cone numbers in the *Prph2$^{Y141C/+}$/Rtbdn$^{-/-}$* were similar to *Prph2$^{Y141C/+}$*, suggesting the reduced photopic ERGs were unrelated to cell loss at this age.

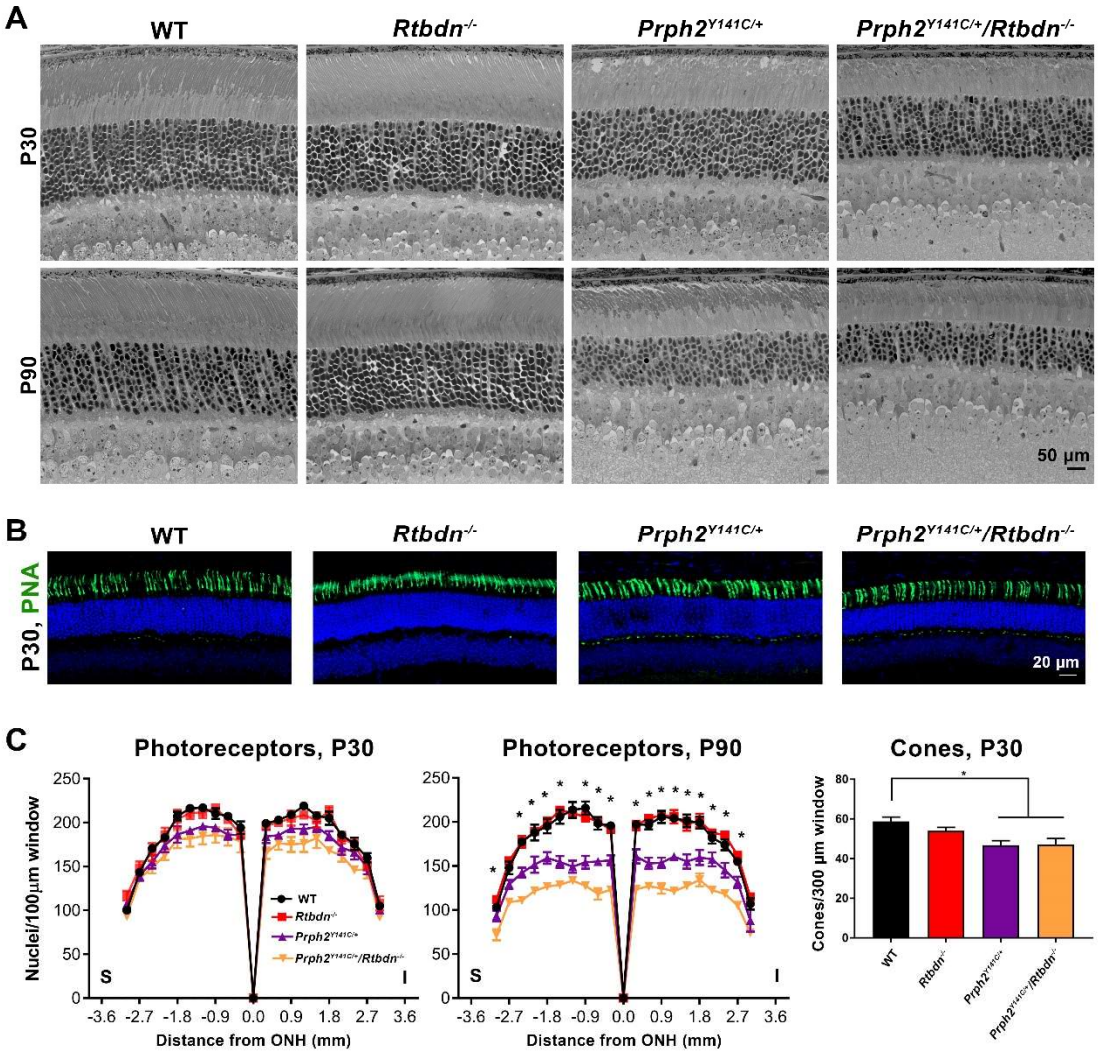

Figure 4.3. Rtbdn absence in *Prph2*$^{Y141C/+}$ retina accelerates photoreceptor loss
A. Light microscopic images of retinal sections **B.** Cone photoreceptors were labeled with PNA **C.** Photoreceptor nuclei count **D.** Cone photoreceptor count.

4.3.4 Prph2$^{Y141C/+}$*/ Rtbdn*$^{-/-}$ *mice exhibited ultrastructural abnormalities within the outer retina, RPE, and Bruch's membrane*

To further characterize the changes observed in light microscopy, ultrastructural examination of the outer retina, as well as RPE, and sub-RPE space was performed. We analyzed the retinas by transmission electron microscopy at P30 when

we observed functional decline, but no photoreceptor nuclei loss in the *Prph2*$^{Y141C/+}$/*Rtbdn*$^{-/-}$ mice, compared to *Prph2*$^{Y141C/+}$. At this age, while ultrastructure of *Rtbdn*$^{-/-}$ retinas were indistinguishable from those in WT ones, elimination of Rtbdn in the *Prph2*$^{Y141C/+}$ mice led to further destruction of photoreceptor OSs. (Fig. 4.4, upper panel). Many photoreceptors in the double mutant were lacked OSs entirely and some of the OSs had whorl like and enlarged morphology (black arrow head). Since the integrity of OSs are crucial for the survival of photoreceptors [150], the reduced photoreceptor nuclei of *Prph2*$^{Y141C/+}$/*Rtbdn*$^{-/-}$ at P90 (Fig 4.3C) might be associated with the prior disturbance of OSs at P30. We also observed vesicular structures (black arrow) at close proximity to the connecting cilium in both *Prph2*$^{Y141C/+}$ and *Prph2*$^{Y141C/+}$/*Rtbdn*$^{-/-}$ retinas (Fig. 4.4, lower panel), however, these vesicles were encountered more frequently in the double mutants.

Moreover, *Prph2*$^{Y141C/+}$ and *Prph2*$^{Y141C/+}$/*Rtbdn*$^{-/-}$ eyes showed presence of undefined structures within RPE cells (white arrow) that were larger and more frequent in the double mutant. We also examined the BM and observed numerous round, electro-lucent, non-membrane bound particles (white arrow head) within the BM of *Rtbdn*$^{-/-}$ and *Prph2*$^{Y141C/+}$/*Rtbdn*$^{-/-}$ mice. These particles in the per unit length of *Prph2*$^{Y141C/+}$/*Rtbdn*$^{-/-}$ BM was more in number, compared to *Rtbdn*$^{-/-}$. These electro-lucent particles that scattered throughout the BM may be lipid associated materials similar to prior findings [151, 152]. Finally, we observed thickening of BM in the *Prph2*$^{Y141C/+}$/*Rtbdn*$^{-/-}$ mice.

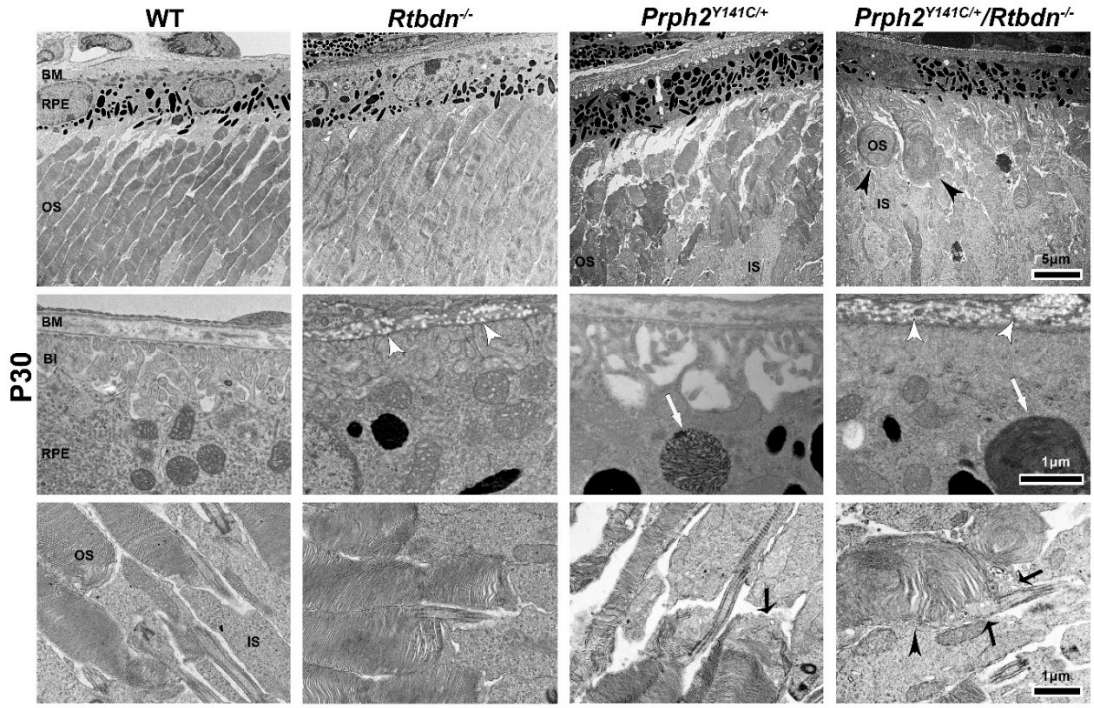

Figure 4.4. Genetic deficiency of Rtbdn in the *Prph2*$^{Y141C/+}$ causes ultrastructural changes in the Bruch's membrane, RPE and retina.
Representative EM images of outer retina/RPE and the OS/IS junction

4.3.5 Rtbdn lacked Prph2$^{Y141C/+}$ *mice exhibited fundus abnormalities and signs of neovascularization*

We examined the ocular phenotype of *Prph2*$^{Y141C/+}$*/Rtbdn*$^{-/-}$ mice and age matched controls by means of fundus photography and fundus angiography. Fundoscopic images of *Rtbdn*$^{-/-}$ mice were indistinguishable from those in WT animals (Fig. 4.5). Confirming the previous study [50], fundus photography revealed widespread flecks (black arrows) that increased with age in P90-P150 *Prph2*$^{Y141C/+}$ mice. These speckles were strikingly, larger in the *Prph2*$^{Y141C/+}$*/Rtbdn*$^{-/-}$ animals and they had patchy pigmentary appearance. Additionally, some of the double mutants

displayed bright spots (white arrow head) which were suggested as drusen-like deposits in the Apo E knock-out mice [153].

Retinal vasculature was analyzed by fluorescein angiography. Signs of neovascularization such as dense capillary bed and neovascular tufts (white arrows) were observed in *Prph2*$^{Y141C/+}$/*Rtbdn*$^{-/-}$ eyes. These features were absent or attenuated in age matched *Prph2*$^{Y141C/+}$ mice.

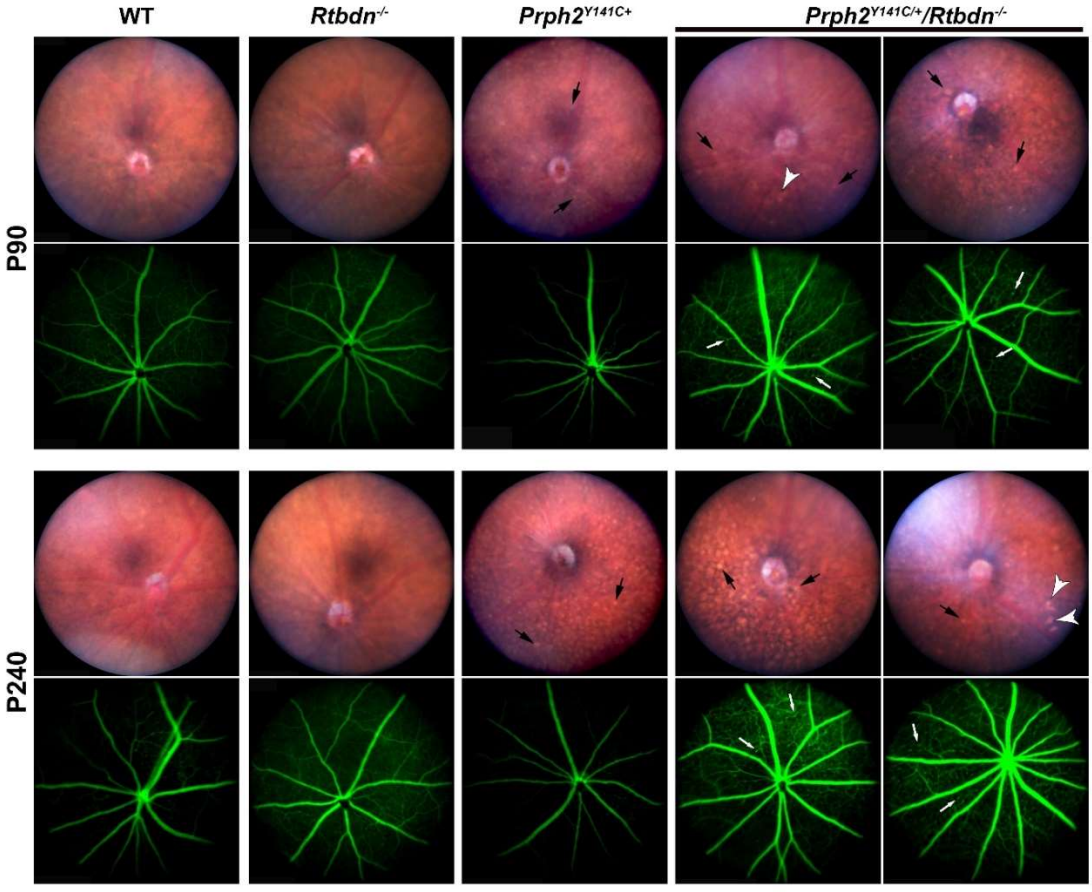

Figure 4.5. Fundus abnormalities and subretinal neovascularization in the *Prph2*$^{Y141C/+}$/*Rtbdn*$^{-/-}$ mice. Bright field fundus and fluorescein angiograms of mice from each group. Two different images from *Rtbdn*$^{-/-}$/*Rho*$^{Y141C/+}$ mice were displayed.

4.3.6 Retinal flavin levels display Rtbdn dependent differences

Since we observed significant upregulation of Rtbdn in the *Prph2*$^{Y141C/+}$ retinas (Fig. 4.1A) and Rtbdn is closely associated with flavin acquisition to the retina [60], we performed riboflavin, FMN, and FAD quantification using high-performance liquid chromatography (HPLC) to determine whether presence and absence of Rtbdn modulates the flavin levels in the *Prph2*$^{Y141C/+}$ retinas at P30. The concentration of all three flavins in the *Rtbdn*$^{-/-}$ retinas were significantly reduced, compared to WT samples (Fig. 4.6A-C) that confirms our previous study [60] and supports Rtbdn's role in flavin acquisition in the retina. The *Prph2*$^{Y141C/+}$ retina contained the highest riboflavin concentration that is ~4.1 fold higher compared to WT and ~6.3 and ~4.6 fold higher compared to *Rtbdn*$^{-/-}$ and *Prph2*$^{Y141C/+}$*/Rtbdn*$^{-/-}$ respectively (Fig 4.6A). The FMN levels of *Prph2*$^{Y141C/+}$ was slightly but not significantly higher compared to WT (Fig. 4.6B), while FAD levels were significantly reduced (Fig. 4.6C). This pattern of flavin distribution in the *Prph2*$^{Y141C/+}$ may reflect the need of each flavin type in altered metabolism or defects in conversion to FMN and FAD. Lack of Rtbdn in the *Prph2*$^{Y141C/+}$*/Rtbdn*$^{-/-}$ resulted reduction in all three flavins compared to *Prph2*$^{Y141C/+}$ that is significant in riboflavin and FMN (Fig. 4.6A,B) but not significant in FAD (Fig. 4.6C). Individual flavin values (riboflavin, FMN, and FAD) were added together to calculate the total flavin levels. Fig. 4.6D shows the total flavin levels, in which the significantly increased flavin levels in the *Prph2*$^{Y141C/+}$ is reflective of increased Rtbdn levels.

This data combination with the reduced flavin levels in the *Prph2*$^{Y141C/+}$*/Rtbdn*$^{-/-}$ retinas support the Rtbdn's role in facilitating the enrichment of flavin levels in the retina.

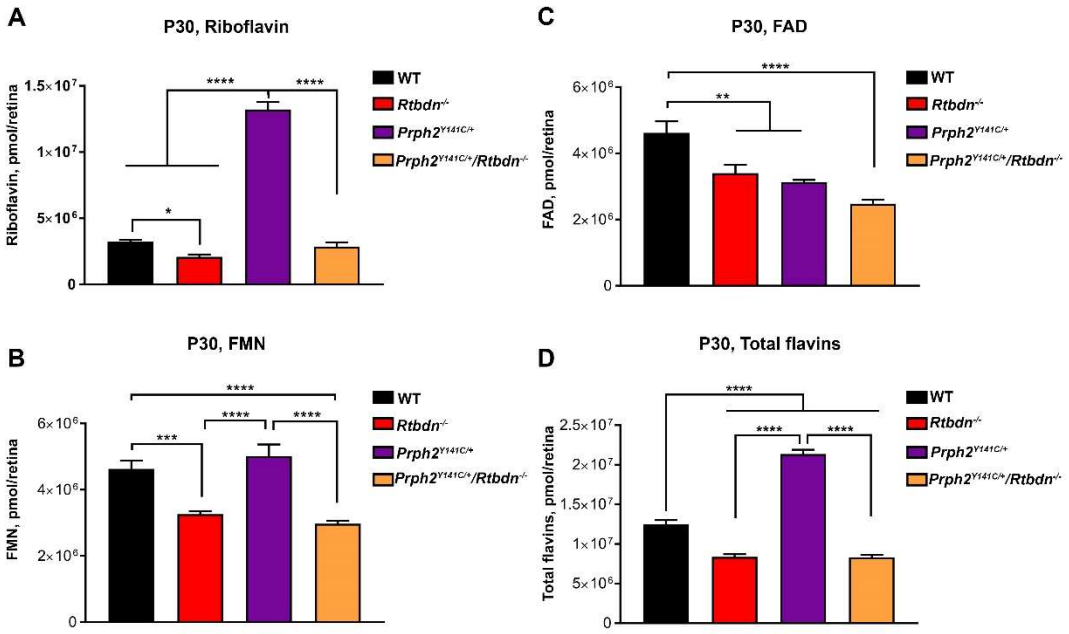

Figure 4.6. Elimination of Rtbdn results reduced flavin levels in the *Prph2*$^{Y141C/+}$ retina.
Steady state levels of **A.** Riboflavin, **B.** FMN, **C.** FAD, and **D.** Total flavins.

ATP production rely on flavoenzymes which are functionally dependent on FMN and FAD that are derived from riboflavin. Thus, disturbance in riboflavin homeostasis may result in mitochondrial dysfunction by means of reduced energy levels. We analyzed ATP levels to gain more insight about the mechanism behind the exacerbated retinal degeneration of *Prph2*$^{Y141C/+}$*/ Rtbdn*$^{-/-}$. The steady state ATP levels (Fig. 4.7) resembled the total flavin levels profile (Fig. 4.6D); however, there was no significance among any of the groups analyzed.

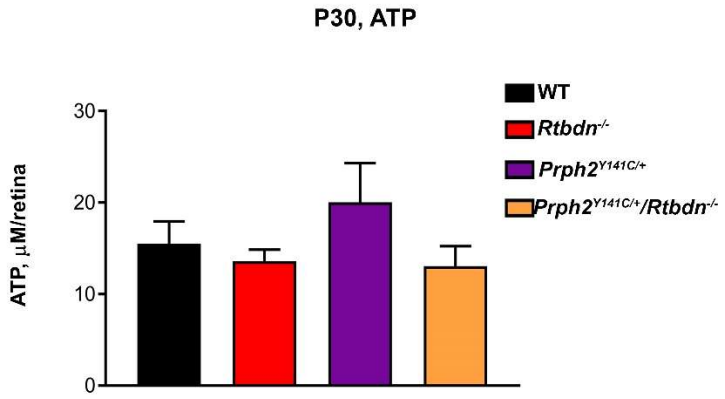

Figure 4.7. Steady state retinal ATP levels.

4.4 Discussion

The *Prph2*$^{Y141C/+}$ knock-in mouse model serves as an established pattern dystrophy model which mimics patients phenotype [50]. In our study, Rtbdn was found to be significantly upregulated in the *Prph2*$^{Y141C/+}$ retinas. To determine the role of Rtbdn in this pathological condition, we studied the *Prph2*$^{Y141C/+}$/*Rtbdn*$^{-/-}$ mice. Elimination of Rtbdn in the *Prph2*$^{Y141C/+}$ mice accelerated the retinal disease progression. The photoreceptor nuclei loss was consistent with the functional deficits shown by the diminished rod and cone ERG responses compared to the *Prph2*$^{Y141C/+}$ control group. Reflecting the increased Rtbdn levels, we observed significantly elevated levels of riboflavin in the *Prph2*$^{Y141C/+}$ retinas compared to WT. Furthermore, genomic deletion of Rtbdn in *Prph2*$^{Y141C/+}$ resulted in significant reduction in riboflavin and FMN levels compared to the control groups. Our findings suggest that Rtbdn might exert neuroprotective effects by modulating the flavin mechanism.

Upregulation of Rtbdn during degenerative process could reflect cell death, or the cell's attempt to switch on tissue protective mechanism. Reduced photoreceptor function and accelerated photoreceptor cell death in the *Prph2*$^{Y141C/+}$/*Rtbdn*$^{-/-}$ mice due to the elimination of Rtbdn suggests that Rtbdn plays role in survival mechanism rather than in apoptosis. Function of flavoenzymes, which protect the cells from oxidative stress and apoptosis, are regulated by flavins. Thus, it is not surprising that any disturbance in flavin metabolism leads to various pathological conditions [127]. Considering the riboflavin binding capability of Rtbdn, its localization at the RPE/OS junction, and reduced flavin levels in the *Rtbdn*$^{-/-}$ retinas, we hypothesized that Rtbdn plays role in acquisition and enrichment of flavins in the retina. Supporting our hypothesis we observed significantly elevated levels of total flavins in the *Prph2*$^{Y141C/+}$ retinas compared to WT. Despite the very high riboflavin and slightly increased FMN levels in the *Prph2*$^{Y141C/+}$, FAD levels were significantly lower compared to WT. This might be either due to an insufficient conversion of FMN into FAD or the specific need to FMN in the diseased retina. In our previous study, we observed similar results: in which P30 Rhodopsin knock-out (*Rho*$^{-/-}$) retinas displayed reduced FAD, while FMN levels were comparable to WT [90]. The photoreceptor cell number is not compromised in P30 *Rho*$^{-/-}$ retinas while there is no OSs [150]. In the *Prph2*$^{Y141C/+}$ we also didn't observe any reduction in the photoreceptor cell count at the age which we performed flavin quantification, however, OSs were diminished. This suggest an association between FAD levels and photoreceptor OS health status.

Consistent with the potential flavin enrichment role of Rtbdn, we observed reduced flavin levels in the *Prph2*$^{Y141C/+}$*/Rtbdn*$^{-/-}$ retinas. In the electron transport chain, FMN is utilized by NADH-Coenzyme Q reductase in complex I, while FAD participate in the activity of complex II and acts as a cofactor for succinate dehydrogenase in the Kreb's cycle. Defects in electron transport chain enhance the production of reactive oxygen species (ROS) and the excess amounts leads membrane lipid peroxidation and DNA damage that ultimately cause neuronal cell death [154-158]. The oxidative damage and degeneration was found to be reduced by glutathione that is catalyzed by glutathione reductase which is an FAD dependent enzyme [159]. Considering the interaction between riboflavin and flavoproteins in terms their role in protecting cells from oxidative stress and apoptosis, exacerbated functional decline and cell death in the *Prph2*$^{Y141C/+}$*/Rtbdn*$^{-/-}$ retinas could be the reason of reduced FMN and FAD, which are the active form of riboflavin.

One interesting observation in the *Prph2*$^{Y141C/+}$*/Rtbdn*$^{-/-}$ eyes is the presence of neovascular tufts and dense capillary bed. Previous studies have evidenced that early photoreceptor dysfunction further affects the blood supply and induce neovascularization [123, 160, 161]. Metabolic demands push angiogenesis [145, 160, 161] and also disturbances in flavin homeostasis accompanied by oxidative stress triggers retinal vascular abnormalities. While the precise mechanism is *unknown*, our findings demonstrated that disturbed photoreceptor activity induced pathological vascular remodeling during degeneration which suggests that this is a Rtbdn mediated mechanism, as additional deletion of Rtbdn resulted in signs of neovascularization.

A surprising finding in the Rtbdn$^{-/-}$ and *Prph2*$^{Y141C/+}$/*Rtbdn*$^{-/-}$ mice is the electro-lucent particles in the BM. These particles were more per unit area in the *Prph2*$^{Y141C/+}$/*Rtbdn*$^{-/-}$ ones. Curcio and colleagues analyzed the electro-lucent droplets recognized in BM using ultrastructural techniques that preserve lipid particle morphology and they demonstrated that these droplets are esterified fatty acid particles [152]. A potential source of cholesterol deposition in the BM is lipid rich OS membranes that are regularly ingested by RPE. Although there is currently no concreate reason to suspect that RPE is the source of cholesterol deposition in the BM, it is possible that retaining components could be released into BM due to the burden on the RPE upon cell death. Upregulation of vascular endothelial growth factor was correlated with accumulation of lipids particles in BM of low density lipo-protein receptor deficient mice [151]. Also, accumulation of lipids in BM is believed to alter its diffusion characteristics and potentially compromises the metabolic exchange between choroid and retina affecting photoreceptor function [162]. Altogether, suggest a link between lipid accumulation, neovascularization, and photoreceptor cell death. These data support the rationale for seeking the link between pathogenic mechanism of other conditions which display lipid associated deposits in BM and the Rtbdn deficient mice.

Our findings demonstrate upregulation of Rtdbn as a molecular response to the insults and exacerbation of retinal disease progression as a consequence of its elimination. It is necessary to test whether Rtbdn overexpression or activation of its signaling components prevent photoreceptor degeneration associated with pattern

dystrophy. Our results correlate the elevation of endogenous Rtbdn with higher flavin levels that play important role in metabolism and support photoreceptor survival. The precise molecular mechanism by which Rtbdn protects damaged photoreceptor cells remains elusive. To determine if flavin related pathways are the reason behind the photoreceptor dysfunction, the metabolome of the *Prph2*$^{Y141C/+}$/*Rtbdn*$^{-/-}$ retina should be analyzed in reference to *Prph2*$^{Y141C/+}$. Additional studies will be necessary to understand how widely Rtbdn is operative not only in retia but in the surrounding tissues as well. Future studies should investigate whether overexpression of Rtbdn mediates protection over photoreceptor cells and the mechanism by which Rtbdn regulates. Understanding such a mechanism is important to develop new treatment strategies. Our findings suggest that Rtbdn upregulation has potential therapeutic value in pattern dystrophy. We show that ablation of Rtbdn in *Prph2*$^{Y141C/+}$ resulted in acceleration of photoreceptor cell death with reduction of flavin levels and probably disturbance of subsequent metabolic activities.

Chapter 5 – Developmental pattern of expression of Rtbdn

5.1 Introduction

Ageing in general can be defined as the progressive accumulation of changes which increase susceptibility to disease and death. Evidence suggest that ageing is driven by highly conserved cell processes and studies has been going over on the hallmarks of ageing, however the mechanism about the cell response to these hallmarks and how they arise remains unclear. One of the characteristic of ageing is the neuronal cell loss in the retina. Rods are more susceptible to ageing than cones; in humans, density of rods decrease by 30% in the central area between the ages of 34 and 90, while the cone density in the macular area is not affected [163, 164]. The number of ganglion cells also decrease during ageing. [164, 165]. Moreover, glial fibrillary acidic protein (GFAP) levels increase and higher levels of cytoplasmic organelles are encountered [166]. The increased astrocyte population was suggested as a protective mechanism of ageing retina against free radicals [166]. Another hallmark of ageing retina is the lipofuscin accumulation in RPE, which is a photo inducible source of reactive oxygen species [167]. Mild pathological changes can also be observed in the aged Bruch's membrane such as basal deposits and drusen. Altogether show the cumulative amount of oxidative and metabolic stress in the ageing eye. Especially retina is prone to oxidative damage by ageing due to the light exposure and polyunsaturated fatty acids rich photoreceptor membranes [168].

In the previous chapters, the role of Rtbdn was investigated in three different pathological conditions. Since ageing can lead to metabolic changes in the retina, we determined the developmental pattern of Rtbdn expression.

5.2 Materials and Methods

Animals

All of the animals were on the C57/BL6 background and re free of *rd8* and *rd1* mutations. Mice were raised under 12 hour (h) dim light (30-50 lux) and 12 h dark conditions. Males and females were equally included into the analyses. All animal procedures and experiments were approved by University of Houston institutional Animal Care and Use Committee (IACUC). For the sample collection, animals were euthanized using CO_2 asphyxiation. Retinas were extracted as described [95] and immediately frozen in liquid nitrogen and stored at -80°C until used.

Immunoblotting

The details for the WB analysis using Rtbdn antibody was described previously [56] and in previous chapters. After the membranes were probed with Rtbdn and allowed to dry, they were probed with anti-HRP conjugated beta-Actin for the sake of normalization. The blots were imaged using Bio-Rad ChemiDoc™ MP imaging system. Western blot analyses were repeated four times and blots were quantified densitometrically, using Bio-rad Image Lab v4.1 software.

5.3 Results

5.3.1 Ageing alters the Pattern of Rtbdn Expression

Kelley et al. previously showed the developmental pattern of Rtbdn expression. Accordingly, Rtbdn first appeared at P3 and levels rise and peaks at P21 [169]. Herein, we showed the pattern of Rtbdn expression in the adult retina. To do this, we performed several immunoblots on WT retinas collected at different time points from P30 to P300. Figure 5.1 shows that the levels of Rtbdn decline after P30 and reaches lowest levels by P90 but starts increasing again as the animals get older and levels of at P180 and thereafter. The increase in Rtbdn levels with age suggests that the aged retinas may be undergoing stress, similar to what we observed in our diseases models.

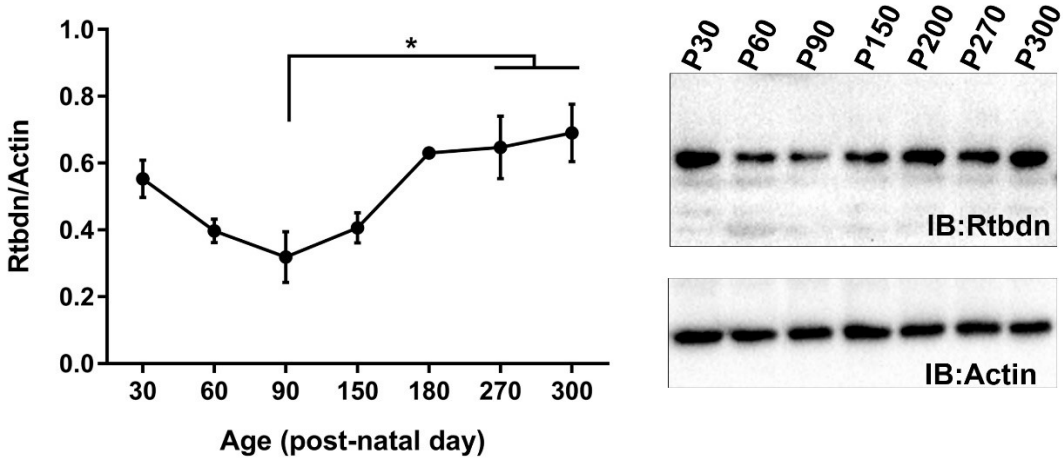

Figure 5.1. Age related expression of Retbindin in mouse retina.
Immunoblot analysis of Rtbdn for WT retinas, which were collected at different postnatal ages of mice.

We demonstrated that Rtbdn levels are significantly upregulated in mouse models of inherited retinal degenerations. Therefore, we became interested in analyzing Rtbdn in healthy aged retinas, as the normal ageing process also leads to progressive physiological changes. Numerous reports suggest that oxidative stress, inflammatory markers, and basal levels of the unfolded protein response increase with age [170, 171], suggesting elevated stress in the retina. Although structural analyses of mouse retina does not show any significant reduction in photoreceptor nuclei, the functional investigation at different ages reveal gradual reduction in both scotopic a- and photopic b- wave amplitudes with age [90]. Elevation of Rtbdn in the healthy aged retina combined with its upregulation in the mice with inherited retinal diseases suggests that the ageing retina undergoes stress and that Rtbdn levels increase as a stress response.

Loss of Rtbdn had no gross effect on photoreceptor viability at young ages, however, by 240 days, *Rtbdn*$^{-/-}$ mice exhibited reduction in photoreceptor numbers. The functional decline and increased photoreceptor cell loss in the aged *Rtbdn*$^{-/-}$ retina was associated with reduced flavin levels from early ages [60]. Sinha et al. studied age–linked pattern of riboflavin cofactors (FAD and FMN) levels in the WT retinas, and they showed stable FAD and FMN levels until P180 and gradual decline after this age [90]. The trend of Rtbdn levels and the flavin cofactor levels are not correlating in the ageing retina. This attributes a secondary role to Rtbdn in stressed condition, other than its potential role in flavin homeostasis.

Chapter 6- Investigation of Retbindin Interacting Partners

6.1 Introduction

Most biological processes involve the action and regulation of multi-protein complexes. Consequently, characterization of the components of multi protein complexes through the identification of specific interacting partners is very important. We show that Rtbdn migrates at a higher molecular weight on native gel. This preliminary data suggests that Rtbdn either self-associates or interacts with other partners. The goal of this study is to identify binding partners of Rtbdn that may be involved in its biosynthetic pathway or function in the retina. This chapter summarizes the investigation of binding candidates of Rtbdn. In the present study, affinity purification method was applied to identify Rtbdn interacting partners by a shotgun proteomic strategy.

6.2 Materials and Methods

Retinal samples and cells

Cell culture was maintained in Dulbecco's modified Eagle's medium supplemented with 10% fetal bovine serum, and penicillin (30 U/ml). Human embryonic kidney (HEK) 293 cells were transfected with a vector that allows the expression of Rtbdn driven by the CMV promoter. The Rtbdn cDNA was C-terminally tagged with Flag and Myc epitopes.

All animal procedures and experiments were approved by University of Houston institutional Animal Care and Use Committee (IACUC). For the sample collection, animals were euthanized using CO_2 asphyxiation and retinas were extracted as described [95] and immediately frozen in liquid nitrogen and stored at -80°C until used.

Immunoblotting

Protein extraction and immunoblot analysis was performed as described previously [56]. Proteins were fractionated by one-dimensional 8% Native-PAGE or SDS-PAGE. Blots were incubated with the following antibodies: rabbit polyclonal anti-Rtbdn (1:500 dilution, 30 min at room temp; in house [56]), mouse monoclonal anti-Rtbdn (serum) (1:50 dilution, at 4°C overnight ; in house 6B6H5E11 or 6B6F7D6), anti-FLAG (1:1000, at 4°C overnight; Cell Signaling Technology, 14793S), and anti-Myc (1:1000, at 4°C overnight, Cell Signaling Technology , 2276S).

OS/IS enrichment

Retinas were pooled and soaked in 1XPBS containing 1%PIN and they were vortexed at 1000 rpm for 1 min to shred the OSs. The pellet was saved for IS enrichment. Supernatant, which contained OSs and soluble S-IPM, was spun at 100,000 rpm for 20 min. The supernatant obtained at this point was discarded and the pellet was considered as OS enriched fraction. The pellet which was saved for IS enrichment was incubated in the 1xPBS, 1%PIN buffer and homogenized with

mechanic homogenizer and was spun at 50,000 rpm for 30 minutes. The pellet was considered as IS enriched fraction. This protocol helped us to isolate the parts where Rtbdn is localized.

Protein Purification

Affinity purification from cells was performed in 4 different ways: 1) immunoprecipitation using monoclonal anti-Myc antibody (cell signaling technology, 2276S) ; 2) running samples through anti-Flag M1 agarose affinity gel, which is a purified mouse IgG2B monoclonal antibody covalently attached to agarose (Millipore Sigma, A4596); 3) traditional immunoprecipitation using the anti-Flag M1 agarose affinity gel beads, (Millipore Sigma, A4596); 4) immunoprecipitation using Myc-trap, magnetic beads (Chromotek, ytma-20). Immunoprecipitations were performed with standard protocol as described previously [172]. Lysates were mixed with primary antibodies and Protein A (for rabbit antibodies) and Protein G (for mouse antibodies)-Sepharose beads at 4°C overnight. The beads were washed three times with 1XPBS before loading buffer (contains 1% SDS and 2.5% BME) was added for elution. Purification using anti-FLAG agarose affinity gel and Myc-trap magnetic beads were performed following supplier's protocol. Elution was performed using Myc peptide (Chromotek, yp-1) when the purification was performed using Myc-trap. Then the samples were subjected to SDS-PAGE.

Proteomics

Affinity purified proteins were subjected to SDS-PAGE and the gel was stained with coomassie blue. After destaining to remove excess dye, band(s) were cut, washed and stored in water at 4°C. Analysis of the protein fragments was carried out by shotgun proteomics (high performance liquid chromatography combined with mass spectrometry) by the University of Rochester Proteomics Center.

6.3 Results

6.3.1 Rtbdn migrates at a higher molecular weight on native gels

Immunoblot of SDS-PAGE shows Rtbdn around 30 kDa in WT retinas. However, we show in Figure 6.1 that Rtbdn migrates at a higher molecular weight (~ 200 kDa) on Native-PAGE. This data suggest that Rtbdn either self-associates or interacts with other partners.

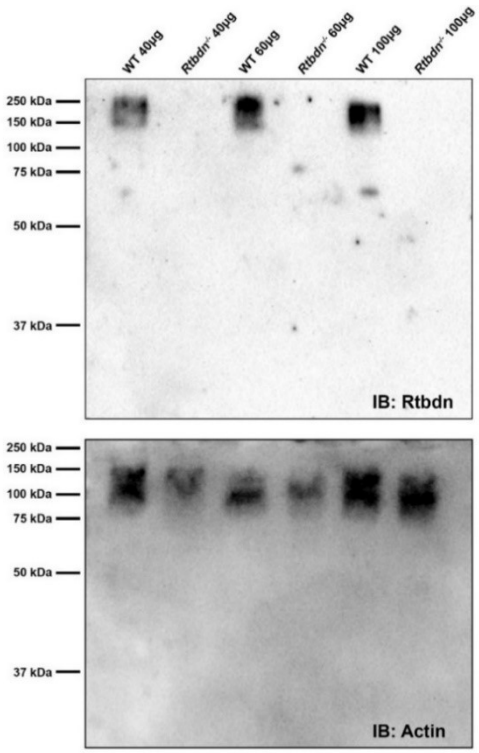

Figure 6.1. Rtbdn migrates to a higher molecular weight on native-PAGE. Blot of WT and *Rtbdn*$^{-/-}$ extracts run on a native gel and probed with anti-Rtbdn and anti-actin antibodies.

6.3.2 Identification of Potential Rtbdn Interacting Partners in Rtbdn transfected cells

To isolate Rtbdn complexes, we have previously tried immunoprecipitation with our validated polyclonal Rtbdn antibody, but unfortunately it did not work for that application. Thus, we transiently transfected FLAG and Myc-tagged Rtbdn in HEK293 cells. This allows us to use commercially available anti-FLAG and -Myc antibodies in pull-downs to study protein-protein interactions.

SDS-PAGE was used to separate lysates from transfected cells and were then analyzed using immunoblotting with antibodies against Rtbdn, Myc, and FLAG. Our rabbit polyclonal anti-Rtbdn antibody showed a single band of the expected size in

mouse WT retinal extracts, while we observed 2 strong and 1 faint bands in transiently transfected Rtbdn in HEK293 cells (Fig. 6.2A). The bands slightly migrated to a higher molecular size due to the addition of FLAG and Myc peptides. The upper band around 50 kDa was not considered since it appeared in the untransfected cells as well. Both anti-Myc and anti-FLAG antibodies showed specific signals in the Rtbdn transfected cell lanes, although no signal was detected in the untransfected cells and retina lysate lanes (Fig. 6.2A&B). This experiment validated that the transfection was successful and the cells express Rtbdn.

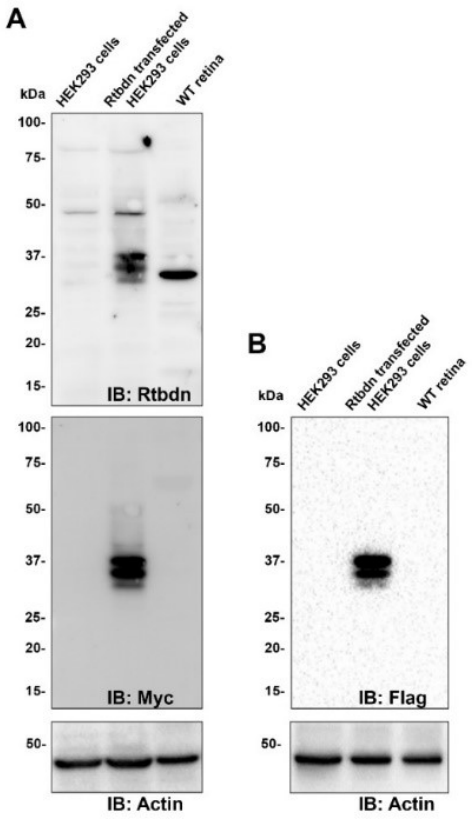

Figure 6.2. Rtbdn transfected HEK293 cells express Rtbdn, FLAG and Myc. Immunoblot analyses of Rtbdn transfected HEK293 cells. Untransfected HEK293 cells and WT retinas, served as negative and positive controls.

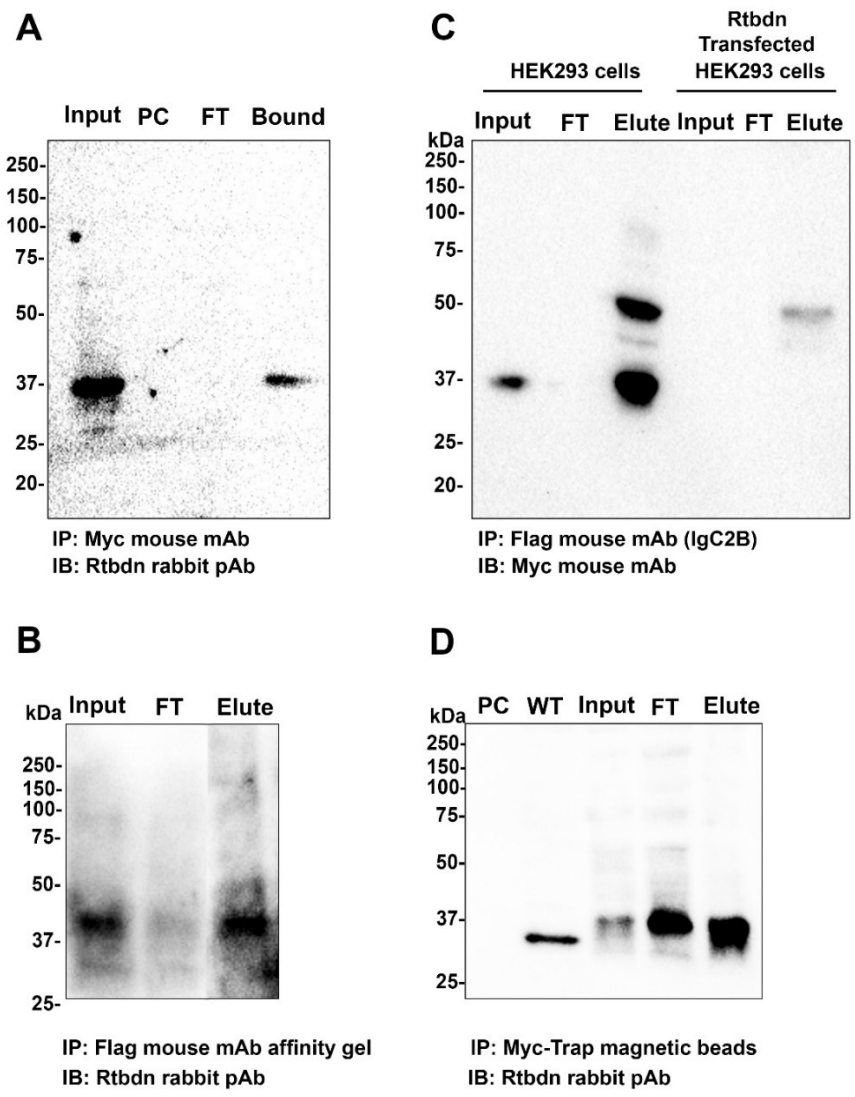

Figure 6.3. Purification of Rtbdn associated proteins from Rtbdn transfected HEK293 cells.

Input: cell lysate, PC; pre-clear, FT; flow through

Next, Rtbdn associated proteins were affinity purified from Rtbdn transfected HEK293 cells in four different ways. First, we performed immunoprecipitation using mouse monoclonal anti-Myc antibody with Sepharose G beads, and the bound was eluted in loading buffer containing SDS and BME (Fig. 6.3A). Second, we performed affinity purification using a mouse IgG2B monoclonal anti-FLAG antibody attached

to agarose. Elution was performed with a solution containing SDS and BME (Fig. 6.3B). Third, we performed traditional immunoprecipitation using anti-FLAG agarose beads. Elution was performed with BME solution (Fig. 6.3C). Fourth, we purified proteins associated with Rtbdn using anti-Myc magnetic beads, and the bound was eluted using the Myc peptide (Fig. 6.3D).

The purified protein complexes were analyzed by mass spectrometry. Since Rtbdn is associated with the plasma membrane protein, we eliminated the proteins that found in the other subcellular localization from the list. Table 2 shows the resulting candidates.

6.3.3 Identification of Rtbdn interacting candidates in mouse retina

The expression of proteins in cell culture to test their interaction is a proper way, however the setting is artificial. Overexpression of proteins in culture can induce aggregation, and tissue culture system cannot copy the photoreceptor like structures. Another limitation of working with cell line was that HEK293 cells may not express the Rtbdn associated partners since they are originally derived from human embryonic kidney cells and Rtbdn is a retina specific protein. To be able to perform immunoprecipitation on retinal samples, we generated a new mouse monoclonal antibody (2 sub-clones: 6B6F7D6, 6B6H5E11) against Rtbdn. This antibody gave a single band of the expected size in mouse retinal extracts on native-PAGE gel (Fig. 6.4A). We observed faint signal in the *Rtbdn*$^{-/-}$ retinal extracts, although PCR validated

the *Rtbdn*$^{-/-}$ homozygous genotype. Our further analyses suggest that our antibody cross-reacts with another protein, likely gfp that was knocked-in in the *Rtbdn* locus.

We next performed immunoprecipitation using extracts from WT and *Rtbdn*$^{-/-}$ retinas with anti-Rtbdn monoclonal antibody. We probed the blot with our rabbit polyclonal anti-Rtbdn antibody and observed strong band, in the bound portion of WT retinal extract, at the expected size (Fig. 6.4B). To confirm whether our immunoprecipitation pulled-down Rtbdn and associated proteins, we performed another immunoprecipitation with Rtbdn transfected and untransfected HEK293 cells using the same antibody. We probed the blot with anti-FLAG antibody and observed a signal in the bound portion of Rtbdn transfected cells at the expected size, while no signal was detected in the untransfected cell extract lanes (Fig. 6.4C).

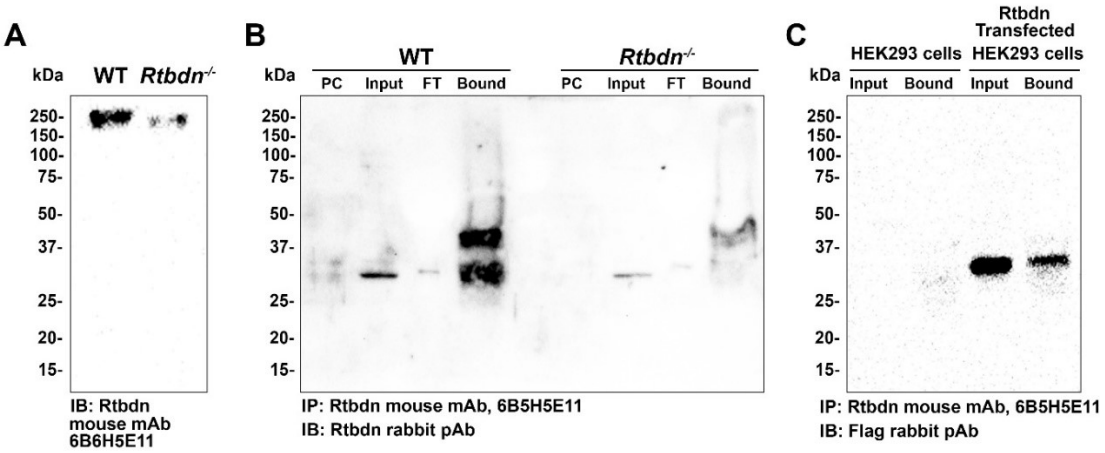

Figure 6.4. Monoclonal anti-Rtbdn antibody is capable of immunoprecipitation.
A. Blot of native-PAGE. **B.** Immunoprecipitation with WT and *Rtbdn*$^{-/-}$ lysates **C.** Immunoprecipitation with Rtbdn-transfected and un-transfected cells.

After validating that the new monoclonal antibody is capable of pulling down Rtbdn, we performed 2 separate experiments for the purification of Rtbdn associated proteins. In the first experiment, we performed immunoprecipitation on extracts from WT and Rtbdn$^{-/-}$ retinas using two different subclones (6B6H5E11 and 6B6F7D6) of our monoclonal anti-Rtbdn antibody (Fig. 6.5A). The WT and *Rtbdn*$^{-/-}$ pulldowns were run on SDS-PAGE for a short period of time until all of the loaded sample pass the stacking gel. The band for each sample was cut out and sent for mass spectrometry analysis. In the second experiment, we prepared OS and IS enriched fractions to purify the OS tips and the membrane of the ISs, where Rtbdn is localized, to avoid too much noise and performed immunoprecipitation separately on these two fractions using the 6B6H5E11 subclone of our monoclonal anti-Rtbdn antibody. The pull downs of the OS and IS fractions were combined and separated in SDS-PAGE and were stained by coomassie blue (Fig 6.5B). The bands were cut out and sent for mass spectrometry analysis separately.

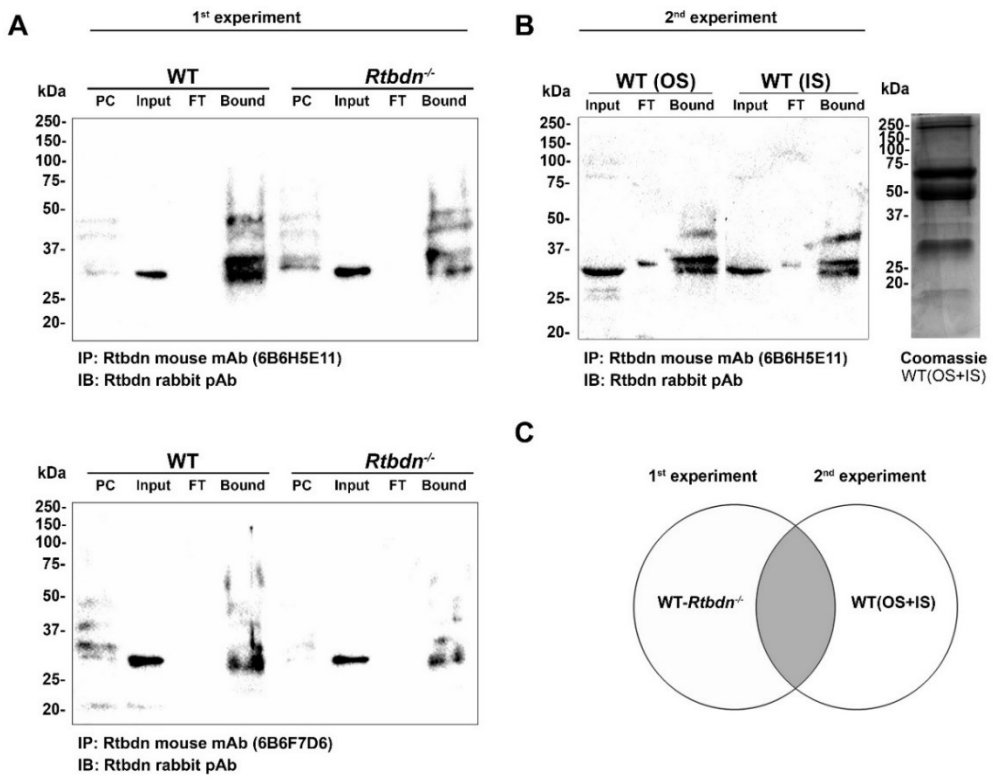

Figure 6.5. Purification of Rtbdn associated proteins from mouse retina. **B.** Immunoprecipitation from WT outer segment and WT inner segment enriched fractions. **C.** Rtbdn associated proteins identified by proteomics.

The protein lists derived from the immunoprecipitation using different subclones of Rtbdn monoclonal antibody were combined for WT and *Rtbdn*$^{-/-}$. The protein candidates derived from the first experiment were selected by subtracting the proteins showing up in the negative control (*Rtbdn*$^{-/-}$) from WT (1st group). For the second experiment, although each band was analyzed via mass spectrometry separately, we combined the protein lists (2nd group). The proteins which were common in both groups were selected for further investigation (Fig. 6.5C). Table 3 shows these selected proteins.

6.3.4 Investigation of potential Rtbdn and PEDF interaction

From our proteomics analysis, we selected pigment epithelium–derived factor (PEDF) to investigate its interaction with Rtbdn considering its localization and functions. PEDF is a member of the serine protease superfamily secreted by the RPE cells into the IPM and it plays critical roles in many physiological and pathophysiological processes, including neuroprotection, angiogenesis, and fibrogenesis [173]. Various studies showed that PEDF suppresses retinal neovascularization and inhibits endothelial cell migration [174, 175]. It is present in the photoreceptors (mostly in the OSs) and in the inner retinal cells [176]. Although, it is generally regarded as a secreted protein, some studies have reported intracellular detection [177, 178]. To begin our validation of interactions between Rtbdn and PEDF, we conducted immunohistochemistry on P30 WT retinal paraffin sections. Rtbdn was localized at the apical portion of OSs and around the ISs confirming our previous findings. PEDF was localized throughout photoreceptor cell layer with a strong signal in the OS area. The 3D view of confocal z-stack images revealed the co-localization of Rtbdn with PEDF throughout the apical side of the photoreceptor OSs and partially at the ISs (yellow color and arrows) (Fig 6.6). Although the distribution of PEDF was similar on the *Rtbdn*$^{-/-}$ retinal section, its intensity was low compared to WT, especially at basal IS area. This observation prompted us to investigate PEDF levels in WT and *Rtbdn*$^{-/-}$ retinas. Our preliminary analysis showed reduced PEDF levels in the *Rtbdn*$^{-/-}$ retinas compared to the WT retinas.

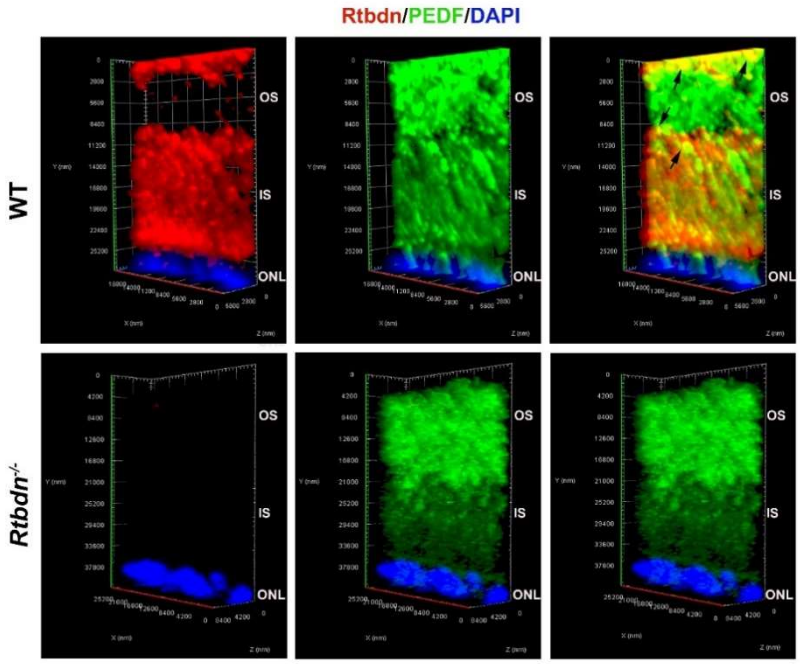

Figure 6.6. PEDF co-localizes with Rtbdn at OS tips and around IS.
P30 retinal sections were double immunolabeled with anti-Rtbdn and -PEDF antibodies. Shown are 3D representation of a confocal stack.

We next conducted immunoprecipitation studies to test potential interaction of Rtbdn with PEDF. The commercial polyclonal PEDF antibody detects two bands; one at approximately 50 kDa and the other at around 150 kDa. Immunoblots of immunoprecipitated proteins probed for Rtbdn and PEDF, showed signals at the same size both in input and bound lanes (Fig. 6.6).

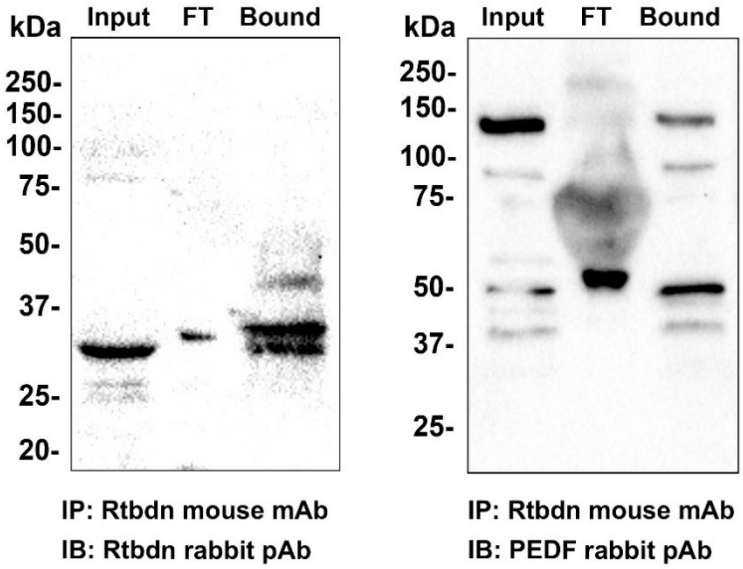

Figure 6.7. Immunoprecipitation using anti-Rtbdn and -PEDF antibodies.
Input: retina lysate, PC; pre-clear, FT; flow through, pAb; polyclonal antibody, mAb; monoclonal antibody, OS; outer segment, IS; inner segment.

6.4 Discussion

Although retbindin is ~30 kDa on SDS-PAGE, our preliminary data show that it migrates at a higher molecular weight on native-PAGE gels, suggesting that it may interact with other proteins. Here we utilized affinity purification methods and mass spectrometry analysis using Rtbdn transfected cells and retinal samples to identify the Rtbdn interacting proteins.

We immunoprecipitated Rtbdn from retinal samples using newly generated anti-Rtbdn monoclonal antibody and have selected PEDF for further investigation from the protein list identified in mass spectrometry analysis. The localization of PEDF and its function directed this selection. It was reported that PEDF has anti-angiogenic, anti-tumorigenic, and neurotrophic functions [174, 179]. Evidence

showed that its role in protection against glutamate neurotoxicity and against both natural and induced apoptosis [180, 181]. Studies on retinal angiogenesis have focused on the balance of PEDF as an angiogenesis inhibitor and VEGF as an angiogenic growth factor [182, 183]. In the previous chapters it was shown that Rtbdn absence results in formation of neovascular tufts and dense capillary bed in the diseased retinas. Rtbdn upregulation in the diseased retina may be playing a role in inhibition of neovascularization and it may mediate this by its interaction with PEDF. Our preliminary data showed reduced PEDF levels in *Rtbdn*$^{-/-}$ retina compared to WT. We have initiated the investigation of potential interaction between Rtbdn and PEDF. Co-localization of Rtbdn and PEDF in the distal OSs and IS area is a promising finding in terms of possible interaction among these two proteins. However, further reciprocal co-immunoprecipitation studies are essential to validate this interaction. We have started this exploration but couldn't finalize yet due to problems arising from antibodies. To verify interaction between these two proteins, proximity ligation assay should also be performed. Furthermore, the cells can be co-transfected with vectors to express Rtbdn and PEDF to perform reciprocal immunoprecipitations.

In summary, we present here the workflow that was applied to analyze affinity-purified Rtbdn complexes isolated using either tagged fusion proteins or via immunoprecipitation of endogenous Rtbdn.

Chapter 7- Conclusions and future directions

This dissertation presented the effect of Rtbdn absence in different retinal disease models to investigate the role of Rtbdn in the degenerative process. While we don't fully understand the mechanisms that cause certain mutations to lead to cell death in retinal degenerations, there is a wealth of literature suggesting that metabolic aberrations may underlay or at least contribute to the degeneration [142, 143]. Since flavins are involved in enzymatic reactions in metabolism, we hypothesized that Rtbdn, as a flavin binding protein, plays a role in modulating the degenerative process in the retina. In support of our hypothesis, we found that levels of Rtbdn increase during retinal degeneration in different mouse models of inherited retinal diseases (Fig. 2.1, Fig. 3.1, Fig. 4.1). The upregulation of Rtbdn during the degenerative process could be due to its protective role or contributor to the dying photoreceptor cells. To determine which of the two possibilities is likely, we backcrossed mouse models of retinal degenerative diseases onto the *Rtbdn*$^{-/-}$ background.

It is important to study different diseases to determine whether the protein alteration is mutant protein-specific or it is common to different blinding disorders. To address this, we chose *Prph2*^{R172W} transgenic mice with late onset cone-rod dystrophy, *Rho*$^{P23H/+}$ knock-in retinitis pigmentosa model and *Prph2*$^{Y141C/+}$ knock-in pattern dystrophy mouse model. All of these are well characterized inherited retinal disease models that mimic patient phenotypes [47, 52, 92]. They have different rates of degeneration, different etiology and associated histopathology. Table 5 summarizes the genotypic and phenotypic properties of each disease model. Identifying elements

that promote photoreceptor survival is crucial for the management of these retinal degenerations. Our ultimate goal is to determine whether Rtbdn can serve as a potential therapeutic target for the treatment of these diseases.

R172W mutation is characterized by primary cone degeneration with secondary rod involvement. Eliminating Rtbdn in *Prph2*^{R172W} mutants had a larger effect on rod function (was reduced ~52% compared to *Prph2*^{R172W} control group) than the cone function (was reduced 21% compared to *Prph2*^{R1472W} control group). We next examined the effect of Rtbdn absence in the *Rho*$^{P23H/+}$ mice, which is characterized by extensive, rapid rod loss and secondary cone involvement. Analysis of effects of eliminating Rtbdn in the *Rho*$^{P23H/+}$ mouse showed more pronounced deleterious effects on cone function (~33% reduction in cones, ~22% reduction in rods). Lastly, investigating the elimination of Rtdbn on retinas expressing the Y141C mutation, which effects both rods and cones equally, resulted in ~34% reduction in cone or cone pathway function and ~25% reduction in rod function. These findings suggests that the negative effects of removing Rtbdn are more pronounced in models where rod loss is secondary, and in models where degeneration is not early onset. In addition to functional manifestations, lack of Rtbdn in all disease models resulted in evident shortening of OS and ISs and reduced photoreceptor numbers. Upregulation of Rtbdn in diseased retinas combined with the accelerated degeneration in its absence suggest that Rtbdn plays a protective role during degeneration.

Mutation screening in panels of Lebers Congenital Amaurosis , Retinitis Pigmentosa, and Cone-Rod patients have not identified any pathological mutations in

Rtbdn. However, two missense polymorphisms (Gly106Ser, Gly265Ala) were encountered in large number of these patients, as well as control DNA's [184]. This and our findings may have implications that Rtbdn is not necessary for the initiation of disease, but it rather plays modulatory roles in the progression of retinal diseases. This approach is consistent with the role of metabolic dysregulation as a secondary mechanism in retinal degeneration.

Although Rtbdn is expressed only in rod photoreceptors [56], its deficiency led to significant functional decline and cell loss in both rods and cones. Therefore, it is of interest to determine whether Rtbdn levels will increase in models of cone degeneration. That is likely the scenario since we observed significantly elevated levels of Rtbdn in the $Prph2^{R172W}$ late onset cone-rod dystrophy even before the onset of degeneration. Interestingly, the effect of Rtbdn absence on the cones was more pronounced in the mouse model harboring mutation in rod specific gene ($Rho^{P23H/+}$) compared to other mouse models studied. Therefore, Rtbdn is a likely contributor to cone homeostasis.

One interesting observation is that absence of Rtbdn resulted in neovascular tufts and dense capillary bed in the retina of all the inherited disease models we studied. Akula at al. showed that early photoreceptor dysfunction in rats is predictive of ensuing neurovascularization [123]. Moreover, other studies demonstrated that photoreceptor energy demand controls the vascular supply and drive vessel growth [124-126]. The metabolic and energy needs of retina has been assumed to be largely met by glucose. The metabolomics study of $Rtbdn^{-/-}$ retinas revealed reduced glucose

levels and disturbed glycolysis [61]. Other lines of evidence show that reduced nutrient and oxygen availability triggers the compensatory misguided neovascularization in proliferative retinopathies [147]. The neovascularization in the diseased animals with no Rtbdn could be either due to reduced glucose flux and altered glycolysis or secondary pathological remodeling of blood vessels as a compensatory mechanism against accelerated cell death due to loss of a protective factor (i.e., Rtbdn). Since no signs of neovascularization were observed in the *Rtdbn*$^{-/-}$, the latter possibility is more plausible. Although, evidence show that metabolic need influence the blood vessel supply in the retina, the specific mediators that link metabolism with angiogenesis during retinal degeneration remain elusive. Our results suggest that Rtbdn is one such mediator.

We also demonstrated that lack of Rtbdn cause accelerated induction of glial fibrillary acidic protein (GFAP) in diseased retina. Müller cells play important role in the development and preservation of retinal cells [185]. They express low levels of GFAP at normal conditions. However, multiple studies showed higher levels of GFAP in cases of retinal stress and vascular diseases [186-188]. Although, it has been suggested as a stress marker in diseases, the mechanism underlying the upregulation of GFAP has not been determined. We observed accelerated induction of GFAP in the retina of double mutants compared to the single mutant control group. Therefore, upregulated and altered pattern of GFAP labeling in the Müller cells of the diseased retina in elimination of Rtbdn suggest that Rtbdn absence triggers the stress in the pathological conditions and makes the retina more vulnerable to neovascularization as

higher levels of GFAP is associated with vascular diseases and we observed neovascularization in its absence.

Although Rtbdn is photoreceptor specific, our study suggests impairment of the inner postreceptoral retina in addition to the dominant effects on photoreceptors. The reduced photopic b- wave in the double mutants we observed could be due to effects on cone photoreceptors, as well as to postreceptoral effects on transmission to cone bipolar cells and other factors affecting cone bipolar cell function such as neovascularization and gliosis we observed. We also observed low scotopic b- wave amplitudes in the double mutants. More generally, the stimulus used would put the b-wave in saturation. The b- wave must have been affected by the loss and damage to rod photoreceptors. This would be detected using weaker stimulus flash that does not saturate rod-driven bipolar cells response.

Another interesting finding from our studies is the electro-lucent particles in the Bruch's membrane of Rtbdn deficient mice. Although we have not characterized these particles, other studies showed very similar material in Bruch's membrane and demonstrated them to be lipid particles [151, 152]. Accumulation of lipid particles in Bruch's membrane was correlated with compromised diffusion and subsequent elevated oxidative stress due to accumulating metabolic end products [162, 189], as well as increased vascular endothelial growth factor expression in the retina [151]. These observations seems to bridge the gap between photoreceptor degeneration, Bruch's membrane changes, and neovascularization in the diseased retinas that lack Rtbdn.

We performed flavin quantification to see whether mis-regulation of flavins is the reason for the accelerated cell death in the diseased retina. Compared to WT, the levels of FAD was found to be significantly, yet equally, reduced in *Rtbdn*$^{-/-}$, all control disease models, and in all models in absence of Rtbdn. However, riboflavin and FMN levels showed model-dependent alterations. Significant elevation of riboflavin and FMN levels in *Prph2*$^{Y141C/+}$ retinas, compared to WT levels, correlates with the increased levels of Rtbdn. Moreover, depression of these two flavin levels in the *Prph2*$^{Y141C/+}$*/Rtbdn*$^{-/-}$ retinas reflects flavin binding capacities of Rtbdn. However, we observed similar riboflavin and FMN levels in the *Prph2*^{R172W} and reduced levels in *Rho*$^{P23H/+}$ retinas, compared to WT, despite the upregulation of Rtbdn. The changes in flavin levels could be indicative of the independent mechanism that contribute to the varying phenotypes. Despite the model-dependent fluctuations, there appears to be an association with vascular abnormalities and flavin levels. Elevated levels of riboflavin were observed in the *Prph2*^{R172W}*/Rtbdn*$^{-/-}$ and *Rho*$^{P23H/+}$*/Rtbdn*$^{-/-}$ retinas which exhibit increased vasculature and leakage. Although FAD is the predominant cofactor in the energy metabolism, interestingly, ATP levels resembled the FMN profile. Our ATP quantification experiments fell short of demonstrating a clear correlation between flavins and ATP levels. It is well known that flavins are involve in a broad spectrum of biological activities in addition to energy metabolism. They serve as co-factor for more than 200 flavoproteins in several different processes. The disturbance of other metabolites in absence of Rtbdn may be the reason for the accelerated degeneration in the diseased retinas. Without any supporting data, it is not

possible within the scope of this dissertation to discuss these metabolites and their interaction with flavins.

Examining Rtbdn in various disease models reveals more information about the processes in which this protein may be involved. However, in order to be able to elucidate its role in binding riboflavin as well as any potentially other function, its binding partners need to be identified. Although the size of Rtbdn is ~30 kDa on the SDS-PAGE, we showed that it migrates at a higher molecular weight on native gels, suggesting that it either self-associates or interacts with other partners. We made attempts to identify these binding partners, however, more investigation is required to be able to have solid data. In addition, protein crystallography should also be performed to determine the three dimensional structure of this protein and identify the riboflavin binding pocket.

In conclusion, we demonstrated significantly increased levels of Rtbdn in *Prph2*^{R172W}, *Rho*$^{P23H/+}$, and *Prph2*$^{Y141C/+}$ mouse models, suggesting that Rtbdn plays a protective role in retinal degenerative diseases. This hypothesis was supported by our findings that the *Prph2*^{R172W}, *Rho*$^{P23H/+}$, and *Prph2*$^{Y141C/+}$ mice lacking Rtbdn exhibit functional and structural defects in both rod and cone photoreceptors, compared to age matched controls. Eliminating Rtbdn in these inherited retinal disease models caused exacerbation of other degenerative processes including retinal gliosis, neovascularization, and thickening of Bruch's membrane. Retinal flavin levels showed Rtbdn as well as model-dependent alterations. These results indicate that Rtbdn is essential for retinal homeostasis and it plays a protective role during retinal

degeneration. The outcome of this study should help to define the processes in which Rtbdn participates and to identify new therapeutic targets. The ultimate goal of the lab is to investigate Rtbdn in donor eyes from patients with inherited retinal degenerative diseases and perform gene therapy experiments to validate Rtbdn as therapeutic target.

Table 1 Antibodies

Antigen	Antibody	Species	Source	Concentration
Retbindin	Anti-Rtbdn	Rbt PC	In-House [56, 169]	1:500 (WB/IF)
Prph2	RDS-2B7	Ms MC	In-House	1:1,000 (WB)
IRBP	Anti-IRBP	Rbt PC	[132]	1:1,000 (WB)
GAPDH	Ab8245	Ms MC	Abcam, Cambridge, MA	1:1,000 (WB)
beta-Actin-HRP	A3854	Ms MC	Sigma-Aldrich St. Louis, MO	1:50,000
GFAP	MAB360	Ms MC	Millipore Burlington, MA	1:1,000 (IF)
FLAD1	G-4, sc-376819	Ms MC	Santa Cruz Biotechnology, Dallas, TX	1:1000 (WB)
Rabbit-HRP	AP187P	Goat PC	Sigma-Aldrich St. Louis, MO	1:25,000 (WB)
Mouse-HRP	AP181P	Goat PC	Sigma-Aldrich St. Louis, MO	1:25,000 (WB)
Alexa Fluor-anti rabbit 647	A21245	Goat PC	Thermo Fisher Scientific Waltham, MA	1:1,000 (IF)
Alexa Fluor-anti mouse 555	A31570	Donkey PC	Thermo Fisher Scientific Waltham, MA	1:1,000 (IF)
PNA Alexa Fluor 488	L21409	N/A	Thermo Fisher Scientific Waltham, MA	1:50 (IF)
Isolectin B4 Alexa Fluor 568	L21412	N/A	Thermo Fisher Scientific Waltham, MA	1:50 (IF)
DAPI (stain)	62248	N/A	Thermo Fisher Scientific Waltham, MA	1:1,000 (IF)

Table 2 Potential Rtbdn associated proteins identified in Mass Spectrometry analysis of Rtbdn transfected HEK293 cells.

+ shows the presence of the protein in the Mass spectrometry analysis for the indicated sample that are bound/elute(s) shown in Fig 6.3: Sample 1 (A), Sample 2(B), Sample 3(C), and Sample 4 (D).

Protein ID	Sample 1	Sample 2	Sample 3	Sample 4	Subcellular localization
P13639	+	+	+	+	Plasma membrane, Cytosol
P49327	+	+	+	+	Plasma membrane, Cytosol
P06733	+	+	+	+	Plasma membrane, Cytosol
P21333	+	+	+	+	Plasma membrane, Cytosol
P04406	+	+	+	+	Plasma membrane, Cytosol
P04792	+	+	+	+	Plasma membrane, Cytosol
P49368	+	+	+	+	Plasma membrane, Cytosol
P35579	+	+	+		Plasma membrane, Cytosol
Q16658	+	+	+	+	Plasma membrane, Cytosol
P08865	+	+	+	+	Plasma membrane, Cytosol
P30041	+	+		+	Plasma membrane, Cytosol
P31939	+	+	+	+	Plasma membrane, Cytosol
P54709	+	+	+	+	Plasma membrane
Q9UBB4		+	+	+	Plasma membrane, Cytosol
P15311	+	+	+	+	Plasma membrane
Q9Y5M8	+	+	+	+	Plasma membrane
P46940	+	+	+	+	Plasma membrane, Junctions
Q9UJZ1	+	+	+	+	Plasma membrane, Cytosol
Q15758	+	+	+	+	Plasma membrane
Q13642		+	+	+	Plasma membrane, Cytosol
Q9HDC9	+	+	+	+	Plasma membrane
P30520	+	+	+	+	Plasma membrane, Cytosol
P11166		+	+	+	Plasma membrane
P55010		+	+	+	Plasma membrane, Cytosol
P06737		+	+	+	Plasma membrane, Cytosol
P20020	+	+	+		Plasma membrane
O43795		+	+		Plasma membrane
P00390	+			+	Plasma membrane, Cytosol
P13796	+	+		+	Plasma membrane, Cytosol
Q9H2G2		+	+	+	Plasma membrane, Cytosol
P13797	+	+		+	Plasma membrane, Cytosol
Q9H2M9		+	+	+	Plasma membrane, Cytosol
P26038	+	+		+	Plasma membrane
Q9Y2J2		+	+	+	Plasma membrane
P30086	+	+		+	Plasma membrane
Q9BR76	+	+	+		Plasma membrane, Cytosol
O60841		+	+	+	Plasma membrane, Cytosol
P09104		+	+	+	Plasma membrane, Cytosol
Q14166		+	+	+	Plasma membrane, Cytosol
O60610		+	+	+	Plasma membrane
P35222		+	+	+	Plasma membrane
Q9Y5X1		+	+	+	Plasma membrane Cytosol
O75083		+	+	+	Plasma membrane, Junctions
Q07021	+	+		+	Plasma membrane, Mitochondria

Table 2 to be continued

Q16555		+	+	+	Plasma membrane, Cytosol
Q8IZP0		+		+	Plasma membrane, Cell Junctions
Q9H223			+	+	Plasma membrane
O60716		+	+		Plasma membrane
Q9H074	+			+	Plasma membrane, Cytosol
Q9UHB6		+		+	Plasma membrane, Cytosol
P50579		+		+	Plasma membrane, Cytosol
Q8IZH2		+	+		Plasma membrane, Cytosol
Q9HAV0		+	+		Plasma membrane
Q96I99		+	+		Plasma membrane, Mitochondria
P53985		+	+		Plasma membrane, Cell Junctions
P07947		+	+		Plasma membrane, Cytosol
Q8TDB8		+	+		Plasma membrane
Q7KYR7		+			Plasma membrane
P13591		+			Plasma membrane, Cytosol
Q8N3E9			+		Plasma membrane
P80723	+				Plasma membrane
Q01484		+			Plasma membrane
Q9P2W9		+			Plasma membrane
Q13554		+			Plasma membrane, Cell Junctions, Cytosol
P17252		+			Plasma membrane, Cytosol
Q9Y6U3		+			Plasma membrane
Q7Z4S6		+			Plasma membrane, Cytosol
Q16643		+			Plasma membrane, Actin filaments
Q13332		+			Plasma membrane, Cytosol
Q14126		+			Plasma membrane, Cell Junctions
P52569					Plasma membrane, Cell Junctions
P53597			+		Plasma membrane, Mitochondria
P11171		+			Plasma membrane, Cell Junctions, Cytosol
P16422	+				Plasma membrane
P50748			+		Plasma membrane, Cytosol
Q8N6Q8		+			Plasma membrane, Mitochondria, Cytosol
Q8NCG7		+			Plasma membrane
P33527		+			Plasma membrane
Q16625		+			Plasma membrane, Cell Junctions
Q02952		+			Plasma membrane, Cytosol
Q99523		+			Golgi apparatus, Plasma membrane, Cytosol
Q8WXG6			+		Plasma membrane, Cytosol
Q01469				+	Plasma membrane, Cytosol
P46108				+	Plasma membrane
Q96BN8				+	Plasma membrane, Mitochondria
Q9Y5K6				+	Plasma ,
Q14847				+	Plasma membrane, Focal adhesion sites, Cytosol
O00233				+	Plasma membrane, Cytosol

Table 2 to be continued

Q9UQB8				+	Plasma membrane, Cytosol
O00151				+	Plasma membrane, Cell Junctions, Actin filaments
P60033				+	Plasma membrane
Q8N8S7				+	Plasma membrane, Focal adhesion sites, Cytosol
Q09666				+	Plasma membrane, Cytosol
Q9UHD9				+	Plasma membrane, Cytosol
P30419				+	Plasma membrane, Cytosol
Q00536				+	Plasma membrane, Microtubules, Cytosol
P58546				+	Plasma membrane,Cytosol
P50552				+	Plasma membrane, Cell Junctions, Focal adhesion sites
Q9Y6W5				+	Plasma membrane, Cytosol
P34949				+	Plasma membrane, Cytosol
O95817				+	Plasma membrane, Cytosol
P27816				+	Plasma membrane, Microtubules, Cytosol
Q9C0D2				+	Plasma membraneCytosol
P26885				+	Plasma membrane

Table 3 Potential Rtbdn associated proteins identified in Mass Spectrometry analysis of retinal extracts

Protein ID	Protein Name
Q9WVJ5	Beta-crystallin B1
P04344	Gamma-crystallin
Q9JJU9	Beta-crystallin
P17742	Peptidyl-prolyl cis-trans isomerase A
P02525	Beta-crystallin A1
P23927	Alpha-crystallin B chain
Q8R1A4	Dedicator of cytokinesis protein
P15105	Glutamine synthetase
P97298	Pigment epithelium-derived factor
P28798	Granulins
Q03265	ATP synthase subunit alpha, mitochondrial
P06151	L-lactate dehydrogenase A chain
P48962	ADP/ATP translocase 1
P62874	Guanine nucleotide-binding protein G(I)/G(S)/G(T) subunit beta-1
P51881	ADP/ATP translocase 2
Q04447	Creatine kinase B-type
P04342	Gamma-crystallin D
P62827	GTP-binding nuclear protein Ran
P01821	Ig heavy chain V region MC101
Q9JLZ3	Methylglutaconyl-CoA hydratase, mitochondrial
Q6PDM2	Serine/arginine-rich splicing factor 1
P06684	Complement C5
P62259	14-3-3 protein epsilon
Q6VNB8	WD repeat and FYVE domain-containing protein 3
P08113	Endoplasmin
P50247	Adenosylhomocysteinase
Q5U405	Transmembrane protease serine 13

Table 4 Inherited retinal degenerative mouse models

Mouse model	***Prph2*^{R172W}**	***Rho*$^{P23H/+}$**	***Prph2*$^{Y141C/+}$**
Genetic construction	Transgenic	Knock-in	Knock-in
Name of disease	Cone- Rod dystrophy	Retinitis Pigmentosa	Pattern Dystrophy
Rate of degeneration	Late	Early	Early
Cell type affected	Cone first, than rods	Rods first, than cones	Rods and cones

Bibliography

1. Saladin, K.S., *Anatomy & Physiology: The unity of Form and Function, fifth edition*. 5th ed ed, ed. J.F. Connely. 2010, 1221 Avenue of the Americas, New York, NY: Michelle Watnick.
2. Fu, Z., C.T. Chen, G. Cagnone, E. Heckel, Y. Sun, B. Cakir, Y. Tomita, S. Huang, Q. Li, W. Britton, S.S. Cho, T.S. Kern, A. Hellstrom, J.S. Joyal, and L.E. Smith, *Dyslipidemia in retinal metabolic disorders.* EMBO Mol Med, 2019. **11**(10): p. e10473.
3. Reichenbach, A. and A. Bringmann, *New functions of Muller cells.* Glia, 2013. **61**(5): p. 651-78.
4. Terakita, A., *The opsins.* Genome Biol, 2005. **6**(3): p. 213.
5. Dale Purves, G.J.A., David Fitzpatrick, Lawrence C Katz, Anthony-Samuel LaMantia, James O McNamara, and S Mark Williams., *Neuroscience, 2nd edition*. 2nd ed ed. 2001.
6. Volland, S., J. Esteve-Rudd, J. Hoo, C. Yee, and D.S. Williams, *A comparison of some organizational characteristics of the mouse central retina and the human macula.* PLoS One, 2015. **10**(4): p. e0125631.
7. Kefalov, V.J., *Phototransduction: Phototransduction in Cones*, in *Encyclopedia of the Eye*, D.A. Dartt, Editor. 2010, Oxford: Academic Press. p. 389-395.

8. Fu, Y., *Phototransduction in Rods and Cones*, in *Webvision: The Organization of the Retina and Visual System*, H. Kolb, E. Fernandez, and R. Nelson, Editors. 1995: Salt Lake City (UT).

9. Hafler, B.P., *Clinical Progress in Inherited Retinal Degenerations: Gene Therapy Clinical Trials and Advances in Genetic Sequencing.* Retina, 2017. **37**(3): p. 417-423.

10. Scholl, H.P., R.W. Strauss, M.S. Singh, D. Dalkara, B. Roska, S. Picaud, and J.A. Sahel, *Emerging therapies for inherited retinal degeneration.* Sci Transl Med, 2016. **8**(368): p. 368rv6.

11. Rajappa, M., A. Goyal, and J. Kaur, *Inherited metabolic disorders involving the eye: a clinico-biochemical perspective.* Eye (Lond), 2010. **24**(4): p. 507-18.

12. Poll-The, B.T., L.J. Maillette de Buy Wenniger-Prick, P.G. Barth, and M. Duran, *The eye as a window to inborn errors of metabolism.* J Inherit Metab Dis, 2003. **26**(2-3): p. 229-44.

13. Brand, C.S., *Management of retinal vascular diseases: a patient-centric approach.* Eye (Lond), 2012. **26 Suppl 2**: p. S1-16.

14. Buschini, E., A. Piras, R. Nuzzi, and A. Vercelli, *Age related macular degeneration and drusen: neuroinflammation in the retina.* Prog Neurobiol, 2011. **95**(1): p. 14-25.

15. Yoshida, N., Y. Ikeda, S. Notomi, K. Ishikawa, Y. Murakami, T. Hisatomi, H. Enaida, and T. Ishibashi, *Clinical evidence of sustained chronic inflammatory reaction in retinitis pigmentosa.* Ophthalmology, 2013. **120**(1): p. 100-5.

16. Joussen, A.M., V. Poulaki, M.L. Le, K. Koizumi, C. Esser, H. Janicki, U. Schraermeyer, N. Kociok, S. Fauser, B. Kirchhof, T.S. Kern, and A.P. Adamis, *A central role for inflammation in the pathogenesis of diabetic retinopathy.* FASEB J, 2004. **18**(12): p. 1450-2.

17. Ehlers, J.P. and S. Fekrat, *Retinal vein occlusion: beyond the acute event.* Surv Ophthalmol, 2011. **56**(4): p. 281-99.

18. Knudson, A.G., Jr., *Mutation and cancer: statistical study of retinoblastoma.* Proc Natl Acad Sci U S A, 1971. **68**(4): p. 820-3.

19. Friend, S.H., R. Bernards, S. Rogelj, R.A. Weinberg, J.M. Rapaport, D.M. Albert, and T.P. Dryja, *A human DNA segment with properties of the gene that predisposes to retinoblastoma and osteosarcoma.* Nature, 1986. **323**(6089): p. 643-6.

20. Fletcher, A.E., G.C. Bentham, M. Agnew, I.S. Young, C. Augood, U. Chakravarthy, P.T. de Jong, M. Rahu, J. Seland, G. Soubrane, L. Tomazzoli, F. Topouzis, J.R. Vingerling, and J. Vioque, *Sunlight exposure, antioxidants, and age-related macular degeneration.* Arch Ophthalmol, 2008. **126**(10): p. 1396-403.

21. Ma, L., H.L. Dou, Y.M. Huang, X.R. Lu, X.R. Xu, F. Qian, Z.Y. Zou, H.L. Pang, P.C. Dong, X. Xiao, X. Wang, T.T. Sun, and X.M. Lin, *Improvement of retinal function in early age-related macular degeneration after lutein and zeaxanthin supplementation: a randomized, double-masked, placebo-controlled trial.* Am J Ophthalmol, 2012. **154**(4): p. 625-634 e1.

22. Seddon, J.M., B. Rosner, R.D. Sperduto, L. Yannuzzi, J.A. Haller, N.P. Blair, and W. Willett, *Dietary fat and risk for advanced age-related macular degeneration.* Arch Ophthalmol, 2001. **119**(8): p. 1191-9.

23. Chiu, C.J., R. Klein, R.C. Milton, G. Gensler, and A. Taylor, *Does eating particular diets alter the risk of age-related macular degeneration in users of the Age-Related Eye Disease Study supplements?* Br J Ophthalmol, 2009. **93**(9): p. 1241-6.

24. Sapieha, P., J. Chen, A. Stahl, M.R. Seaward, T.L. Favazza, A.M. Juan, C.J. Hatton, J.S. Joyal, N.M. Krah, R.J. Dennison, J. Tang, T.S. Kern, J.D. Akula, and L.E. Smith, *Omega-3 polyunsaturated fatty acids preserve retinal function in type 2 diabetic mice.* Nutr Diabetes, 2012. **2**: p. e36.

25. Udhayabanu, T., A. Manole, M. Rajeshwari, P. Varalakshmi, H. Houlden, and B. Ashokkumar, *Riboflavin Responsive Mitochondrial Dysfunction in Neurodegenerative Diseases.* J Clin Med, 2017. **6**(5).

26. Boon, C.J., A.I. den Hollander, C.B. Hoyng, F.P. Cremers, B.J. Klevering, and J.E. Keunen, *The spectrum of retinal dystrophies caused by mutations in the peripherin/RDS gene.* Prog Retin Eye Res, 2008. **27**(2): p. 213-35.

27. Travis, G.H., J.G. Sutcliffe, and D. Bok, *The retinal degeneration slow (rds) gene product is a photoreceptor disc membrane-associated glycoprotein.* Neuron, 1991. **6**(1): p. 61-70.

28. Sanyal, S. and H.G. Jansen, *Absence of receptor outer segments in the retina of rds mutant mice.* Neurosci Lett, 1981. **21**(1): p. 23-6.

29. Connell, G., R. Bascom, L. Molday, D. Reid, R.R. McInnes, and R.S. Molday, *Photoreceptor peripherin is the normal product of the gene responsible for retinal degeneration in the rds mouse.* Proc Natl Acad Sci U S A, 1991. **88**(3): p. 723-6.

30. Conley, S.M., M.W. Stuck, J.N. Watson, R. Zulliger, J.L. Burnett, and M. Naash, *Prph2 initiates outer segment morphogenesis but maturation requires Prph2/Rom1 oligomerization.* Human Molecular Genetics, 2018. **https://doi.org/10.1093/hmg/ddy359**: p. ddy359.

31. Jansen, H.G. and S. Sanyal, *Development and degeneration of retina in rds mutant mice: electron microscopy.* J Comp Neurol, 1984. **224**(1): p. 71-84.

32. Moritz, O.L. and R.S. Molday, *Molecular cloning, membrane topology, and localization of bovine rom-1 in rod and cone photoreceptor cells.* Invest Ophthalmol Vis Sci, 1996. **37**(2): p. 352-62.

33. Arikawa, K., L.L. Molday, R.S. Molday, and D.S. Williams, *Localization of peripherin/rds in the disk membranes of cone and rod photoreceptors: relationship to disk membrane morphogenesis and retinal degeneration.* J Cell Biol, 1992. **116**(3): p. 659-67.

34. Ding, X.Q., H.M. Stricker, and M.I. Naash, *Role of the second intradiscal loop of peripherin/rds in homo and hetero associations.* Biochemistry, 2005. **44**(12): p. 4897-904.

35. Loewen, C.J. and R.S. Molday, *Disulfide-mediated oligomerization of Peripherin/Rds and Rom-1 in photoreceptor disk membranes. Implications for*

photoreceptor outer segment morphogenesis and degeneration. J Biol Chem, 2000. **275**(8): p. 5370-8.

36. Ding, X.Q., M. Nour, L.M. Ritter, A.F. Goldberg, S.J. Fliesler, and M.I. Naash, *The R172W mutation in peripherin/rds causes a cone-rod dystrophy in transgenic mice.* Human Molecular Genetics, 2004. **13**(18): p. 2075-87.
37. Michaelides, M., G.E. Holder, K. Bradshaw, D.M. Hunt, and A.T. Moore, *Cone-rod dystrophy, intrafamilial variability, and incomplete penetrance associated with the R172W mutation in the peripherin/RDS gene.* Ophthalmology, 2005. **112**(9): p. 1592-8.
38. Rath, P.P., S. Jenkins, M. Michaelides, A. Smith, M.G. Sweeney, M.B. Davis, F.W. Fitzke, and A.C. Bird, *Characterisation of the macular dystrophy in patients with the A3243G mitochondrial DNA point mutation with fundus autofluorescence.* Br J Ophthalmol, 2008. **92**(5): p. 623-9.
39. Hartong, D.T., E.L. Berson, and T.P. Dryja, *Retinitis pigmentosa.* Lancet, 2006. **368**(9549): p. 1795-809.
40. Uren, P.J., J.T. Lee, M.M. Doroudchi, A.D. Smith, and A. Horsager, *A profile of transcriptomic changes in the rd10 mouse model of retinitis pigmentosa.* Mol Vis, 2014. **20**: p. 1612-28.
41. Jones, B.W., R.L. Pfeiffer, W.D. Ferrell, C.B. Watt, M. Marmor, and R.E. Marc, *Retinal remodeling in human retinitis pigmentosa.* Exp Eye Res, 2016. **150**: p. 149-65.

42. Moreno, M.L., S. Merida, F. Bosch-Morell, M. Miranda, and V.M. Villar, *Autophagy Dysfunction and Oxidative Stress, Two Related Mechanisms Implicated in Retinitis Pigmentosa.* Front Physiol, 2018. **9**: p. 1008.

43. Trachsel-Moncho, L., S. Benlloch-Navarro, A. Fernandez-Carbonell, D.T. Ramirez-Lamelas, T. Olivar, D. Silvestre, E. Poch, and M. Miranda, *Oxidative stress and autophagy-related changes during retinal degeneration and development.* Cell Death Dis, 2018. **9**(8): p. 812.

44. Dryja, T.P., T.L. McGee, L.B. Hahn, G.S. Cowley, J.E. Olsson, E. Reichel, M.A. Sandberg, and E.L. Berson, *Mutations within the rhodopsin gene in patients with autosomal dominant retinitis pigmentosa.* N Engl J Med, 1990. **323**(19): p. 1302-7.

45. Sohocki, M.M., S.P. Daiger, S.J. Bowne, J.A. Rodriquez, H. Northrup, J.R. Heckenlively, D.G. Birch, H. Mintz-Hittner, R.S. Ruiz, R.A. Lewis, D.A. Saperstein, and L.S. Sullivan, *Prevalence of mutations causing retinitis pigmentosa and other inherited retinopathies.* Hum Mutat, 2001. **17**(1): p. 42-51.

46. Sung, C.H., C.M. Davenport, J.C. Hennessey, I.H. Maumenee, S.G. Jacobson, J.R. Heckenlively, R. Nowakowski, G. Fishman, P. Gouras, and J. Nathans, *Rhodopsin mutations in autosomal dominant retinitis pigmentosa.* Proc Natl Acad Sci U S A, 1991. **88**(15): p. 6481-5.

47. Sakami, S., T. Maeda, G. Bereta, K. Okano, M. Golczak, A. Sumaroka, A.J. Roman, A.V. Cideciyan, S.G. Jacobson, and K. Palczewski, *Probing*

mechanisms of photoreceptor degeneration in a new mouse model of the common form of autosomal dominant retinitis pigmentosa due to P23H opsin mutations. J Biol Chem, 2011. **286**(12): p. 10551-67.

48. Sakami, S., A.V. Kolesnikov, V.J. Kefalov, and K. Palczewski, *P23H opsin knock-in mice reveal a novel step in retinal rod disc morphogenesis.* Hum Mol Genet, 2014. **23**(7): p. 1723-41.

49. Francis, P.J., D.W. Schultz, A.M. Gregory, M.B. Schain, R. Barra, J. Majewski, J. Ott, T. Acott, R.G. Weleber, and M.L. Klein, *Genetic and phenotypic heterogeneity in pattern dystrophy.* Br J Ophthalmol, 2005. **89**(9): p. 1115-9.

50. Stuck, M.W., S.M. Conley, and M.I. Naash, *The Y141C knockin mutation in RDS leads to complex phenotypes in the mouse.* Hum Mol Genet, 2014. **23**(23): p. 6260-74.

51. Vaclavik, V., H.V. Tran, M.C. Gaillard, D.F. Schorderet, and F.L. Munier, *Pattern dystrophy with high intrafamilial variability associated with Y141C mutation in the peripherin/RDS gene and successful treatment of subfoveal CNV related to multifocal pattern type with anti-VEGF (ranibizumab) intravitreal injections.* Retina, 2012. **32**(9): p. 1942-9.

52. Stuck, M.W., S.M. Conley, and M.I. Naash, *The Y141C knockin mutation in RDS leads to complex phenotypes in the mouse.* Human Molecular Genetics, 2014. **23**(23): p. 6260-74.

53. Khani, S.C., A.J. Karoukis, J.E. Young, R. Ambasudhan, T. Burch, R. Stockton, R.A. Lewis, L.S. Sullivan, S.P. Daiger, E. Reichel, and R. Ayyagari, *Late-onset autosomal dominant macular dystrophy with choroidal neovascularization and nonexudative maculopathy associated with mutation in the RDS gene.* Invest Ophthalmol Vis Sci, 2003. **44**(8): p. 3570-7.

54. Conley, S.M., M.W. Stuck, J.N. Watson, and M.I. Naash, *Rom1 converts Y141C-Prph2-associated pattern dystrophy to retinitis pigmentosa.* Hum Mol Genet, 2017. **26**(3): p. 509-518.

55. Wistow, G., S.L. Bernstein, M.K. Wyatt, S. Ray, A. Behal, J.W. Touchman, G. Bouffard, D. Smith, and K. Peterson, *Expressed sequence tag analysis of human retina for the NEIBank Project: retbindin, an abundant, novel retinal cDNA and alternative splicing of other retina-preferred gene transcripts.* Mol Vis, 2002. **8**: p. 196-204.

56. Kelley, R.A., M.R. Al-Ubaidi, and M.I. Naash, *Retbindin is an extracellular riboflavin-binding protein found at the photoreceptor/retinal pigment epithelium interface.* J Biol Chem, 2015. **290**(8): p. 5041-52.

57. Geer, L.Y., A. Marchler-Bauer, R.C. Geer, L. Han, J. He, S. He, C. Liu, W. Shi, and S.H. Bryant, *The NCBI BioSystems database.* Nucleic Acids Res, 2010. **38**(Database issue): p. D492-6.

58. Farrell, H.M., Jr., M.F. Mallette, E.G. Buss, and C.O. Clagett, *The nature of the biochemical lesion in avian renal riboflavinuria. 3. The isolation and*

characterization of the riboflavin-binding protein from egg albumen. Biochim Biophys Acta, 1969. **194**(2): p. 433-42.

59. Ostrowski, W., Z. Zak, and A. Krawczyk, *Riboflavin flavoprotein from egg yolk. Analytical and biophysical data.* Acta Biochim Pol, 1968. **15**(3): p. 241-60.

60. Kelley, R.A., M.R. Al-Ubaidi, T. Sinha, A.M. Genc, M.S. Makia, L. Ikelle, and M.I. Naash, *Ablation of the riboflavin-binding protein retbindin reduces flavin levels and leads to progressive and dose-dependent degeneration of rods and cones.* J Biol Chem, 2017. **292**(51): p. 21023-21034.

61. Tirthankar Sinha, J.D., James B. Hurley, Muna I. Naash and Muayyad R. Al-Ubaidi *Retbindin's ablation leads to metabolic dysregulation prior to the onset of retinal degeneration*. 2020.

62. Merrill, A.H., Jr., J.D. Lambeth, D.E. Edmondson, and D.B. McCormick, *Formation and mode of action of flavoproteins.* Annu Rev Nutr, 1981. **1**: p. 281-317.

63. Huang, S.N. and P.W. Swaan, *Involvement of a receptor-mediated component in cellular translocation of riboflavin.* J Pharmacol Exp Ther, 2000. **294**(1): p. 117-25.

64. Bro-Rasmussen, F. and M.K. Horwitt, *Riboflavin requirement of animal and man, related to protein requirement or energy turnover.* Am J Clin Nutr, 1967. **20**(5): p. 507-10.

65. Tu, B.P., S.C. Ho-Schleyer, K.J. Travers, and J.S. Weissman, *Biochemical basis of oxidative protein folding in the endoplasmic reticulum.* Science, 2000. **290**(5496): p. 1571-4.

66. Mazur-Bialy, A.I., B. Buchala, and B. Plytycz, *Riboflavin deprivation inhibits macrophage viability and activity - a study on the RAW 264.7 cell line.* Br J Nutr, 2013. **110**(3): p. 509-14.

67. Sanches, S.C., L.N. Ramalho, M. Mendes-Braz, V.A. Terra, R. Cecchini, M.J. Augusto, and F.S. Ramalho, *Riboflavin (vitamin B-2) reduces hepatocellular injury following liver ischaemia and reperfusion in mice.* Food Chem Toxicol, 2014. **67**: p. 65-71.

68. Powers, H.J., *Riboflavin (vitamin B-2) and health.* Am J Clin Nutr, 2003. **77**(6): p. 1352-60.

69. Irinoda, K. and S. Sato, *Contribution to the ocular manifestation of riboflavin deficiency.* Tohoku J Exp Med, 1954. **61**(1): p. 93-104.

70. Deluca, C. and N.O. Kaplan, *Flavin adenine dinucleotide synthesis in animal tissues.* Biochim Biophys Acta, 1958. **30**(1): p. 6-11.

71. Foraker, A.B., C.M. Khantwal, and P.W. Swaan, *Current perspectives on the cellular uptake and trafficking of riboflavin.* Adv Drug Deliv Rev, 2003. **55**(11): p. 1467-83.

72. Akiyama, T., J. Selhub, and I.H. Rosenberg, *FMN phosphatase and FAD pyrophosphatase in rat intestinal brush borders: role in intestinal absorption of dietary riboflavin.* J Nutr, 1982. **112**(2): p. 263-8.

73. Kubo, Y., S. Miki, S.I. Akanuma, and K.I. Hosoya, *Riboflavin transport mediated by riboflavin transporters (RFVTs/SLC52A) at the rat outer blood-retinal barrier.* Drug Metab Pharmacokinet, 2019. **34**(6): p. 380-386.

74. Kubo, Y., S. Yahata, S. Miki, S.I. Akanuma, and K.I. Hosoya, *Blood-to-retina transport of riboflavin via RFVTs at the inner blood-retinal barrier.* Drug Metab Pharmacokinet, 2017. **32**(1): p. 92-99.

75. Ganea, E. and J.J. Harding, *Glutathione-related enzymes and the eye.* Curr Eye Res, 2006. **31**(1): p. 1-11.

76. Ashoori, M. and A. Saedisomeolia, *Riboflavin (vitamin B(2)) and oxidative stress: a review.* Br J Nutr, 2014. **111**(11): p. 1985-91.

77. Batey, D.W., K.K. Daneshgar, and C.D. Eckhert, *Flavin levels in the rat retina.* Exp Eye Res, 1992. **54**(4): p. 605-9.

78. Batey, D.W. and C.D. Eckhert, *Identification of FAD, FMN, and riboflavin in the retina by microextraction and high-performance liquid chromatography.* Anal Biochem, 1990. **188**(1): p. 164-7.

79. Batey, D.W. and C.D. Eckhert, *Analysis of flavins in ocular tissues of the rabbit.* Invest Ophthalmol Vis Sci, 1991. **32**(7): p. 1981-5.

80. Said, H.M., S. Wang, and T.Y. Ma, *Mechanism of riboflavin uptake by cultured human retinal pigment epithelial ARPE-19 cells: possible regulation by an intracellular Ca2+-calmodulin-mediated pathway.* J Physiol, 2005. **566**(Pt 2): p. 369-77.

81. Kansara, V., D. Pal, R. Jain, and A.K. Mitra, *Identification and functional characterization of riboflavin transporter in human-derived retinoblastoma cell line (Y-79): mechanisms of cellular uptake and translocation.* J Ocul Pharmacol Ther, 2005. **21**(4): p. 275-87.

82. Thresher, R.J., M.H. Vitaterna, Y. Miyamoto, A. Kazantsev, D.S. Hsu, C. Petit, C.P. Selby, L. Dawut, O. Smithies, J.S. Takahashi, and A. Sancar, *Role of mouse cryptochrome blue-light photoreceptor in circadian photoresponses.* Science, 1998. **282**(5393): p. 1490-4.

83. Eckhert, C.D., M.H. Hsu, and N. Pang, *Photoreceptor damage following exposure to excess riboflavin.* Experientia, 1993. **49**(12): p. 1084-7.

84. Rohlich, P., *The interphotoreceptor matrix: electron microscopic and histochemical observations on the vertebrate retina.* Exp Eye Res, 1970. **10**(1): p. 80-6.

85. Jorns, M.S., B. Wang, and S.P. Jordan, *DNA repair catalyzed by Escherichia coli DNA photolyase containing only reduced flavin: elimination of the enzyme's second chromophore by reduction with sodium borohydride.* Biochemistry, 1987. **26**(21): p. 6810-6.

86. Susin, S.A., H.K. Lorenzo, N. Zamzami, I. Marzo, B.E. Snow, G.M. Brothers, J. Mangion, E. Jacotot, P. Costantini, M. Loeffler, N. Larochette, D.R. Goodlett, R. Aebersold, D.P. Siderovski, J.M. Penninger, and G. Kroemer, *Molecular characterization of mitochondrial apoptosis-inducing factor.* Nature, 1999. **397**(6718): p. 441-6.

87. Entsch, B. and W.J. van Berkel, *Structure and mechanism of para-hydroxybenzoate hydroxylase.* FASEB J, 1995. **9**(7): p. 476-83.

88. Kim, H.J. and D.R. Winge, *Emerging concepts in the flavinylation of succinate dehydrogenase.* Biochim Biophys Acta, 2013. **1827**(5): p. 627-36.

89. Thorpe, C., R.G. Matthews, and C.H. Williams, Jr., *Acyl-coenzyme A dehydrogenase from pig kidney. Purification and properties.* Biochemistry, 1979. **18**(2): p. 331-7.

90. Sinha, T., M. Makia, J. Du, M.I. Naash, and M.R. Al-Ubaidi, *Flavin homeostasis in the mouse retina during aging and degeneration.* J Nutr Biochem, 2018. **62**: p. 123-133.

91. Reuter, J.H. and S. Sanyal, *Development and degeneration of retina in rds mutant mice: the electroretinogram.* Neurosci Lett, 1984. **48**(2): p. 231-7.

92. Conley, S.M., M.W. Stuck, J.L. Burnett, D. Chakraborty, S. Azadi, S.J. Fliesler, and M.I. Naash, *Insights into the mechanisms of macular degeneration associated with the R172W mutation in RDS.* Human Molecular Genetics, 2014. **23**(12): p. 3102-14.

93. Ekstrom, U., S. Andreasson, V. Ponjavic, M. Abrahamson, O. Sandgren, P. Nilsson-Ehle, and B. Ehinger, *A Swedish family with a mutation in the peripherin/RDS gene (Arg-172-Trp) associated with a progressive retinal degeneration.* Ophthalmic Genet, 1998. **19**(3): p. 149-56.

94. Ding, X.Q., M. Nour, L.M. Ritter, A.F. Goldberg, S.J. Fliesler, and M.I. Naash, *The R172W mutation in peripherin/rds causes a cone-rod dystrophy in transgenic mice.* Hum Mol Genet, 2004. **13**(18): p. 2075-87.

95. Winkler, B.S., *The electroretinogram of the isolated rat retina.* Vision Res, 1972. **12**(6): p. 1183-98.

96. Cheng, T., N.S. Peachey, S. Li, Y. Goto, Y. Cao, and M.I. Naash, *The effect of peripherin/rds haploinsufficiency on rod and cone photoreceptors.* J Neurosci, 1997. **17**(21): p. 8118-28.

97. Stricker, H.M., X.Q. Ding, A. Quiambao, S.J. Fliesler, and M.I. Naash, *The Cys214-->Ser mutation in peripherin/rds causes a loss-of-function phenotype in transgenic mice.* Biochemical Journal, 2005. **388**(Pt 2): p. 605-13.

98. Koirala, A., R.S. Makkia, M.J. Cooper, and M.I. Naash, *Nanoparticle-mediated gene transfer specific to retinal pigment epithelial cells.* Biomaterials, 2011. **32**(35): p. 9483-93.

99. Lieth, E., A.J. Barber, B. Xu, C. Dice, M.J. Ratz, D. Tanase, and J.M. Strother, *Glial reactivity and impaired glutamate metabolism in short-term experimental diabetic retinopathy. Penn State Retina Research Group.* Diabetes, 1998. **47**(5): p. 815-20.

100. Hernandez, M.R., H. Miao, and T. Lukas, *Astrocytes in glaucomatous optic neuropathy.* Prog Brain Res, 2008. **173**: p. 353-73.

101. Gallego, B.I., J.J. Salazar, R. de Hoz, B. Rojas, A.I. Ramirez, M. Salinas-Navarro, A. Ortin-Martinez, F.J. Valiente-Soriano, M. Aviles-Trigueros, M.P.

Villegas-Perez, M. Vidal-Sanz, A. Trivino, and J.M. Ramirez, *IOP induces upregulation of GFAP and MHC-II and microglia reactivity in mice retina contralateral to experimental glaucoma.* J Neuroinflammation, 2012. **9**: p. 92.

102. Penn, J.S., A. Madan, R.B. Caldwell, M. Bartoli, R.W. Caldwell, and M.E. Hartnett, *Vascular endothelial growth factor in eye disease.* Prog Retin Eye Res, 2008. **27**(4): p. 331-71.

103. Venkataswamy, G., *Ocular manifestations of vitamin B-complex deficiency.* Br J Ophthalmol, 1967. **51**(11): p. 749-54.

104. Wong-Riley, M.T., *Energy metabolism of the visual system.* Eye Brain, 2010. **2**: p. 99-116.

105. McCormick, D.B., *Two interconnected B vitamins: riboflavin and pyridoxine.* Physiol Rev, 1989. **69**(4): p. 1170-98.

106. Calaza, K.C., J.H. Kam, C. Hogg, and G. Jeffery, *Mitochondrial decline precedes phenotype development in the complement factor H mouse model of retinal degeneration but can be corrected by near infrared light.* Neurobiol Aging, 2015. **36**(10): p. 2869-76.

107. Yonezawa, A. and K. Inui, *Novel riboflavin transporter family RFVT/SLC52: identification, nomenclature, functional characterization and genetic diseases of RFVT/SLC52.* Mol Aspects Med, 2013. **34**(2-3): p. 693-701.

108. Balasubramaniam, S., J. Christodoulou, and S. Rahman, *Disorders of riboflavin metabolism.* J Inherit Metab Dis, 2019. **42**(4): p. 608-619.

109. Huvaere, K., D.R. Cardoso, P. Homem-de-Mello, S. Westermann, and L.H. Skibsted, *Light-induced oxidation of unsaturated lipids as sensitized by flavins.* J Phys Chem B, 2010. **114**(16): p. 5583-93.

110. Song, P.S. and D.E. Metzler, *Photochemical degradation of flavins. IV. Studies of the anaerobic photolysis of riboflavin.* Photochem Photobiol, 1967. **6**(10): p. 691-709.

111. Treadwell, G.E., W.L. Cairns, and D.E. Metzler, *Photochemical degradation of flavins. V. Chromatographic studies of the products of photolysis of riboflavin.* J Chromatogr, 1968. **35**(3): p. 376-88.

112. Kelley, R.A., M.R. Al-Ubaidi, and M.I. Naash, *Retbindin Is Capable of Protecting Photoreceptors from Flavin-Sensitized Light-Mediated Cell Death In Vitro.* Adv Exp Med Biol, 2018. **1074**: p. 485-490.

113. Kushnareva, Y. and D.D. Newmeyer, *Bioenergetics and cell death.* Ann N Y Acad Sci, 2010. **1201**: p. 50-7.

114. Mansoorabadi, S.O., C.J. Thibodeaux, and H.W. Liu, *The diverse roles of flavin coenzymes--nature's most versatile thespians.* J Org Chem, 2007. **72**(17): p. 6329-42.

115. Lienhart, W.D., V. Gudipati, and P. Macheroux, *The human flavoproteome.* Arch Biochem Biophys, 2013. **535**(2): p. 150-62.

116. Nomura, K., H. Imai, T. Koumura, M. Arai, and Y. Nakagawa, *Mitochondrial phospholipid hydroperoxide glutathione peroxidase suppresses apoptosis*

mediated by a mitochondrial death pathway. J Biol Chem, 1999. **274**(41): p. 29294-302.

117. Zamaraeva, M.V., R.Z. Sabirov, E. Maeno, Y. Ando-Akatsuka, S.V. Bessonova, and Y. Okada, *Cells die with increased cytosolic ATP during apoptosis: a bioluminescence study with intracellular luciferase.* Cell Death Differ, 2005. **12**(11): p. 1390-7.

118. Perez de Lara, M.J., A. Guzman-Aranguez, P. de la Villa, J.I. Diaz-Hernandez, M.T. Miras-Portugal, and J. Pintor, *Increased levels of extracellular ATP in glaucomatous retinas: Possible role of the vesicular nucleotide transporter during the development of the pathology.* Mol Vis, 2015. **21**: p. 1060-70.

119. Skulachev, V.P., *Bioenergetic aspects of apoptosis, necrosis and mitoptosis.* Apoptosis, 2006. **11**(4): p. 473-85.

120. Nicotera, P. and G. Melino, *Regulation of the apoptosis-necrosis switch.* Oncogene, 2004. **23**(16): p. 2757-65.

121. Ankarcrona, M., J.M. Dypbukt, E. Bonfoco, B. Zhivotovsky, S. Orrenius, S.A. Lipton, and P. Nicotera, *Glutamate-induced neuronal death: a succession of necrosis or apoptosis depending on mitochondrial function.* Neuron, 1995. **15**(4): p. 961-73.

122. Perez de Lara, M.J. and J. Pintor, *Presence and release of ATP from the retina in an Alzheimer's disease model.* J Alzheimers Dis, 2015. **43**(1): p. 177-81.

123. Akula, J.D., R.M. Hansen, R. Tzekov, T.L. Favazza, T.C. Vyhovsky, I.Y. Benador, J.A. Mocko, D. McGee, R. Kubota, and A.B. Fulton, *Visual cycle*

modulation in neurovascular retinopathy. Exp Eye Res, 2010. **91**(2): p. 153-61.

124. Fu, Z., C.A. Lofqvist, R. Liegl, Z. Wang, Y. Sun, Y. Gong, C.H. Liu, S.S. Meng, S.B. Burnim, I. Arellano, M.T. Chouinard, R. Duran, A. Poblete, S.S. Cho, J.D. Akula, M. Kinter, D. Ley, I.H. Pupp, S. Talukdar, A. Hellstrom, and L.E. Smith, *Photoreceptor glucose metabolism determines normal retinal vascular growth.* EMBO Mol Med, 2018. **10**(1): p. 76-90.

125. Sapieha, P., *Eyeing central neurons in vascular growth and reparative angiogenesis.* Blood, 2012. **120**(11): p. 2182-94.

126. Joyal, J.S., M.L. Gantner, and L.E.H. Smith, *Retinal energy demands control vascular supply of the retina in development and disease: The role of neuronal lipid and glucose metabolism.* Prog Retin Eye Res, 2018. **64**: p. 131-156.

127. Barile, M., T.A. Giancaspero, C. Brizio, C. Panebianco, C. Indiveri, M. Galluccio, L. Vergani, I. Eberini, and E. Gianazza, *Biosynthesis of flavin cofactors in man: implications in health and disease.* Curr Pharm Des, 2013. **19**(14): p. 2649-75.

128. Powers, H.J., B.M. Corfe, and E. Nakano, *Riboflavin in development and cell fate.* Subcell Biochem, 2012. **56**: p. 229-45.

129. Futterman, S. and J.H. Kinoshita, *Metabolism of the retina. I. Respiration of cattle retina.* J Biol Chem, 1959. **234**(4): p. 723-6.

130. Hu, Z., Y. Zhang, J. Wang, P. Mao, X. Lv, S. Yuan, Z. Huang, Y. Ding, P. Xie, and Q. Liu, *Knockout of Ccr2 alleviates photoreceptor cell death in*

rodent retina exposed to chronic blue light. Cell Death Dis, 2016. **7**(11): p. e2468.

131. Conley, S.M., H.M. Stricker, and M.I. Naash, *Biochemical analysis of phenotypic diversity associated with mutations in codon 244 of the retinal degeneration slow gene.* Biochemistry, 2010. **49**(5): p. 905-11.

132. Redmond, T.M., B. Wiggert, F.A. Robey, N.Y. Nguyen, M.S. Lewis, L. Lee, and G.J. Chader, *Isolation and characterization of monkey interphotoreceptor retinoid-binding protein, a unique extracellular matrix component of the retina.* Biochemistry, 1985. **24**(3): p. 787-93.

133. Cheng, T., M.R. al Ubaidi, and M.I. Naash, *Structural and developmental analysis of the mouse peripherin/rds gene.* Somat Cell Mol Genet, 1997. **23**(3): p. 165-83.

134. Hung, M.C. and W. Link, *Protein localization in disease and therapy.* J Cell Sci, 2011. **124**(Pt 20): p. 3381-92.

135. Bridges, C.D., *Lectin receptors of rods and cones. Visualization by fluorescent label.* Invest Ophthalmol Vis Sci, 1981. **20**(1): p. 8-16.

136. Blanks, J.C. and L.V. Johnson, *Specific binding of peanut lectin to a class of retinal photoreceptor cells. A species comparison.* Invest Ophthalmol Vis Sci, 1984. **25**(5): p. 546-57.

137. Kivela, T. and A. Tarkkanen, *A lectin cytochemical study of glycoconjugates in the human retina.* Cell Tissue Res, 1987. **249**(2): p. 277-88.

138. Majumder, A., J. Pahlberg, K.K. Boyd, V. Kerov, S. Kolandaivelu, V. Ramamurthy, A.P. Sampath, and N.O. Artemyev, *Transducin translocation contributes to rod survival and enhances synaptic transmission from rods to rod bipolar cells.* Proc Natl Acad Sci U S A, 2013. **110**(30): p. 12468-73.

139. Chen, J., M.I. Simon, M.T. Matthes, D. Yasumura, and M.M. LaVail, *Increased susceptibility to light damage in an arrestin knockout mouse model of Oguchi disease (stationary night blindness).* Invest Ophthalmol Vis Sci, 1999. **40**(12): p. 2978-82.

140. Song, X., S.A. Vishnivetskiy, J. Seo, J. Chen, E.V. Gurevich, and V.V. Gurevich, *Arrestin-1 expression level in rods: balancing functional performance and photoreceptor health.* Neuroscience, 2011. **174**: p. 37-49.

141. Liu, H., J. Tang, Y. Du, A. Saadane, D. Tonade, I. Samuels, A. Veenstra, K. Palczewski, and T.S. Kern, *Photoreceptor Cells Influence Retinal Vascular Degeneration in Mouse Models of Retinal Degeneration and Diabetes.* Invest Ophthalmol Vis Sci, 2016. **57**(10): p. 4272-81.

142. Punzo, C., W. Xiong, and C.L. Cepko, *Loss of daylight vision in retinal degeneration: are oxidative stress and metabolic dysregulation to blame?* J Biol Chem, 2012. **287**(3): p. 1642-8.

143. Griciuc, A., M.J. Roux, J. Merl, A. Giangrande, S.M. Hauck, L. Aron, and M. Ueffing, *Proteomic survey reveals altered energetic patterns and metabolic failure prior to retinal degeneration.* J Neurosci, 2014. **34**(8): p. 2797-812.

144. Ngo, S.T. and F.J. Steyn, *The interplay between metabolic homeostasis and neurodegeneration: insights into the neurometabolic nature of amyotrophic lateral sclerosis.* Cell Regen (Lond), 2015. **4**(1): p. 5.

145. Joyal, J.S., Y. Sun, M.L. Gantner, Z. Shao, L.P. Evans, N. Saba, T. Fredrick, S. Burnim, J.S. Kim, G. Patel, A.M. Juan, C.G. Hurst, C.J. Hatton, Z. Cui, K.A. Pierce, P. Bherer, E. Aguilar, M.B. Powner, K. Vevis, M. Boisvert, Z. Fu, E. Levy, M. Fruttiger, A. Packard, F.A. Rezende, B. Maranda, P. Sapieha, J. Chen, M. Friedlander, C.B. Clish, and L.E. Smith, *Retinal lipid and glucose metabolism dictates angiogenesis through the lipid sensor Ffar1.* Nat Med, 2016. **22**(4): p. 439-45.

146. Bellhorn, R.W., *Control of blood vessel development.* Trans Ophthalmol Soc U K, 1980. **100**(3): p. 328-31.

147. Chen, J. and L.E. Smith, *Retinopathy of prematurity.* Angiogenesis, 2007. **10**(2): p. 133-40.

148. Bernstein, F.C., T.F. Koetzle, G.J. Williams, E.F. Meyer, Jr., M.D. Brice, J.R. Rodgers, O. Kennard, T. Shimanouchi, and M. Tasumi, *The Protein Data Bank: a computer-based archival file for macromolecular structures.* J Mol Biol, 1977. **112**(3): p. 535-42.

149. Joosten, V. and W.J. van Berkel, *Flavoenzymes.* Curr Opin Chem Biol, 2007. **11**(2): p. 195-202.

150. Lem, J., N.V. Krasnoperova, P.D. Calvert, B. Kosaras, D.A. Cameron, M. Nicolo, C.L. Makino, and R.L. Sidman, *Morphological, physiological, and*

biochemical changes in rhodopsin knockout mice. Proc Natl Acad Sci U S A, 1999. **96**(2): p. 736-41.

151. Rudolf, M., B. Winkler, Z. Aherrahou, L.C. Doehring, P. Kaczmarek, and U. Schmidt-Erfurth, *Increased expression of vascular endothelial growth factor associated with accumulation of lipids in Bruch's membrane of LDL receptor knockout mice.* Br J Ophthalmol, 2005. **89**(12): p. 1627-30.

152. Curcio, C.A., C.L. Millican, T. Bailey, and H.S. Kruth, *Accumulation of cholesterol with age in human Bruch's membrane.* Invest Ophthalmol Vis Sci, 2001. **42**(1): p. 265-74.

153. Tode, J., E. Richert, S. Koinzer, A. Klettner, C. von der Burchard, R. Brinkmann, R. Lucius, and J. Roider, *Thermal Stimulation of the Retina Reduces Bruch's Membrane Thickness in Age Related Macular Degeneration Mouse Models.* Transl Vis Sci Technol, 2018. **7**(3): p. 2.

154. Barile, M., C. Brizio, D. Valenti, C. De Virgilio, and S. Passarella, *The riboflavin/FAD cycle in rat liver mitochondria.* Eur J Biochem, 2000. **267**(15): p. 4888-900.

155. Mancuso, M., F. Coppede, L. Migliore, G. Siciliano, and L. Murri, *Mitochondrial dysfunction, oxidative stress and neurodegeneration.* J Alzheimers Dis, 2006. **10**(1): p. 59-73.

156. Droge, W., *Free radicals in the physiological control of cell function.* Physiol Rev, 2002. **82**(1): p. 47-95.

157. Cui, H., Y. Kong, and H. Zhang, *Oxidative stress, mitochondrial dysfunction, and aging.* J Signal Transduct, 2012. **2012**: p. 646354.

158. Nita, M. and A. Grzybowski, *The Role of the Reactive Oxygen Species and Oxidative Stress in the Pathomechanism of the Age-Related Ocular Diseases and Other Pathologies of the Anterior and Posterior Eye Segments in Adults.* Oxid Med Cell Longev, 2016. **2016**: p. 3164734.

159. Winkler, B.S., S.M. Orselli, and T.S. Rex, *The redox couple between glutathione and ascorbic acid: a chemical and physiological perspective.* Free Radic Biol Med, 1994. **17**(4): p. 333-49.

160. De Benedetto, U., G. Querques, R. Lattanzio, E. Borrelli, G. Triolo, G. Maestranzi, G. Calori, L. Querques, and F. Bandello, *Macular dysfunction is common in both type 1 and type 2 diabetic patients without macular edema.* Retina, 2014. **34**(11): p. 2171-7.

161. Pescosolido, N., A. Barbato, A. Stefanucci, and G. Buomprisco, *Role of Electrophysiology in the Early Diagnosis and Follow-Up of Diabetic Retinopathy.* J Diabetes Res, 2015. **2015**: p. 319692.

162. Ambati, J., B.K. Ambati, S.H. Yoo, S. Ianchulev, and A.P. Adamis, *Age-related macular degeneration: etiology, pathogenesis, and therapeutic strategies.* Surv Ophthalmol, 2003. **48**(3): p. 257-93.

163. Curcio, C.A., C.L. Millican, K.A. Allen, and R.E. Kalina, *Aging of the human photoreceptor mosaic: evidence for selective vulnerability of rods in central retina.* Invest Ophthalmol Vis Sci, 1993. **34**(12): p. 3278-96.

164. Gao, H. and J.G. Hollyfield, *Aging of the human retina. Differential loss of neurons and retinal pigment epithelial cells.* Invest Ophthalmol Vis Sci, 1992. **33**(1): p. 1-17.

165. Curcio, C.A. and D.N. Drucker, *Retinal ganglion cells in Alzheimer's disease and aging.* Ann Neurol, 1993. **33**(3): p. 248-57.

166. Ramirez, J.M., A.I. Ramirez, J.J. Salazar, R. de Hoz, and A. Trivino, *Changes of astrocytes in retinal ageing and age-related macular degeneration.* Exp Eye Res, 2001. **73**(5): p. 601-15.

167. Wassell, J., S. Davies, W. Bardsley, and M. Boulton, *The photoreactivity of the retinal age pigment lipofuscin.* J Biol Chem, 1999. **274**(34): p. 23828-32.

168. Winkler, B.S., M.E. Boulton, J.D. Gottsch, and P. Sternberg, *Oxidative damage and age-related macular degeneration.* Mol Vis, 1999. **5**: p. 32.

169. Kelley, R.A., M.R. Al-Ubaidi, and M.I. Naash, *The Potential Role of Flavins and Retbindin in Retinal Function and Homeostasis.* Adv Exp Med Biol, 2016. **854**: p. 643-8.

170. Steinle, J.J., S. Sharma, C.P. Smith, and L.S. McFayden-Ketchum, *Normal aging involves modulation of specific inflammatory markers in the rat retina and choroid.* J Gerontol A Biol Sci Med Sci, 2009. **64**(3): p. 325-31.

171. Lenox, A.R., Y. Bhootada, O. Gorbatyuk, R. Fullard, and M. Gorbatyuk, *Unfolded protein response is activated in aged retinas.* Neurosci Lett, 2015. **609**: p. 30-5.

172. Zulliger, R., S.M. Conley, M.L. Mwoyosvi, M.W. Stuck, S. Azadi, and M.I. Naash, *SNAREs Interact with Retinal Degeneration Slow and Rod Outer Segment Membrane Protein-1 during Conventional and Unconventional Outer Segment Targeting.* PLoS One, 2015. **10**(9): p. e0138508.

173. Rychli, K., K. Huber, and J. Wojta, *Pigment epithelium-derived factor (PEDF) as a therapeutic target in cardiovascular disease.* Expert Opin Ther Targets, 2009. **13**(11): p. 1295-302.

174. Dawson, D.W., O.V. Volpert, P. Gillis, S.E. Crawford, H. Xu, W. Benedict, and N.P. Bouck, *Pigment epithelium-derived factor: a potent inhibitor of angiogenesis.* Science, 1999. **285**(5425): p. 245-8.

175. Mori, K., E. Duh, P. Gehlbach, A. Ando, K. Takahashi, J. Pearlman, K. Mori, H.S. Yang, D.J. Zack, D. Ettyreddy, D.E. Brough, L.L. Wei, and P.A. Campochiaro, *Pigment epithelium-derived factor inhibits retinal and choroidal neovascularization.* J Cell Physiol, 2001. **188**(2): p. 253-63.

176. Chen, Y., J. Yang, H. Geng, L. Li, J. Li, B. Cheng, X. Ma, H. Li, and L. Hou, *Photoreceptor degeneration in microphthalmia (Mitf) mice: partial rescue by pigment epithelium-derived factor.* Dis Model Mech, 2019. **12**(1).

177. Tombran-Tink, J., S.M. Shivaram, G.J. Chader, L.V. Johnson, and D. Bok, *Expression, secretion, and age-related downregulation of pigment epithelium-derived factor, a serpin with neurotrophic activity.* J Neurosci, 1995. **15**(7 Pt 1): p. 4992-5003.

178. Karakousis, P.C., S.K. John, K.C. Behling, E.M. Surace, J.E. Smith, A. Hendrickson, W.X. Tang, J. Bennett, and A.H. Milam, *Localization of pigment epithelium derived factor (PEDF) in developing and adult human ocular tissues.* Mol Vis, 2001. **7**: p. 154-63.

179. Tombran-Tink, J., G.G. Chader, and L.V. Johnson, *PEDF: a pigment epithelium-derived factor with potent neuronal differentiative activity.* Exp Eye Res, 1991. **53**(3): p. 411-4.

180. Araki, T., T. Taniwaki, S.P. Becerra, G.J. Chader, and J.P. Schwartz, *Pigment epithelium-derived factor (PEDF) differentially protects immature but not mature cerebellar granule cells against apoptotic cell death.* J Neurosci Res, 1998. **53**(1): p. 7-15.

181. Pang, I.H., H. Zeng, D.L. Fleenor, and A.F. Clark, *Pigment epithelium-derived factor protects retinal ganglion cells.* BMC Neurosci, 2007. **8**: p. 11.

182. Gao, G., Y. Li, D. Zhang, S. Gee, C. Crosson, and J. Ma, *Unbalanced expression of VEGF and PEDF in ischemia-induced retinal neovascularization.* FEBS Lett, 2001. **489**(2-3): p. 270-6.

183. Ohno-Matsui, K., I. Morita, J. Tombran-Tink, D. Mrazek, M. Onodera, T. Uetama, M. Hayano, S.I. Murota, and M. Mochizuki, *Novel mechanism for age-related macular degeneration: an equilibrium shift between the angiogenesis factors VEGF and PEDF.* J Cell Physiol, 2001. **189**(3): p. 323-33.

184. Bhattacharya, S.S., R.J. Patel, L. AbuSafieh, C. Chakarova, M. Papaioannou, E. Vithana, B. Leroy, and A.J. Hardcastle, *Evaluation of the Retbindin gene as a candidate for retinal diseases.* Investigative Ophthalmology & Visual Science, 2003. **44**: p. U400-U400.

185. Wang, X., A. Iannaccone, and M.M. Jablonski, *Contribution of Muller cells toward the regulation of photoreceptor outer segment assembly.* Neuron Glia Biol, 2005. **1**: p. 1-6.

186. Vessey, K.A., J.L. Wilkinson-Berka, and E.L. Fletcher, *Characterization of retinal function and glial cell response in a mouse model of oxygen-induced retinopathy.* J Comp Neurol, 2011. **519**(3): p. 506-27.

187. Lewis, G.P. and S.K. Fisher, *Up-regulation of glial fibrillary acidic protein in response to retinal injury: its potential role in glial remodeling and a comparison to vimentin expression.* Int Rev Cytol, 2003. **230**: p. 263-90.

188. Ekstrom, P., S. Sanyal, K. Narfstrom, G.J. Chader, and T. van Veen, *Accumulation of glial fibrillary acidic protein in Muller radial glia during retinal degeneration.* Invest Ophthalmol Vis Sci, 1988. **29**(9): p. 1363-71.

189. Beatty, S., H. Koh, M. Phil, D. Henson, and M. Boulton, *The role of oxidative stress in the pathogenesis of age-related macular degeneration.* Surv Ophthalmol, 2000. **45**(2): p. 115-34.